INVESTIGATIONS ON PEAK-TO-AVERAGE POWER RATIO REDUCTION TECHNIQUES FOR SC-FDMA SYSTEMS

Submitted in partial fulfilment of the requirements

for the award of the degree of

Doctor of Philosophy

by

K. Shri Ramtej

(Roll No. 716028)

Supervisor

Dr. S. Anuradha

Associate Professor, Dept. of ECE

Department of Electronics & Communication Engineering
NATIONAL INSTITUTE OF TECHNOLOGY WARANGAL – 506004, T.S, INDIA
March-2020

APPROVAL SHEET

This thesis entitled "**Investigations on Peak-to-Average Power Ratio Reduction Techniques for SC-FDMA Systems**" by Mr. **K. Shri Ramtej** is approved for the degree of **Doctor of Philosophy**.

Examiners

_____

_____

Supervisor

_____

Dr. S. Anuradha

Associate Professor, Electronics and Communication Engineering Department,

NIT WARANGAL

Chairman

_____

Prof. L. Anjaneyulu

Head, Electronics and Communication Engineering Department,

NIT WARANGAL

Date:

Place:

DECLARATION

This is to certify that the work presented in the thesis entitled "**Investigations on Peak-to-Average Power Ratio Reduction Techniques for SC-FDMA Systems**" is a bonafide work done by me under the supervision of **Dr. S. Anuradha**, Department of Electronics and Communication Engineering, National Institute of Technology Warangal, and was not submitted elsewhere for the award of any degree.

I declare that this written submission represents my ideas in my own words and where others' ideas or words have been included, I have adequately cited and referenced the original sources. I also declare that I have adhered to all principles of academic honesty and integrity and have not misrepresented or fabricated or falsified any idea/date/fact/source in my submission. I understand that any violation of the above will be cause for disciplinary action by the institute and can also evoke penal action from the sources which have thus not been properly cited or from whom proper permission has not been taken when needed.

K. Shri Ramtej
Roll No: 716028

Date:
Place: Warangal

Department of Electronics and Communication Engineering
National Institute of Technology
Warangal – 506 004, Telangana, India

CERTIFICATE

This is to certify that the dissertation work entitled **"Investigations on Peak-to-Average Power Ratio Reduction Techniques for SC-FDMA Systems"**, which is being submitted by Mr. K. Shri Ramtej (Roll No.716028), is a bonafide work submitted to National Institute of Technology Warangal in partial fulfilment of the requirement for the award of the degree of *Doctor of Philosophy in Electronics and Communication Engineering*.

To the best of our knowledge, the work incorporated in this thesis has not been submitted elsewhere for the award of any degree.

Dr. S. Anuradha
Supervisor
Department of ECE
National Institute of Technology
Warangal – 506004

Dedicated to My

Family, Gurus, & Friends

Contents

ACKNOWLEDGEMENTS

I am grateful to many people who made this work possible and helped me during my Ph.D studies. I am greatly indebted to my research supervisor Dr. S. Anuradha for giving me excellent support during my research activity at NIT Warangal. She encouraged me in choosing my research topic, her vision in my research area leads to successful investigations. I am very much thankful for giving research freedom and guidance, support in non-academic matters and for the humanity shown to me. With her inimitable qualities as a good teacher, she chiseled my path towards perfection. Ever since I met her, she has been an eternal source of motivation, inspiration, encouragement and enlightenment. She is responsible for making the period of my research work as an educative and enjoyable learning experience. The thesis would not have seen the light of the day without her insistent support and cooperation.

I am also grateful to Prof. L. Anjaneyulu, Head of the Department, Dept. of Electronics and Communication Engineering, for his valuable suggestions and support that he shared during my research tenure.

I take this privilege to thank all my Doctoral Scrutiny Committee members, Prof. D. M. Vinod Kumar, Department of Electrical Engineering, Dr. P. Sreehari Rao, Associate Professor, Department of Electronics and Communication Engineering, Dr. D.Vakula, Associate Professor, Department of Electronics and Communication Engineering for their detailed review, constructive suggestions and excellent advice during the progress of this research work.

I am grateful to the former Heads of the ECE department Prof. N. Bheema Rao and Prof. T. Kishore Kumar for their continuous support and encouragement. I would also appreciate the encouragement from teaching, non-teaching members and fraternity of Dept. of E.C.E. of N.I.T. Warangal. They have always been encouraging and supportive.

I take this opportunity to convey my regards to my closest friends for being always next to me. Thanks to V. Sandeep Kumar, M. Ranjeeth, D. Srikar, and Ch. Vijaya Durga Department of Electronics and Communication Engineering for their motivation and support throughout my work.

I acknowledge my gratitude to all my teachers and colleagues at various places for supporting and cooperating me to complete this work.

I would like to thank my family members (K. M. M. Krishna, K. Malliswari, Y. Bheemeswara Rao, Y. S. K. Madhavi, and K. Shri Vidya Krishna) for giving me mental support and inspiration. They have motivated and helped me to complete my thesis work successfully.

Finally, I thank God, for filling me every day with new hopes, strength, purpose and faith.

K. Shri Ramtej

ABSTRACT

Single carrier frequency division multiple access (SC-FDMA) is a promising technique that is currently being used in the uplink communications of the third-generation partnership project (3GPP) long term evolution (LTE) standard. It is also referred to as DFT spread orthogonal frequency division multiple access (OFDMA) and has nearly the same complexity and similar performance as that of OFDMA. One notable advantage of SC-FDMA over OFDMA is that it has a lower peak-to-average power ratio (PAPR) because of its single carrier nature.

Although SC-FDMA has low PAPR, the dynamic range of the signal increases with higher-order modulations, especially with localized mapping. Therefore further limiting the PAPR in localized SC-FDMA systems for higher-order modulations is a key issue, as decreasing PAPR results in lower power consumption and hence an extended battery life. Reducing PAPR without degrading power usage efficiency and bit error rate (BER) is a challenging issue in improving communication performance. So, this thesis aims to investigate PAPR reduction techniques for SC-FDMA systems.

In this thesis, we first studied the performance of various companding schemes developed for OFDM systems, to mitigate PAPR in SC-FDMA systems. Then an improved exponential companding technique with two different companding levels is introduced that can offer more flexibility than the conventional exponential companding technique.

As companding transforms are designed based on the distribution of the signal, the distribution of the SC-FDMA signal is approximated by using a curve fitting tool, and then a companding technique is proposed to transform it into a uniform distribution. Also, the distribution of the DCT SC-FDMA signal is approximated by using a curve fitting tool, and then a companding technique is proposed to transform it into a triangular distribution.

Also, an SC-FDMA transceiver based on Walsh Hadamard Transform (WHT) is proposed, and the performance of different ordered WHT systems over AWGN and multipath fading environments is studied. The time-domain symbols for different ordered WHT systems have also been derived.

Finally, the proposed techniques have been verified experimentally considering a real-time indoor channel by using Wireless Open-Access Research Platform (WARP) hardware.

List of Figures

List of Tables

Nomenclature

3GPP	3rd Generation Partnership Project
ACC	Adjustable Circle Constraint
ACE	Active Constellation Extension
AEXP	Absolute EXPonential
AWGN	Additive White Gaussian Noise
BER	Bit Error Rate
CCDF	Complementary Cumulative Distribution Function
CDF	Cumulative Distributive Function
CP	Cyclic Prefix
CR	Clipping Ratio
DCT	Discrete Cosine Transform
DFT	Discrete Fourier Transform
DST	Discrete Sine Transform
DWT	Discrete Wavelet Transform
EC	Exponential Companding
FDE	Frequency Domain Equalization
FFT	Fast Fourier Transform
HPA	High Power Amplifier
IBI	Inter Block Interference
IBO	Input Back-Off
ICI	Inter Carrier interference
IEC	Improved Exponential Companding
IFFT	Inverse Fast Fourier Transform
ISI	Inter Symbol Interference
LTE	Long Term Evolution
MCM	Multi Carrier Communication

MMC	Modified μ-law Companding
MMSE	Minimum Mean Square Error
MSE	Mean Square Error
NDC	No De-Companding
NL	Non Linear
NLOS	Non Line Of Sight
OFDM	Orthogonal Frequency Division Multiplexing
OFDMA	Orthogonal Frequency Division Multiple Access
OOB	Out-Of-Band
PA	Power Amplifier
PAPR	Peak-to-Average Power Ratio
PDF	Probability Density Function
POCS	Projection-Onto Convex Sets
PSD	Power Spectral Density
PTS	Partial Transmit Sequence
QAM	Quadrature Amplitude Modulation
QPSK	Quadrature Phase Shift Keying
RC	Raised Cosine
SC-FDMA	Single Carrier Frequency Division Multiple Access
SGP	Smart Gradient Projection
SI	Side Information
SLM	SeLective Mapping
SNR	Signal to Noise Ratio
SRRC	Square Root Raised Cosine
SSPA	Solid State Power Amplifier
TI	Tone Injection
TR	Tone Reservation
TS	Trellis Shaping
WARP	Wireless open Access Research Platform
WHT	Walsh Hadamard Transform

Chapter-1

Introduction

1.1. Introduction

To meet the requirements of media-rich wireless services, broadband wireless communications came into existence. But they are subject to multipath frequency selective fading. Also they require complex time domain equalizers which are not practical.

Orthogonal frequency division multiplexing (OFDM) is a widely accepted multicarrier communication system in broadband wireless communications owing to its robustness to frequency selective fading channels [1]. OFDM that supports multiple users simultaneously is referred to as orthogonal frequency division multiple access (OFDMA). OFDM/OFDMA is being implemented in wireless LAN (IEEE 802.11a and 11g), WiMAX (IEEE 802.16), and third-generation partnership project (3GPP) long term evolution (LTE) downlink systems. Despite these advantages, OFDM and OFDMA systems suffer from a high peak to average power ratio (PAPR).

Single carrier frequency division multiple access (SC-FDMA), also referred to as DFT spread OFDMA, has nearly the same complexity and similar performance as that of OFDMA [2]. One notable advantage of SC-FDMA over OFDMA is that it has lower PAPR because of its single carrier nature. This enabled SC-FDMA to replace OFDMA in the uplink communications, as lower PAPR extremely helps the mobile device in terms of manufacturing cost and power efficiency. In 3GPP LTE standard, OFDMA and SC-FDMA are currently being implemented in the downlink and the uplink communications, respectively [2]–[4].

The signal with excessive PAPR generates nonlinear distortion if the power amplifier (PA) does not have highly linear characteristics, and if the input back-off (IBO) is not set properly. If IBO is not set sufficiently, the transmit signal is corrupted by the nonlinear distortion and causes adjacent channel interference, thereby decreasing the system's spectral efficiency. Contrarily, if IBO is increased, the efficiency of PA is reduced, and the heat dissipation is increased. Additionally, a high PAPR requires digital-to-analog (D/A) converters with higher dynamic ranges. For uplink communications, the reduction of PAPR leads to PA efficiency improvement, thereby increasing its coverage.

Although SC-FDMA has low PAPR, the signal's dynamic range increases with higher order modulations, especially with localized mapping [5], [6]. Therefore further limiting the PAPR in localized SC-FDMA systems for higher order modulations is a key issue, as decreasing PAPR results in lower power consumption and hence an extended battery life. Reducing PAPR without degrading power usage efficiency and bit error rate (BER) is a challenging issue in improving communication performance.

1.2. Motivation

Various methods have been adopted to limit PAPR in OFDM systems [7]–[11]. Clipping is one of the simplest method, but it causes both in band distortion and out of band radiation, there by degrading the system performance. An improved clipping and filtering technique reduces the out of band radiation, but causes some peaks to regrow [7]. Companding scheme, which was basically developed for speech processing applications [8], [9] is the most popular technique due to its low complexity, no bandwidth expansion and good system performance. Partial transmit sequence [11] and selected mapping [10] techniques limit PAPR at the cost of high system complexity, and the need of side information.

Recently, the methods adopted in OFDM systems have been used to further limit the PAPR in SC-FDMA systems [12], [13]. μ-law [14], power function [15], and raised cosine-like companding [16] are some of the techniques used to mitigate PAPR in SC-FDMA system. Other than these, not many companding schemes have been studied in the literature to mitigate the PAPR of SC-FDMA systems. This motivated us to study different companding techniques to mitigate PAPR in SC-FDMA systems without significantly degrading the system performance.

Also Discrete Cosine Transform (DCT) [17] and Discrete Wavelet Transform (DWT) [18] based SC-FDMA systems have superior performance than the conventional DFT based SC-FDMA system. This motivated us to investigate the performance of Walsh Hadamard Transform (WHT) based SC-FDMA system.

1.3. Research Objectives

The objectives of the proposed work, carried out in order to diminish PAPR in the SC-FDMA system are:

1. To study the performance of various companding schemes developed for OFDM systems for PAPR mitigation in SC-FDMA systems. To introduce an improved exponential companding technique with two different companding levels that can offer more flexibility than the conventional exponential companding technique.
2. To approximate the distribution of SC-FDMA signal by using curve fitting tool and then to propose a companding technique that transforms the approximated distribution into a uniform distribution, that can reduce PAPR without increasing average power of the signal. To propose a hybrid technique where the companded signal is clipped to a specific threshold value. To approximate the distribution of discrete cosine transform (DCT) based SC-FDMA signal, and to propose a companding technique to transform the approximated distribution into a triangular distribution to diminish PAPR in DCT SC-FDMA system.
3. To investigate the performance of an SC-FDMA transceiver based on Walsh Hadamard Transform (WHT). To derive the time domain symbols for different ordered WHT based systems.
4. To verify the proposed techniques experimentally over real time indoor channel by using Wireless Open-Access Research Platform (WARP) hardware.

1.4. Thesis Organization

The thesis is organized into seven chapters. This section gives the summary of all chapters.

Chapter 1: Gives the introduction, background, and reasons for choosing the problem.

Chapter 2: The second chapter begins with an overview of the traditional SC-FDMA system. The PAPR in SC-FDMA system is defined, and the effect of high power amplifiers on the PAPR is introduced, which further demonstrates the importance of PAPR reduction. Finally, the common methods of PAPR reduction in conventional OFDM system are summarized, including clipping, tone reservation, selective mapping and partial transmission sequences. Then, some techniques used in literature to mitigate PAPR in SC-FDMA systems conclude this chapter.

Chapter 3: In this chapter, various companding techniques like error function, exponential, rooting, logarithmic and airy companding techniques have been studied to mitigate PAPR in SC-FDMA systems. The performance of these techniques is compared with the well-known μ-law companding technique. An improved exponential companding technique with two different companding levels that offer more flexibility than the conventional exponential companding technique has been introduced.

Chapter 4: In this chapter, the distribution of SC-FDMA signal is approximated, and a companding technique is proposed to transform the approximated distribution into a uniform distribution, which decreases PAPR without increasing average power of the signal. For further improvement in PAPR, a hybrid technique is also proposed where the companded signal is clipped to a specific threshold value. Also the distribution of DCT based SC-FDMA signal is approximated, and a companding technique is proposed to transform the approximated distribution into a triangular distribution to diminish PAPR in DCT SC-FDMA system.

Chapter 5: This chapter introduces a new transceiver for SC-FDMA system based on WHT. The performance of different ordered WHT systems has been studied over AWGN and multipath fading environments. The time domain symbols for different ordered WHT systems have been derived. Exponential companding technique is used to further reduce its PAPR without degrading its BER.

Chapter 6: This chapter introduces WARP (Wireless Open-Access Research Platform) hardware. The performance of all the proposed techniques have been verified by considering real-time indoor channel by using WARP hardware.

Chapter 7: This chapter presents a summary of the results and conclusions from work carried out in the earlier chapters. The scope for future research is also indicated.

Chapter-2

Single Carrier FDMA and PAPR Reduction Schemes

2.1. Introduction

In this chapter, the concepts of SC-FDMA system are introduced. The SC-FDMA signal PAPR is defined first, and then its statistical properties are analysed. Subsequently, the correlation model of the high power amplifier is used to analyse the influence of high PAPR signal on the system when passing through the high power amplifier. Finally, a brief introduction to the traditional common methods of reducing PAPR in OFDM system is provided. Then, the PAPR reduction methods for SC-FDMA systems existing in literature close off this chapter.

Table 2.1. List of Symbols

Symbol	Description
x_n	Modulated symbols
N	Input block size
X_k	DFT of x_n
$\bar{X}_l$	Frequency-domain samples after the subcarriers mapping
M	Number of subcarriers
$\bar{x}_m$	IDFT of $\bar{X}_l$
$p(t)$	Pulse shaping filter
α	roll-off factor
$x(t)$	Complex pass-band SC-FDMA signal
η	power efficiency

$\phi(t)$	Phase of $x(t)$
α	roll-off factor
v_{sat}	Saturation voltage of power amplifier
p	Smoothing factor
P_{avg}	Average power

2.2. Overview of SC-FDMA System

Fig. 2.1 presents the block diagram of an SC-FDMA system [19]. SC-FDMA can be treated as a DFT precoded OFDMA, as the DFT block before OFDMA modulation transforms the time domain symbols to frequency domain symbols. As each user occupies distinct subcarriers in the frequency domain, the users are orthogonal to each other, similar to OFDMA. As the overall transmit signal has lower signal envelope fluctuations with single carrier nature, PAPR is naturally low when compared to OFDMA.

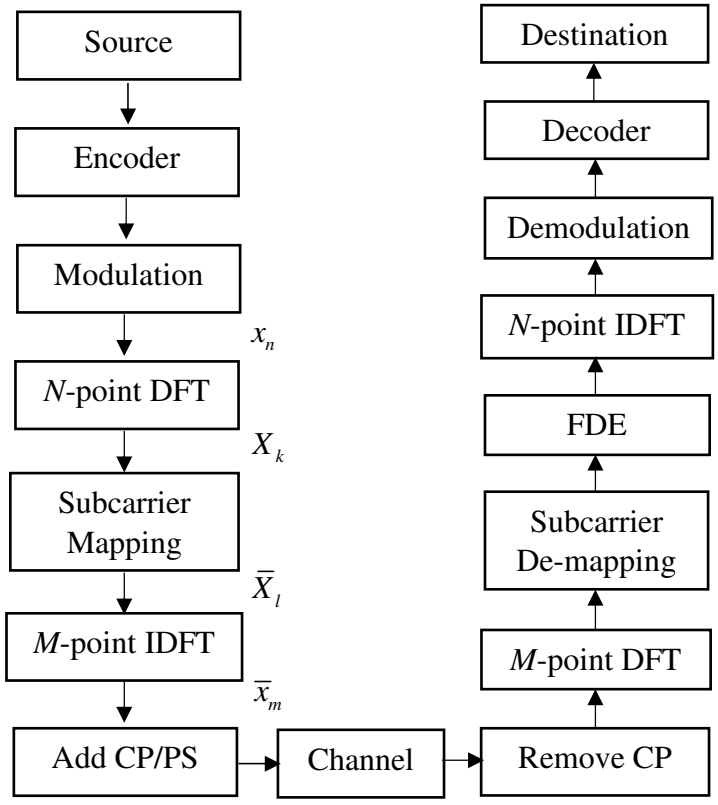

Fig.2.1. Block diagram of SC-FDMA system.

At the input to the transmitter, the encoded input is modulated by using one of the available modulation techniques, such as QPSK and QAM. These modulated symbols $\{x_n\}$ are then grouped into blocks, each comprising *N* symbols. Now an *N*-point DFT is carried out to generate a frequency domain representation X_k as given by [19]

$$X_k = \sum_{n=0}^{N-1} x_n e^{-j\frac{2\pi}{N}kn} \quad , k = 0,1,....,N-1 \tag{2.1}$$

These *N* symbols are now mapped to *M* subcarriers ($N < M$). $\bar{X}_l$ ($l = 0,1,2...,M-1$) is the result of the subcarrier mapping, where *N* of the amplitudes are non-zero. For subcarrier mapping in SC-FDMA systems, we have two techniques, namely Distributed FDMA (DFDMA) and Localized FDMA (LFDMA), as shown in Fig. 2.2. Interleaved FDMA (IFDMA) is one realization of DFDMA. In DFDMA, the subcarriers are spread across the entire bandwidth where unused subcarriers are occupied with zeros, whereas in LFDMA, each terminal transmits its symbols over consecutive subcarriers. In distributed mode, when the subcarriers are equidistantly occupied with $M = Q \times N$, then it is called IFDMA. Here *Q* is the bandwidth expansion factor. So the system can manage *Q* concurrent transmissions without co-channel interference. An example of subcarrier mapping with $N = 4$, $M = 12$ and $Q = 3$ is depicted in Fig. 2.3.

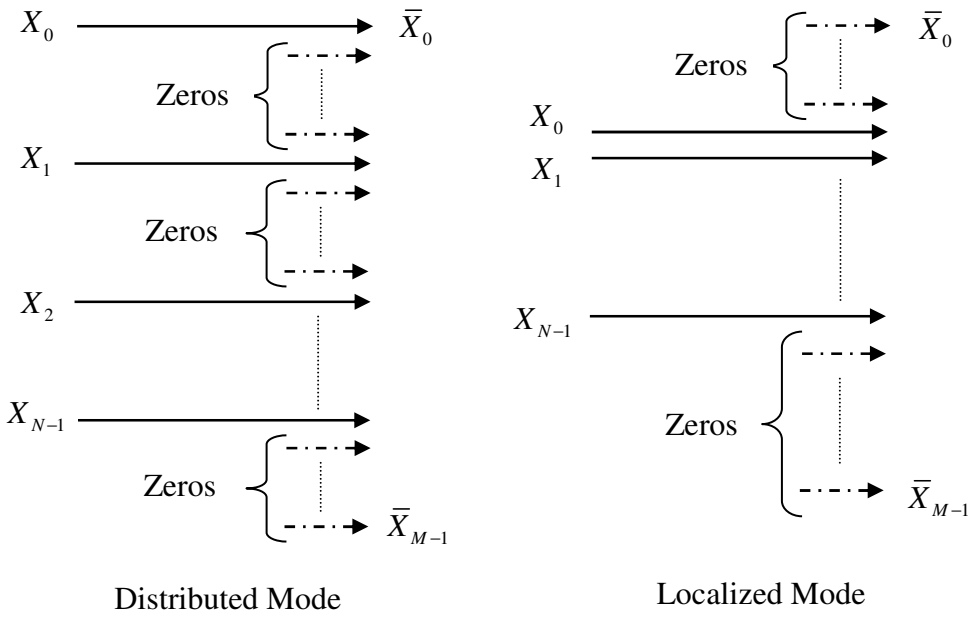

Fig.2.2. Subcarrier mapping modes; distributed and localized.

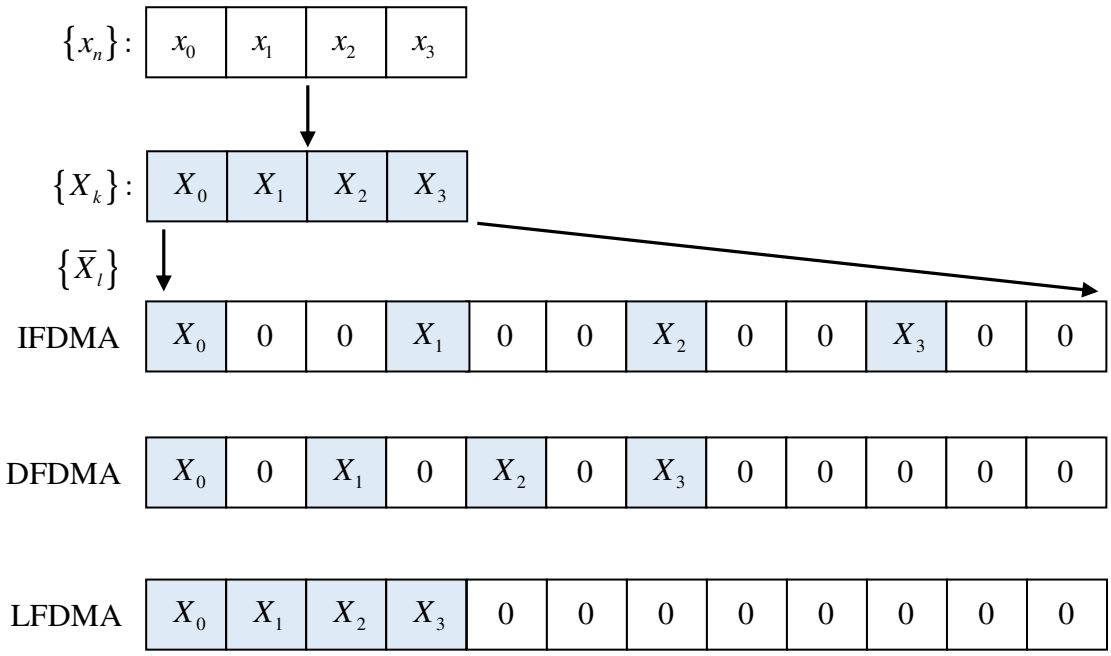

Fig.2.3. An example of subcarrier mapping with $N = 4$, $M = 12$ and $Q = 3$.

If localized subcarrier mapping is used then $\bar{X}_l$ is given by [19]

$$\bar{X}_l = \begin{cases} X_l, & (0 \le l \le N-1) \\ 0, & (N \le l \le M-1) \end{cases} \tag{2.2}$$

If interleaved subcarrier mapping is used then $\bar{X}_l$ is given by [19]

$$\bar{X}_l = \begin{cases} X_k(l/Q),\ l = Q.k & (0 \le k \le N-1) \\ 0 & otherwise \end{cases} \tag{2.3}$$

After subcarrier mapping, $\bar{X}_l$ are passed through M-point IDFT and the resulting time domain complex signal $\bar{x}_m$ is given by [19]

$$\bar{x}_m = \frac{1}{M}\sum_{l=0}^{M-1} \bar{X}_l e^{j\frac{2\pi}{M}ml}, \quad m = 0,....,M-1 \tag{2.4}$$

The transmitter appends a cyclic prefix (CP) to hinder the inter-block interference (IBI) caused by multiple paths. CP is a copy of the last part of the block, which is concatenated at the beginning of each block for two reasons. First, if CP's length is more than the channel's maximum delay spread or the channel impulse response's length, then it acts as a guard time between consecutive blocks, thereby eliminating IBI. Second, CP transforms a discrete-time

linear convolution into a discrete-time circular convolution. Hence the data propagated through the channel can be represented as a circular convolution between the transmitted data block and the channel impulse response, which is a point-wise multiplication of DFT samples in the frequency domain. Later, to eliminate the channel distortion, the DFT of the received signal can be divided point-wise by the DFT of the channel impulse response, or a more advanced frequency domain equalization (FDE) method can be applied.

The transmitter also performs a linear filtering operation named pulse shaping to decrease out-of-band radiation. Raised-cosine filter is one of the most used pulse shaping filter whose time domain and frequency domain representations are given by [19]

$$p(t) = \frac{\sin(\pi t / T)}{\pi t / T} \times \frac{\cos(\pi \alpha t / T)}{1 - 4\alpha^2 t^2 / T^2} \tag{2.5}$$

$$P(f) = \begin{cases} T & ,0 \le |f| \le \dfrac{1-\alpha}{2T} \\ \dfrac{T}{2}\left\{1 + \cos\left[\dfrac{\pi T}{\alpha}\left(|f| - \dfrac{1-\alpha}{2T}\right)\right]\right\} & ,\dfrac{1-\alpha}{2T} \le |f| \le \dfrac{1+\alpha}{2T} \\ 0 & ,|f| \ge \dfrac{1+\alpha}{2T} \end{cases} \tag{2.6}$$

where T represents the symbol period, and α represents the roll-off factor which lies between 0 and 1.

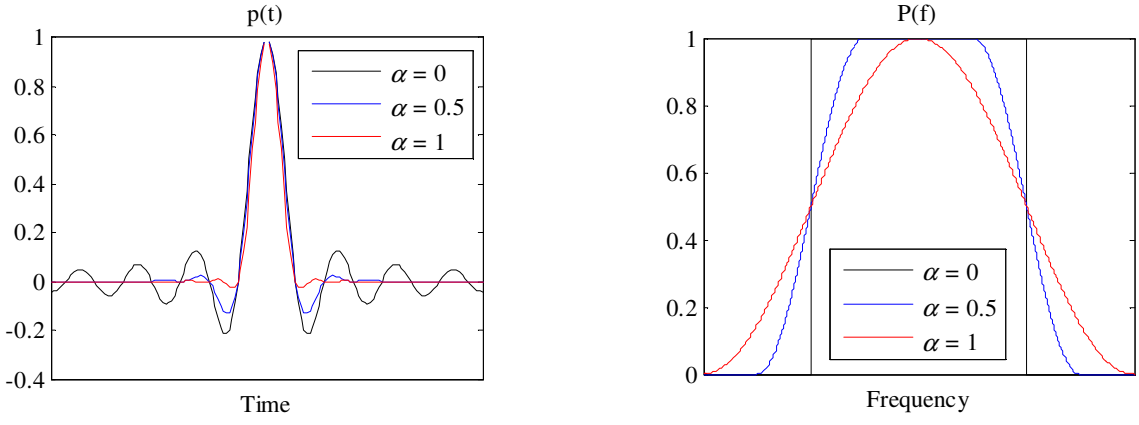

Fig.2.4. Raised-cosine filter.

Fig. 2.4 presents the graphical representation of raised-cosine filter in the time domain and frequency domain. When α is close to 0, the pulse has higher side lobes in the time domain,

thus increasing the peak power of the transmitted signal. On the other hand, when $\alpha = 0$ there is no out-of-band radiation and increasing α, increases the out-of-band radiation.

At the receiver side, the received signal is transformed into the frequency domain by using DFT, then subcarriers are de-mapped, and FDE is performed to reduce inter-symbol interference (ISI). Now IDFT transforms the equalized symbols back to the time domain, and demodulation and decoding operations are performed to detect the transmitted data.

2.3. Introduction to PAPR

Let $x(t)$ represent the complex pass-band transmit signal of SC-FDMA as [19]

$$x(t) = e^{jw_c t} \sum_{m=0}^{M-1} \overline{x}_m \, p(t - mT) \tag{2.7}$$

where $p(t)$ is pulse shaping filter, w_c is the carrier frequency of the system, and T is the symbol duration of the transmitted symbol $\overline{x}_m$. PAPR of this continuous-time baseband signal can be expressed as the ratio of maximum instantaneous signal power to the average signal power as [19]

$$\text{PAPR}_{x(t)} = \frac{\max_{0 \le t \le T} \left| x(t) \right|^2}{E\left[\left| x(t) \right|^2 \right]} \tag{2.8}$$

where $E[.]$ is the expectation operator. In general, PAPR of the oversampled discrete-time domain signal gives a precise estimate of the PAPR of the continuous-time domain signal if the oversampling factor is ≥ 4. For the discrete-time signal $x(n)$, PAPR is defined as [19]

$$\text{PAPR}_{x(n)} = \frac{\max_{n=0,1,2,\ldots,N-1} \left| x(n) \right|^2}{\frac{1}{N} \sum_{n=0}^{N-1} \left| x(n) \right|^2} \tag{2.9}$$

PAPR is a performance measure that designates the power efficiency of the transmitter. Transmit power efficiency and PAPR [dB] are theoretically related to each other as [19], [20]:

$$\eta = \eta_{\max} 10^{-PAPR/20} \tag{2.10}$$

where η_{max} is the maximum power efficiency and η is the power efficiency. For class A power amplifier, η_{max} is 50% and for class B, η_{max} is 78.5% [21]. From Fig. 2.5 it is apparent that high PAPR worsens the performance of transmit power efficiency.

In practice, the empirical Complementary Cumulative Distribution Function (CCDF) is used to evaluate the PAPR. PAPR reducing capacity is measured by the amount of CCDF reduction obtained. CCDF indicates the probability that PAPR is greater than a specific PAPR threshold $PAPR_0$ ($Pr\{PAPR>PAPR_0\}$).

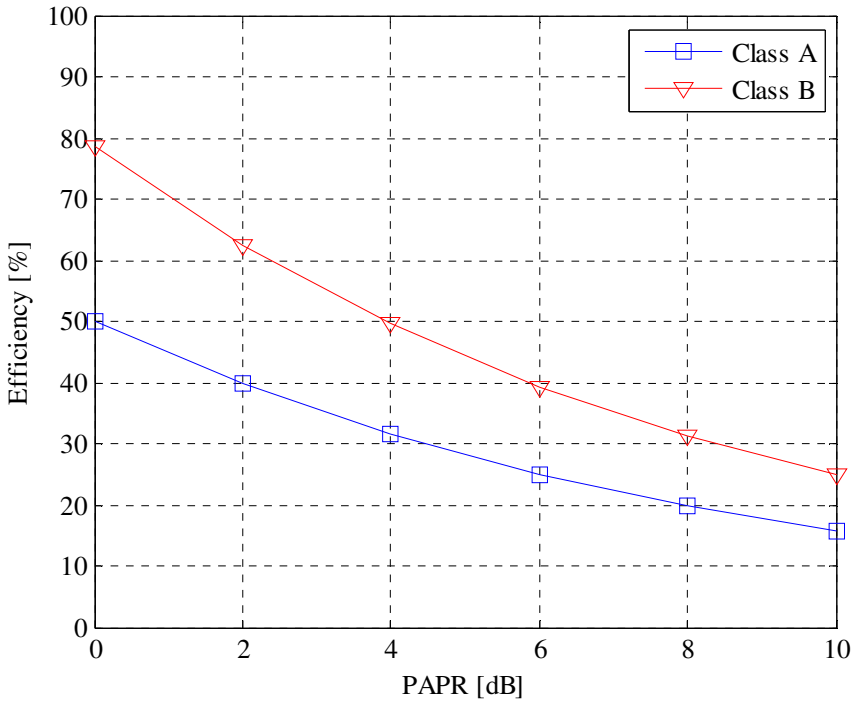

Fig.2.5. Relationship between transmit power efficiency and PAPR.

2.4. Nonlinearity and Power Amplifier Models

The Power Amplifier (PA) is one of the essential components of wireless mobile communications. It compensates for the attenuation induced by free-space propagation. But, it is an analog component and is naturally Non-Linear (NL) as the amplifier circuits are composed of active elements like transistors, which are NL in nature.

In general, PA modelling is sophisticated, but a general method is to model them as memoryless nonlinearities with a frequency-nonselective response [22]. Let the input of the power amplifier be

$$\tilde{x}(t) = \left|\tilde{x}(t)\right| e^{j\phi(t)} \tag{2.11}$$

where $\phi(t)$ and $\left|\tilde{x}(t)\right|$ are the phase and amplitude of the input signal, respectively, then the output of PA is given by [22]

$$y(t) = G\left[\left|\tilde{x}(t)\right|\right] e^{j\left\{\phi(t)+\Phi\left[\left|\tilde{x}(t)\right|\right]\right\}} \tag{2.12}$$

where $\Phi[.]$ and $G[.]$ are amplitude/phase (AM/PM) and amplitude/amplitude (AM/AM) conversions, respectively. $G[.]$ describes the impact of nonlinearity on the amplitude $\left|\tilde{x}(t)\right|$, and $\Phi[.]$ describes the impact of nonlinearity on the phase $\phi(t)$.

Solid state power amplifier (SSPA) model is the most commonly used PA model which is given by [22]

$$G\left[\left|\tilde{x}(t)\right|\right] = \frac{\left|\tilde{x}(t)\right|}{\left[1+\left(\frac{\left|\tilde{x}(t)\right|}{v_{sat}}\right)^{2p}\right]^{1/2p}} \tag{2.13}$$

$$\Phi\left(\left|\tilde{x}(t)\right|\right) = 0 \tag{2.14}$$

where v_{sat} is the saturation level of PA and p is a parameter that controls the smoothness of transition from linear region to saturation region. From Fig. 2.6, with $v_{sat} = 1$, it can be observed as p increases, the SSPA model approaches that of a soft-limiter.

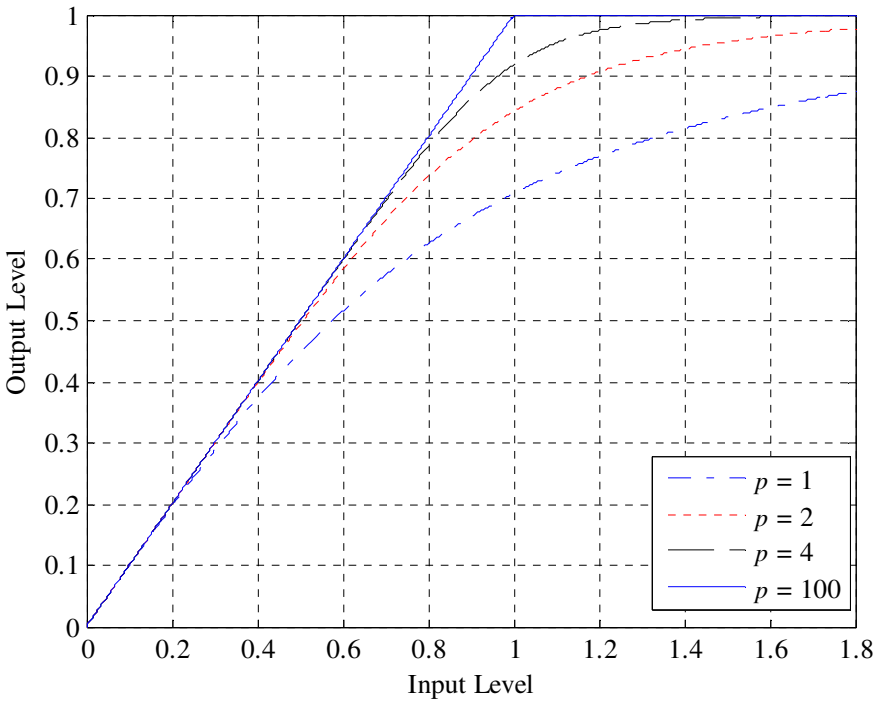

Fig.2.6. AM/AM characteristics of SSPA for different values of *p*.

The most effective operating point for a power amplifier is at the saturation level. Nevertheless, high peaks encountered in SC-FDMA signals can drive the power amplifier into saturation. Hence, input backoff (IBO) is needed to shift the operating point to the left, as depicted in Fig. 2.7. The IBO is defined as the ratio of saturation power of the power amplifier to the average power of the input signal, as given by [22]

$$\text{IBO} = 10\log_{10}\left[\frac{P_{sat}}{P_{avg}}\right] = 10\log_{10}\left[\frac{v_{sat}^2}{E\left[\left|\tilde{x}(t)\right|^2\right]}\right] \tag{2.15}$$

where P_{avg} and P_{sat} are average and saturation powers, respectively. To assure that the amplified peaks do not exceed the saturation level, IBO should be at least equal to PAPR. But, this drives the power amplifier to operate at reduced efficiency.

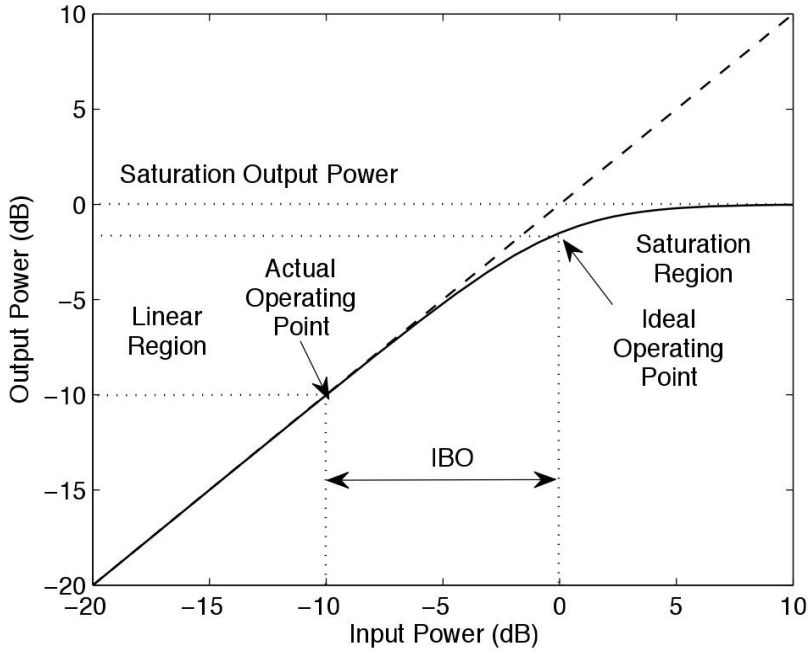

Fig.2.7. Typical output power vs input power characteristics curve.

2.5. Overview of Traditional PAPR Reduction Methods

Numerous approaches exist in the literature to reduce the PAPR of an OFDM system. These methods can be mainly divided into three types: signal distortion, coding, and multiple signaling and probabilistic techniques, as illustrated in Fig. 2.8 [22]–[24].

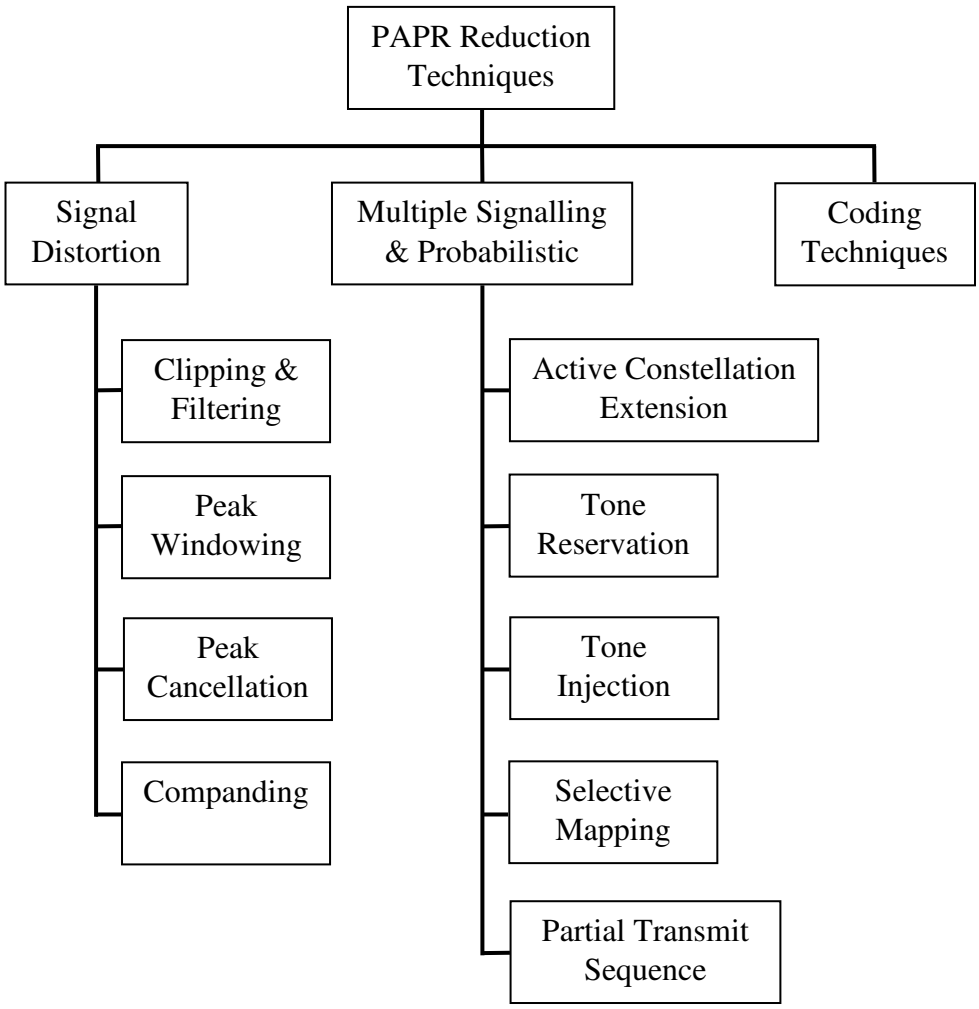

Fig.2.8. Classification of PAPR reduction techniques.

These techniques reduce the PAPR by either clipping, distorting, or adding additional side information to the signal. But, PAPR reduction may result in degradation of the BER performance, due to the change in the nature of a QAM modulated signal, which is already at the highest efficiency achievable (in terms of Euclidean distance between bits). Adding additional side-information reduces the capacity and results in additional energy being added to the signal, thereby degrading the efficiency of the system.

Therefore PAPR reduction techniques may increase BER of the system and might add complexity and cost required for additional signal processing operations. Consequently, the actual advantages of PAPR reduction techniques are found in the systems that can reduce PAPR without a significant effect on BER performance and avoids additional system

complexity. Hence there is a trade-off among PAPR reduction, BER degradation, and system complexity.

2.5.1. Clipping & Filtering

Clipping is the simplest signal distortion based PAPR reduction method. In this technique, the signal peaks of $x(t)$ are clipped when the peak values exceed a specific threshold, α_0 as described by [25]

$$x_c(t) = \begin{cases} x(t), & |x(t)| \le \alpha_0 \\ \alpha_0 e^{j\phi(t)}, & |x(t)| > \alpha_0 \end{cases} \tag{2.16}$$

where $\phi(t)$ is the phase of $x(t)$. This is a straightforward PAPR reduction method, as no side information is necessary to transmit to the receiver. However, clipping causes both in-band and out-of-band distortions [25]. Therefore it is essential to filter the clipped signal to reduce out-of-band distortions. But filtering cannot reduce in-band distortions, which causes BER degradation [26]. Nevertheless, oversampling can decrease the effect of in-band distortions as some part of the noise is reshaped out of the signal band, which can be eliminated by filtering operation [27]. Filtering the clipped signal can maintain spectral efficiency by removing the out-of-band radiations, thereby improving the BER performance. However, it can lead to peak power regrowth. Various iterative clipping and filtering [7], [28]–[30] techniques have been proposed to minimize the overall peak power regrowth.

2.5.2. Peak Windowing

Peak windowing reduces higher peaks by multiplying them with a weighting function known as window function [31], [32], in contrast to peak clipping, where the peaks that exceed a predefined threshold are hard-limited. Various window functions with good spectral properties can be used in this process. Hanning, Hamming, and Kaiser windows are the most usually used window functions. To diminish PAPR, a window function is aligned with the signal samples in such a fashion that its higher amplitudes are multiplied by lower amplitude signal samples, and its lower amplitudes are multiplied by the signal peaks. Hence, the signal peaks are attenuated more smoothly in contrast to the hard clipping, thereby causing reduced distortion.

2.5.3. Peak Cancellation

In this method, a peak cancellation waveform is adequately generated, scaled, shifted, and subtracted from the OFDM signal at the segments which exhibit higher peaks. The generated waveform is band limited to specific peak cancellation tones that are not used for transmission [33], [34]. In the OFDM transmitter after the IFFT block, a peak detector is used to detect the peaks higher than a specific threshold. Then a peak cancellation waveform is generated and subtracted from the OFDM signal. Peak cancellation process should be performed carefully so that new peaks are not generated.

2.5.4. Companding

Companding techniques are normally used to optimize the required number of bits per sample in speech signals. As speech signals and OFDM signals have a similar structure i.e., high peaks occur occasionally, the same companding techniques can be employed to decrease the PAPR of OFDM signal [35], [36]. Companding transforms have comparatively low computational complexity in comparison to other PAPR reduction methods, and their complexity is not influenced by the number of subcarriers. Moreover, they do not require the transmission of side information and, therefore, doesn't decrease the bit rate. Due to their implementation simplicity and the benefits they provide, companding techniques become an attractive PAPR reduction method. However, the PAPR reduction achieved by companding techniques comes with the cost of an increase in BER.

The application of the μ-law companding to decrease PAPR is investigated in [8], [37], [38]. μ-law companding enhances the lower amplitudes while maintaining the high peaks of the signal. Hence the peak power is unaltered, and average power is increased, thereby reducing the PAPR. To accommodate this increase in average power, the gain of power amplifier should be adjusted dynamically, which increases the hardware cost. The authors in [8] investigated the impact of companding on the OFDM system's BER performance in the presence of AWGN channel and demonstrated that a reasonable symbol error rate could be obtained by appropriately selecting the companding coefficients.

2.5.5. Coding Techniques

The coding techniques that offer error detection and correction can be modified to perform PAPR reduction with a tolerable extra complexity. One of the well-known methods for

decreasing PAPR is Block coding [39]. In this method, input data is encoded to a codeword where some bits are dedicated to decreasing PAPR instead of enhancing BER. For instance, to decrease the PAPR of a signal with 4 subcarriers, 3-bit input data can be mapped to a 4-bit codeword by adding a parity bit. By optimizing the position of the parity bit, PAPR can be reduced further. Moreover, by dividing the lengthy information sequences into sub-blocks and by employing different coding techniques to encode each sub-block [40], PAPR can be reduced by optimizing their combination. But the information on the coding techniques used and the location of parity bits should be transmitted to the receiver as side information.

Golay complementary sequences can also be employed as codewords, which can assure that OFDM signals with any number of sub-carriers have a PAPR of not more than 3 dB [41]. To reduce PAPR, a soft decision based Reed-Muller decoding algorithm is introduced in [42], and the construction of Golay complementary sequences with 64QAM constellation is suggested in [43]. But using Golay sequences for systems with a large number of subcarriers can increase computational complexity and cause significant rate loss and due to redundancy and exhaustive search for good codes. Another limitation of coding techniques is that they are not downward compatible as the receiver needs to be modified with a decoding algorithm.

2.5.6. Active Constellation Extension (ACE)

The ACE technique for PAPR reduction in OFDM is well reported in [44]–[49]. It is an effective technique to decrease the PAPR without the need for side information transmission. The projection-onto-convex-sets (POCS) algorithm of the ACE technique clips the time domain signal and extends the outer constellation points out of the original constellation without decreasing the minimum Euclidean distance.

The fundamental principle of ACE techniques for PAPR reduction is described in Fig. 2.9. The constellation points may be extended into areas representing gray regions during the reconstruction phase after the time domain signal is clipped. PAPR can be reduced by extending the constellations into these regions at the cost of a small increment in average power. This increment degrades the system's BER performance. But this degradation is somewhat compensated by the fact that the gray regions result in an increase in the minimum Euclidean distance. So there is a fair trade-off between the PAPR reduction and BER

degradation [44]. Also, this method increases the average power of the transmitted signal and has a limitation when applied to modulation schemes with larger constellation sizes [24].

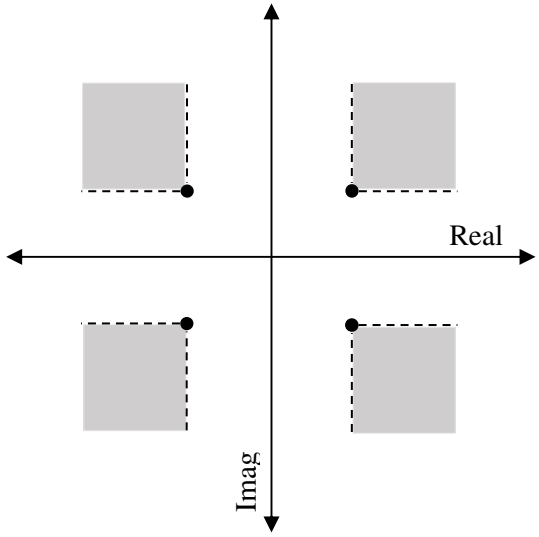

Fig.2.9. Constellation map describing the allowable extension region for ACE considering QPSK modulation.

In [50], an adjustable circle constraint (ACC) method is proposed, which offers the advantages of the ACE technique without iterative computations. This is achieved by setting a circular constraint with various circle centres and radius around the original constellation points. ACC doesn't need additional devices in the receiver and requires much less computation time when compared to ACE.

2.5.7. Tone Reservation (TR)

TR is a method that uses reserved subcarriers to decrease the PAPR of a signal [51]–[56]. Similar to the ACE technique, pre-transmission clipping, and constellation reconstruction are used to reduce the PAPR of a time-domain signal. Nevertheless, the main difference is in the utilization of reserved tones in place of distorted constellations. In this method, a time-domain vector x is added to the OFDM signal to modify its statistical distribution that helps in reducing PAPR. The tricky thing now is to determine x that reduces the maximum peak value of the new OFDM signal. The amount of PAPR reduction in this method depends on the number of reserved subcarriers, their locations, and the optimization complexity. The locations of these reserved subcarriers should be transmitted as side information to the receiver. If the number of subcarriers is small in OFDM systems, these reserved subcarriers

might decrease the data rate. Standard TR has the disadvantage of a slow convergence time as that of POCS ACE [51]. Gradient projection method is suggested to be used in [51] similar to that of Smart Gradient Projection (SGP) ACE to converge quickly.

2.5.8. Tone Injection (TI)

Tellado has introduced TI to overcome the data rate loss problem in TR [57]–[60]. The central idea is to expand the constellation size so that each point in the original constellation is mapped onto various other points in the expanded constellation before IDFT processing. Considering a square QAM constellation with size M and spacing of d between the original points, the minimum distance between each point in the original constellation and its equivalent points in the expanded constellation should be $D = d\sqrt{M}$ [22] to maintain the BER performance.

TI doesn't require any side information transmission, and so there is no loss of bit rate. Despite its benefits, TI increases the complexity of the transmitter. Also, it increases average signal power due to the expansion of the signal constellation. TI offers two degrees of freedom, one being the selection of tones and other being the expanded constellation's size. Discovering the right possible combination requires high complexity.

2.5.9. Selective Mapping (SLM)

SLM is a simple method where L different OFDM signals are generated, which represent the original data, and the signal with the least PAPR is transmitted [10], [61]–[65]. This is accomplished by generating a set of L distinct phase rotated vectors and multiplying them with the original subcarriers, as depicted in Fig. 2.10. This method utilizes the independence of various phase rotated subcarriers and hence ensuring time-domain signals with distinct PAPR values [10].

To decrease the complexity, phase rotation vectors are usually considered as multiples of $\pi/2$. The amount of reduction in PAPR depends on the number of phase sequences generated and their design. The complexity increases due to the need for L modulators to generate L different time-domain signals. Another disadvantage is the requirement of side information of $\lfloor \log_2 L \rfloor$ bits to inform the receiver which sequence was selected for transmission. As this side information is crucial for accurate demodulation, it requires an

additional level of coding, to protect it from corruption. SLM technique, which doesn't require side information, is proposed in [61]. But, this method comes with the price of additional complexity in the form of scramblers with a little redundancy introduced.

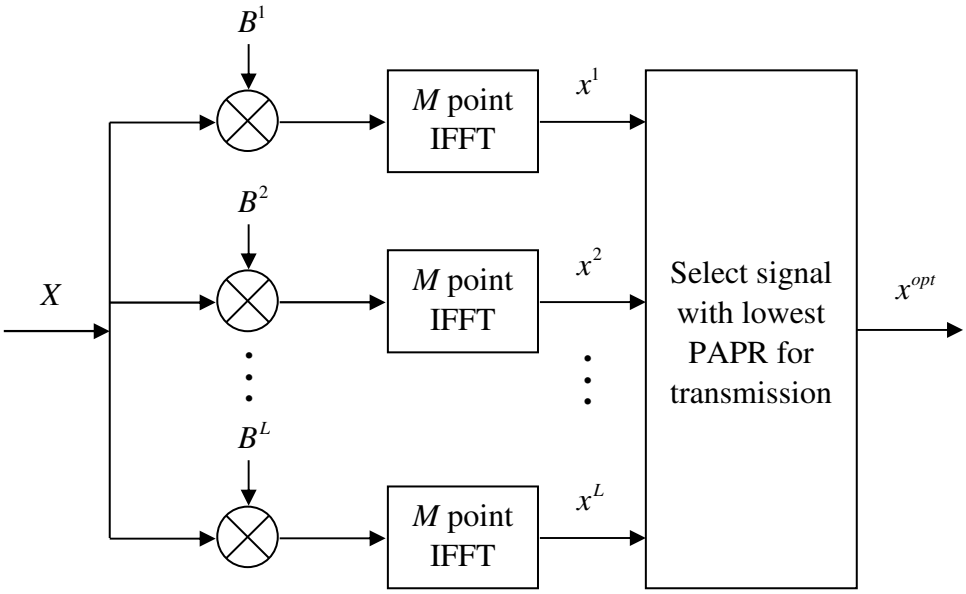

Fig.2.10. SLM technique for OFDM.

If side information is protected by channel coding, no side information is required. At the receiver side, L decoders process the received signal using L possible phase rotated vectors to recover the data [10]. But often, there are space limitations at the receiver side, particularly in the case of mobile devices.

2.5.10. Partial Transmit Sequence (PTS)

In the PTS technique, the input data block is partitioned into N disjoint frames. Then all the frames are weighted by different optimal phase factors and added so that the combined signal has a lower PAPR [66]–[69], as shown in Fig. 2.11. The complexity of the PTS technique is high, as the selection of the optimal phase rotation factor requires an exhaustive search. Also, PTS requires additional N-1 IDFT blocks and side information transmission to demodulate the data-carrying subcarriers perfectly.

PAPR reduction capability can be improved by increasing the number of possible phase rotation factors *W* and the number of disjointed frames *N*. But the complexity of the search algorithm grows exponentially with *N* [24]. So, the complexity is of the form $O\left(W^N\right)$ and to overcome the search complexity, techniques commonly employ only 2 $\{\pm 1\}$ or 4 $\{\pm 1, \pm j\}$ possible rotation factors and restrict the number of disjoint frames to 4. Several techniques are proposed to decrease the computational complexity of the PTS scheme. In [66], a threshold is used to avoid undesirable search, once the required PAPR performance is attained. In [67] a smart search algorithm is employed to decrease the complexity of the search algorithm for optimal phase factors.

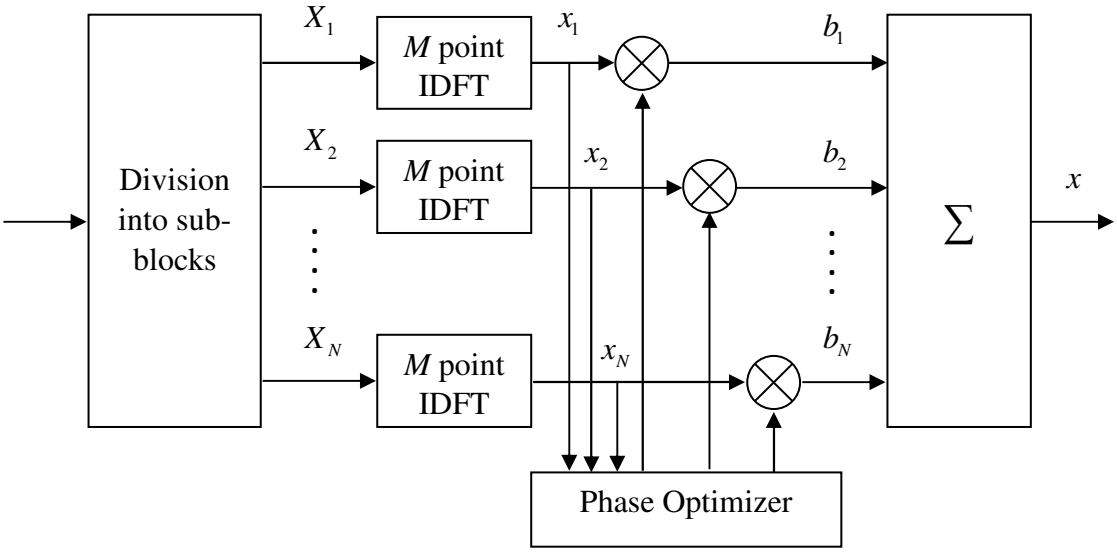

Fig.2.11. PTS technique for OFDM.

2.6. Literature Survey

Many schemes have been adopted to limit PAPR in SC-FDMA systems. But most of the techniques either increase the complexity associated with the additional signal processing elements or require side information to be transmitted. The increased complexity and processing power required, often makes these techniques infeasible for real life applications. The techniques listed here are the most noticeable techniques to decrease PAPR in SC-FDMA systems.

In [3], authors compared PAPR of SC-FDMA signals with OFDMA signals. The results indicate that SC-FDMA signals have lesser PAPR than OFDMA and interleaved

FDMA has lesser PAPR than localized FDMA. Also, the use of pulse shaping filter increases the PAPR and roll-off factor has a notable impact on the performance of PAPR. Hence pulse shaping filter must be designed properly to limit PAPR without demeaning system performance.

In [70], authors presented sinusoidal transforms as a possible alternative to DFT in OFDM. This enabled authors in [17] to propose an SC-FDMA system based on DCT Type-II. DCT's energy compaction property enables it to pack maximum signal energy into first few samples, reducing inter-symbol interference due to relatively small amplitudes at high frequency indices. This results in a lower bit error rate when compared to DFT. Also, it uses only real arithmetic operations instead of complex arithmetic operations used in DFT. Results indicate that DCT SC-FDMA has improved BER but has slightly high PAPR when compared to DFT SC-FDMA.

In [14], μ-law companding scheme is employed to mitigate the PAPR in SC-FDMA systems. Results indicate that SC-FDMA system with μ-law companding scheme has a reduced PAPR than the original SC-FDMA system. Results also reveal that PAPR and BER performances depend on the companding coefficient, which must be selected carefully. But μ-law companding increases the average power and hence improvement in BER is due to this increase in average power but not due to companding.

In [71], a new transceiver scheme where wavelet transform is used after SC-FDMA modulator is proposed. Authors also suggested a hybrid clipping and companding method to mitigate PAPR of the proposed transceiver, without degrading BER performance. Haar and Daubechies wavelets have been used in this article. Results indicate that the proposed Hybrid Wavelet SC-FDMA system offers improved BER and PAPR performances than the original system by properly choosing the clipping and companding parameters. But complexity is slightly increased as compared to the conventional SC-FDMA scheme.

In [16], [72] raised cosine-like companding scheme is employed for PAPR mitigation of SC-FDMA signals. PAPR reduction performance depends on the variable parameter-α. Simulation results demonstrate that it does not increase the average power in the companding operation. But the authors did not discuss the effect of companding on BER performance.

In [73], authors proposed a time-domain partial transmit sequence (PTS) scheme without side information (SI) for SC-FDMA system, where pilots are used to recover the

phase rotation during channel estimation. The proposed scheme has lower complexity and provides similar BER and channel estimation performance when compared to PTS with perfect SI. Hence, the proposed technique offers improved bandwidth and power efficiency. But, time-domain PTS provides a trade-off between PAPR reduction performance and complexity as complexity increases with the number of partitioned sub-blocks.

In [15], a power-function companding technique that transforms the SC-FDMA signals into power-function distributed signals is proposed to mitigate PAPR of SC-FDMA signals. The proposed companding maintains constant average power and reduces PAPR when control parameters are chosen properly. But the authors did not discuss the effect of companding on BER performance.

Precoding technique works by finding the codewords that mitigate PAPR. But, the construction of the codewords require an exhaustive search and huge lookup tables to perform encoding and decoding. In [74], authors first formulated the problem of reducing PAPR by precoding as a combinatorial problem, and then proposed a semi definite relaxation approach which can solve the problem in polynomial time. Proposed scheme reduces the peak power with lesser complexity but increases the transmit power. Hence there is a trade-off amongst the transmit power increase and reduction of peak power.

Falconer [75], suggested to minimize the variance of instantaneous power of a linearly block coded OFDMA signal, instead of the conventional method of PAPR minimization. Beginning with a random precoding matrix, an optimization process is used to reduce the variance of instantaneous power. Irrespective of the starting point, the optimization process always converged to the same solution. The precoder solution found is a small variation to DFT precoder that is being used in LTE standard. But this optimum precoder provides only 1 dB gain over the original SC-FDMA system.

Slimane [76], studied raised-cosine (RC) and square-root raised-cosine (SRRC) window functions. For a given excess bandwidth, numerical results show that SRRC window is preferable than RC window. On the other hand, RC window has smoother edges when compared to SRRC window and hence causes smaller time-domain side-lobes.

Authors in [77], suggested direct optimization of window vector rather than optimizing precoder matrix. They formulated the problem in the form of Lagrange multipliers and analysed its second-order conditions to verify that the optimal window is a strict local

minimizer. They analysed and compensated the noise enhancement drawback of the optimized precoder and confirmed that the optimized precoder indeed has best performance than the precoder with SRRC window.

The time-domain selective mapping technique (TD-SLM) in [12] provides a good PAPR mitigation in localized SC-FDMA systems. However, it causes a minor BER deprivation. The amount of PAPR reduction depends on the number of phases, irrespective of their values. TD-SLM provides a PAPR reduction of about 3.5dB but at the cost of increased computational complexity. So there is a trade-off amongst complexity, cost, and PAPR reduction.

In [18], a novel transceiver design for SC-FDMA system based on discrete wavelet transform (DWT) is proposed. The authors also suggested Walsh Hadamard transform (WHT) as linear precoding technique to enhance the PAPR performance. Simulated results demonstrate that the proposed transceiver has superior BER and PAPR performances when compared to standard DFT based SC-FDMA transceiver.

Authors proposed parametric linear combination of pulses in [78] and α-β pulse shaping filter in [79] to mitigate PAPR in SC-FDMA system. By introducing additional design parameters μ, and β respectively, the proposed pulse shaping filters have the advantage of more flexibility for a certain roll-off factor, α. The proposed filters perform better when compared to the existing filters like raised cosine filter and has simpler impulse response. But PAPR improvement is not more than 1 dB and the impact on BER performance is not discussed.

In [80], authors calculated the PAPR of each SC-FDMA symbol and compared it with a predefined threshold, *A*. If PAPR is greater than *A,* then the modulated symbol causing peaks of the output signal samples to exceed the threshold is modified to an inner constellation by deliberately introducing few bit errors. Channel decoding is used to reduce the effect of deliberately corrupted bits on the BER performance. Proposed scheme reduces the PAPR effectively with nearly similar BER performance as that of original SC-FDMA signals only for SNR values < 35 dB.

In [81], authors proposed the use of discrete cosine/sine transforms as an alternative to DFT for SC-FDMA systems. SC-FDMA systems based on 4 types of DST and 4 types of DCT are studied. The PAPR and BER performances of these 8 DCT/DST based SC-FDMA

systems are compared with the standard DFT-based SC-FDMA system. DCT/DST-based SC-FDMA systems employing interleaved mapping, offer similar BER performance but high PAPR when compared to DFT based system. On the other hand when localized mapping is used, DCT/DST-based SC-FDMA systems offer superior BER and similar PAPR when compared to DFT based system.

In [82], authors proposed a piece-wise linear pulse shaping filter to mitigate PAPR in interleaved SC-FDMA systems. Simulation results indicate that the proposed filter has lower computational complexity, improved PAPR and SER performances when compared to the raised cosine filter but focuses only on interleaved SC-FDMA.

In [83], authors proposed a new transceiver using the DWT and a hybrid clipping and companding technique for PAPR mitigation in both DFT and DCT based SC-FDMA systems. The results indicate that the proposed wavelet based transceiver for the DFT and DCT based systems offer better BER and PAPR performances than the original DFT SC-FDMA system. There is a trade-off between the BER and PAPR performances, as the number of decomposition levels increase, the BER performance improves and PAPR performance degrades.

In [84], authors modified the modulated symbols which cause the peak of SC-FDMA signal by introducing an additive pre-distortion vector. By cautiously designing the pre-distortion vector, the proposed technique can diminish the PAPR without significant degradation in BER.

In [85], authors proposed a novel probabilistic pulse shaping technique with no excess bandwidth to mitigate PAPR of SC-FDMA signals. A set of weighting windows with zero excess bandwidth is used to generate different candidate signal blocks with a low-complexity scheme, and the block with lowest PAPR is chosen for transmission. The received data can be detected by combining the applied weighting window into the defined equivalent channel without side information. The proposed technique achieves decent advancements over the original system in terms of BER and PAPR performances, with little additional complexity at the transmitter.

In [86], PAPR is reduced by deliberately distorting the amplitudes of the complex modulated symbols which cause peaks to cross a predetermined threshold similar to [80]. The location of distorted symbols are marked by the use of a pilot block without the need of side

information. The distorted amplitudes are recovered at the receiver by using these marked location indices. Simulation results show that the proposed method reduces the PAPR effectively with a slight degradation in BER performance.

Selected mapping (SLM) reduces PAPR but requires side information (SI) transmission and increases the system complexity. SI embedding and detection technique is presented in [87] for SLM based SC-FDMA systems, by utilizing the block pilot symbols. The representation of SI index for each data symbol by a location set of few selected subcarriers in the block pilot symbol avoids SI transmission. An optimal pilot-aided maximum-likelihood and a suboptimal log-likelihood ratio SI detectors are introduced for SI detection.

In [88], product-coded modulation and SLM are employed to mitigate PAPR in SC-FDMA system without the need for transmission of side information. The proposed method uses phase-factor generating mechanism to lower the complexity needed to search the optimal phase factors.

In [89], conventional SLM technique is used to mitigate PAPR of localized SC-FDMA signals by considering an experimental setup in Non-line-of-sight (NLOS) outdoor environment. Simulation results present that the SLM technique provides a PAPR reduction gain of 3.78 dB over localized OFDMA system and reasonable BER with and without high power amplifier when compared to Localized SC-FDMA.

A hybrid filter is proposed in [90] to mitigate PAPR in interleaved SC-FDMA system. The suggested filter is designed based on a finite impulse response filter and Nyquist-I pulse. Authors proposed a new family of Nyquist-I pulses called exponential linear pulse with an extra design parameter to mitigate PAPR for a given roll-off factor. Simulation results indicate that the suggested filter has superior performance over existing filters in terms of complexity, SER and PAPR.

In [91], authors proposed a novel trellis shaping (TS) design to reduce peak power of SC-FDMA signals. Due to the circularly periodic structure of SC-FDMA signal, direct application of TS employed for reducing peak power of single carrier signals will cause high peaks at the edges. So authors introduced a modification in TS, such that the symbols located at one edge can control the symbols at the other edge. SC-FDMA with TS outperforms SC-FDMA without TS due to the reduction of average power and PAPR.

In [92], authors proposed to divide a 16-QAM product code into two sub-blocks, one for error correction using encoding, and the other to generate PAPR reduction signals. PAPR reduction signals have been generated by using constellation extension technique as it does not cause any data loss. Simulation results exhibit that the proposed technique outperforms original SC-FDMA signals in terms of PAPR and error correction due to the use of product codes.

In [93], authors used conventional raised cosine and square root raised cosine filters with the absolute exponential companding to reduce PAPR in DCT SCFDMA system. The proposed method achieves significant improvement in PAPR reduction capability over the conventional pulse shaping schemes when used alone in DCT-SCFDMA system. But the impact on BER performance is not discussed.

Authors in [94] suggested the use of tone injection (TI) to enhance the low data transmission rate problem of tone reservation (TR) scheme, caused due to the reserved subcarriers. As the combination of TI and TR techniques require high computational complexity, an iterative flipping algorithm was proposed. Proposed method effectively mitigates the PAPR of the SC-FDMA system and improves the rate of data transmission of the standard TR scheme.

In [95], a Blind Selective Mapping (B-SLM) method which require no side information transmission is introduced to limit the PAPR in SC-FDMA system. PAPR of B-SLM method is nearly identical as that of the conventional SLM method. Also, the proposed method reduces the bandwidth requirement without significant BER degradation.

In [96], a hyperbolic tangent companding is used with standard pulse shaping techniques to mitigate PAPR in DCT-SCFDMA signals. Proposed method offers significant improvements in PAPR reduction and BER over the conventional pulse shaping techniques when used alone in DCT-SCFDMA system.

In [97], authors studied the effect of two PAPR mitigation schemes (interleaver based and SLM) to mitigate the PAPR in SC-FDMA based Cognitive Radio. Then, a hybrid technique of interleaving and SLM to reduce the PAPR in SC-FDMA for Cognitive Radio Network is introduced with a slight increase in system's complexity.

2.7. Conclusion

It is clear from the literature review that PAPR reduction in SC-FDMA systems is well researched topic but is still in an infant stage. It can be observed that all the techniques offer decent PAPR reduction performance and the trade-off comes into play with complexity, BER degradation or data rate loss.

Chapter-3

Performance Analysis of Various Companding Techniques

3.1. Introduction

This chapter discusses various companding techniques to mitigate PAPR in SC-FDMA systems and compare their performance with the well-known μ-law companding technique and conventional SC-FDMA system. These companding techniques do not increase the average signal power. Also, these techniques do not require the transmission of side information and have low complexity.

3.2. Nonlinear Companding Transforms

Nonlinear companding transform is one of the most attractive techniques due to its excellent system performance, including PAPR reduction and BER, the simplicity of implementation, without restriction on the type of constellation, the number of subcarriers, and any bandwidth expansion. Companding is a composite word formed by combining **com**pressing and exp**anding**.

μ-law companding is the first nonlinear companding transform, which is based on the speech processing algorithm μ-law, and it has better performance than that of the clipping technique [8]. μ-law mainly focuses on enlarging small signal amplitudes and keeping peak signals unchanged. Thus it increases the average power of the transmitted signals and probably results in exceeding the saturation region of HPA to make the system performance worse.

The nonlinear companding transform can be considered as a special case of clipping scheme. The differences between nonlinear companding transform and the clipping can be summarized as:

- Clipping scheme deliberately clips large signals when the amplitude of the original signals is greater than the given threshold. Hence the clipped signals cannot be recovered at the receiver. Nevertheless, nonlinear companding transforms compand original signals by using a strict monotone increasing function. Hence, the companded signals at the transmitter can be recovered appropriately through the corresponding inversion operation of the nonlinear transform function at the receiver.
- Nonlinear companding transforms compress the large signals while enlarging the small signals to improve the immunity of small signals from noise, whereas the clipping scheme does not change the small signals. Therefore, the clipping scheme suffers from three major problems: in-band distortion, out-of-band radiation, and peak regrowth after digital to analog conversion. As a result, the system performance degradation due to the clipping may not be promising. However, nonlinear companding transforms can operate well with excellent PAPR reduction while keeping good BER performance [98].

It is apparent that companding transform is an additional operation performed before transmitting the signal. Consequently companding schemes decrease PAPR at the cost of generating companding distortion. Hence, it is essential for the design of companding transform aiming at decreasing the impact of companding distortion on the BER performance.

Table 3.2. List of Symbols

Symbol	Description
x_n	Modulated symbols
N	Input block size
X_k	DFT of x_n
$\bar{X}_l$	Frequency-domain samples after the subcarriers mapping
M	Number of subcarriers
$\bar{x}_m$	IDFT of $\bar{X}_l$
t_m	Companded signal

$h(x)$	Companding function
r_m	Received signal
$\overline{r}_m$	Decompanded signal.
α	Attenuation factor
b_m	Companding noise
w_m	Channel noise.

3.3. SC-FDMA System Model with Companding Technique

SC-FDMA system with companding transform is illustrated in Fig. 3.1. Firstly the data is encoded and modulated by one of the possible modulation techniques (*M*-QAM or QPSK). Then the modulated symbols are grouped into *N* symbol blocks with each block having symbols $(x_n, n = 0,1,2,...,N-1)$. These *N* symbols are sent through an *N*-point DFT to convert them into frequency domain representation X_k as given by

$$X_k = \sum_{n=0}^{N-1} x_n e^{-j\frac{2\pi}{N}nk},\ k = 0,1,....,N-1 \tag{3.1}$$

These *N* symbols will be mapped into *M* subcarriers (*M*>*N*, *M*=*Q*×*N*) by using either localized or interleaved mapping. In localized mapping, the symbols are passed continuously over consecutive subcarriers and in interleaved mapping, the subcarriers are spread over entire bandwidth. With localized subcarrier mapping, the *M* point sequence $\overline{X}_l$ can be expressed as

$$\overline{X}_l = \begin{cases} X_k(l), & (0 \le l \le N-1) \\ 0, & (N \le l \le M-1) \end{cases} \tag{3.2}$$

Now $\overline{X}_l$ is transformed back to time domain signal $\overline{x}_m$ by using *M*-point IDFT as

$$\overline{x}_m = \frac{1}{M}\sum_{l=0}^{M-1} \overline{X}_l e^{j\frac{2\pi}{M}ml},\ m = 0,....,M-1 \tag{3.3}$$

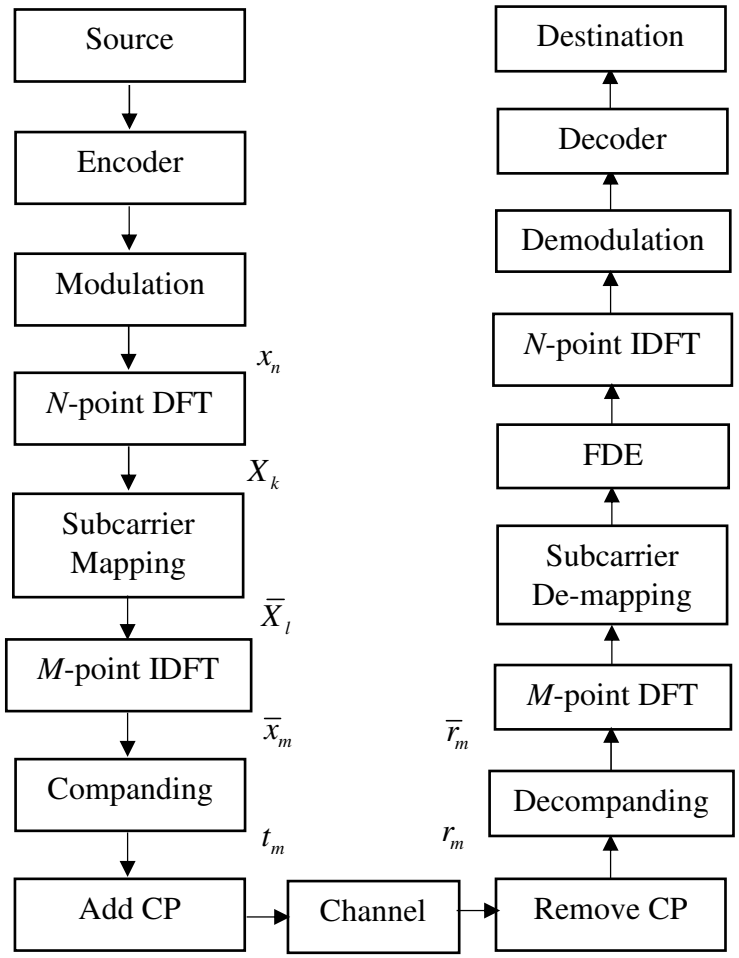

Fig. 3.1. SC-FDMA system with companding.

Now $\bar{x}_m$ is sent through compander $h(x)$ as described by

$$t_m = h(\bar{x}_m) \tag{3.4}$$

where $\bar{x}_m$ is the input signal and t_m is the companded signal. Now cyclic prefix (CP) is inserted before transmission of signal over the channel. After removing CP, r_m is sent through decompander $h^{-1}(x)$ to produce $\bar{r}_m$.

$$\bar{r}_m = h^{-1}(r_m) \tag{3.5}$$

where r_m is the CP removed signal, $\bar{r}_m$ is decompanded signal. Compander and Decompander are the only blocks that have been added additionally to the original system. The respective inverse operations will be implemented at the receiver side. Various companding techniques will be discussed in the subsequent sections.

3.3.1. Modified μ-law Companding (MMC)

In [14], the use of μ-law companding lessened PAPR in SC-FDMA systems. But it increases the average signal power. So we modify μ-law companding such that the average signal power is unaltered. The conventional μ-law companding is given by

$$h(x) = V_{\max} \frac{\ln\left[1+\frac{\mu|x|}{V_{\max}}\right]}{\ln[1+\mu]} \operatorname{sgn}(x) \tag{3.6}$$

where $V_{\max} = \max\left(|\bar{x}_m|\right)$, μ is companding coefficient and sgn indicates the sign function. In order to keep the average signal power unaltered, we modify it as

$$h(x) = A \times V_{\max} \frac{\ln\left[1+\frac{\mu|x|}{V_{\max}}\right]}{\ln[1+\mu]} \operatorname{sgn}(x) \tag{3.7}$$

As average signal power of companded and original signal are same

$$\begin{aligned} E\left[|\bar{x}_m|^2\right] &= E\left[|t_m|^2\right] = E\left[h\left(|\bar{x}_m|^2\right)\right] \\ &= E\left[\left[A \times V_{\max} \frac{\ln\left[1+\frac{\mu|\bar{x}_m|}{V_{\max}}\right]}{\ln[1+\mu]}\right]^2\right] \end{aligned} \tag{3.8}$$

Now A is chosen such that

$$A = \sqrt{\frac{E\left[|\bar{x}_m|^2\right]}{E\left[\left[V_{\max} \frac{\ln\left[1+\frac{\mu|\bar{x}_m|}{V_{\max}}\right]}{\ln[1+\mu]}\right]^2\right]}} \tag{3.9}$$

So by simply multiplying the conventional companding function with *A*, we can make sure that average power of companded signal is unaltered. The decompanding function at the receiver side is characterized by

$$h^{-1}(x) = \frac{V_{\max}}{\mu}\left[\exp\left(\frac{|x|\ln(1+\mu)}{A\times V_{\max}}\right)-1\right]\operatorname{sgn}(x) \tag{3.10}$$

3.3.2. Error Function (ERF) Companding

This companding transform is based on the error function that has been used in OFDM systems [9]. ERF companding function is characterized by

$$h(x) = A\times erf(k|x|)\operatorname{sgn}(x) \tag{3.11}$$

where *erf* denotes error function and '*k*' is the companding coefficient. By keeping the average power of companded signal t_m equal to that of the original signal

$$\begin{aligned} E\left[|\overline{x}_m|^2\right] &= E\left[|t_m|^2\right] = E\left[h\left(|\overline{x}_m|^2\right)\right] \\ &= E\left[\left(A\times erf\left(k|\overline{x}_m|\right)\right)^2\right] \end{aligned} \tag{3.12}$$

Now *A* is given by

$$A = \sqrt{\frac{E\left[|\overline{x}_m|^2\right]}{E\left[\left(erf\left(k|\overline{x}_m|\right)\right)^2\right]}} \tag{3.13}$$

The ERF decompanding function at the receiver side is characterized by

$$h^{-1}(x) = \frac{1}{k}erf^{-1}\left(\frac{|x|}{A}\right)\operatorname{sgn}(x) \tag{3.14}$$

3.3.3. Exponential Companding (EC)

It is based on the exponential function used in OFDM systems [99]. Exponential companding function is defined as

$$h(x) = \operatorname{sgn}(x)\sqrt[d]{A\left[1-\exp\left(-\frac{|x|^2}{\sigma^2}\right)\right]} \tag{3.15}$$

$$A = \left(\frac{E\left[|x|^2 \right]}{E\left[\sqrt[d]{\left[1 - \exp\left(-\frac{|x|^2}{\sigma^2} \right) \right]^2} \right]} \right)^{\frac{d}{2}} \tag{3.16}$$

where exp denotes the exponential function and '*d*' defines the degree parameter controlling the companding process. Exponential decompanding function is described by

$$h^{-1}(x) = \operatorname{sgn}(x) \left| \sqrt{-\sigma^2 \log_e \left(1 - \frac{|x|^d}{A} \right)} \right| \tag{3.17}$$

3.3.4. Logarithmic (log) Companding

Logarithmic companding is based on threshold companding scheme used in OFDM systems [100]. Logarithmic companding function is defined as

$$h(x) = A \times \log_e \left(k|x| + 1 \right) \operatorname{sgn}(x) \tag{3.18}$$

where '*k*' is a positive number which controls the amount of companding. *A* is chosen such that the average power of companded signal doesn't change as given below

$$A = \sqrt{\frac{E\left[|\overline{x}_m|^2 \right]}{E\left[\left(\log_e \left(k|\overline{x}_m| \right) + 1 \right)^2 \right]}} \tag{3.19}$$

The logarithmic decompanding function at the receiver side is characterized by

$$h^{-1}(x) = \frac{1}{k} \left[\exp\left(\frac{|x|}{A} \right) - 1 \right] \operatorname{sgn}(x) \tag{3.20}$$

3.3.5. Rooting Companding

Rooting companding has been inspired by the principle of square root. Rooting companding function is described by

$$h(x) = A \times |x|^R \operatorname{sgn}(x) \tag{3.21}$$

$$A = \sqrt{\frac{E\left[\left|\overline{x}_m\right|^2\right]}{E\left[\left|\overline{x}_m\right|^{2R}\right]}} \tag{3.22}$$

The amount of companding depends on '*R*'. The rooting decompanding function is described by

$$h^{-1}(x) = \left|\frac{x}{A}\right|^{\frac{1}{R}} \operatorname{sgn}(x) \tag{3.23}$$

3.3.6. Airy Companding

This companding technique is based on a special function, called airy function [101]. The airy companding function is given by

$$h(x) = \beta\left[\operatorname{airy}(0) - \operatorname{airy}\left(d\left|x\right|\right)\right]\operatorname{sgn}(x) \tag{3.24}$$

$$\beta = \sqrt{\frac{E\left[\left|\overline{x}_m\right|^2\right]}{E\left[\left|\operatorname{airy}(0) - \operatorname{airy}(d\left|\overline{x}_m\right|)\right|^2\right]}} \tag{3.25}$$

where airy(.) is the airy function, '*k*' controls the degree of companding and β is used to make sure that average signal power of the companded signal remains unaltered. The airy decompanding function is described by

$$h^{-1}(x) = \frac{1}{d}\operatorname{airy}^{-1}\left[\operatorname{airy}(0) - \frac{|x|}{\beta}\right]\operatorname{sgn}(x) \tag{3.26}$$

3.4. Improved Exponential Companding (IEC)

Improved Exponential Companding uses two different companding levels, one if the amplitude of original signal is below the threshold and the other if it is above the threshold. In IEC technique a threshold *T* is introduced such that the signal is companded with d_1 if the amplitude values are below or equal to the threshold and d_2 otherwise. Now the values of $d_1, d_2,$ and *T* can be adjusted accordingly as per the system requirements for better PAPR and BER performances. Hence we have a higher degree of freedom than the conventional exponential companding technique. But, the improved exponential companding technique has

slightly higher complexity when compared to the conventional exponential companding technique as it has to find optimal values for d_2 and T additionally. Hence there is a trade-off between complexity and degree of freedom. The companding function is described by

$$h(x)=\begin{cases}\operatorname{sgn}(x)\left[A(d_1,d_2)\left(1-\exp\left(-\dfrac{|x|^2}{\sigma^2}\right)\right)\right]^{1/d_1}, & |x|\le T\\ \operatorname{sgn}(x)\left[A(d_1,d_2)\left(1-\exp\left(-\dfrac{|x|^2}{\sigma^2}\right)\right)\right]^{1/d_2}, & |x|>T\end{cases} \tag{3.27}$$

$A(d_1,d_2)$ is a normalization factor to keep the average powers of companded and original signals equal. The decompanding function is described by

$$h^{-1}(x)=\begin{cases}\operatorname{sgn}(x)\left|\sqrt{-\sigma^2\log_e\left(1-\dfrac{|x|^{d_1}}{A(d_1,d_2)}\right)}\right|, & |x|\le T\\ \operatorname{sgn}(x)\left|\sqrt{-\sigma^2\log_e\left(1-\dfrac{|x|^{d_2}}{A(d_1,d_2)}\right)}\right|, & |x|>T\end{cases} \tag{3.28}$$

3.5. No Decompanding (NDC) Operation

Let the companded signal t_m be

$$t_m=\alpha\bar{x}_m+b_m \tag{3.29}$$

where b_m is companding noise and α is attenuation factor as defined by [102]

$$\alpha=\frac{E\left\{t_m\bar{x}_m^*\right\}}{E\left\{\bar{x}_m\bar{x}_m^*\right\}} \tag{3.30}$$

As the companded and original signals have same average signal power,

$$\begin{aligned}P_{\bar{x}_m}&=P_{t_m}=P_{\alpha\bar{x}_m}+P_{b_m}=\alpha^2P_{\bar{x}_m}+P_{b_m}\\ P_{b_m}&=\left(1-\alpha^2\right)P_{\bar{x}_m}\end{aligned} \tag{3.31}$$

This illustrates that $\alpha<1$ and P_{b_m} will be smaller, when α is close to one. The received signal considering AWGN channel can be described as

$$r_m = t_m + w_m \tag{3.32}$$

where w_m is channel noise. After decompanding operation, the recovered signal can be represented as

$$\overline{r}_m = \frac{r_m - b_m}{\alpha} = \frac{t_m + w_m - b_m}{\alpha} = \overline{x}_m + \frac{w_m}{\alpha} \tag{3.33}$$

This shows that decompanding operation amplifies the channel noise w_m to w_m / α. Without the decompanding operation, the equivalent noise is the companding noise plus channel noise. Now, the corresponding noise without and with decompanding operation can be written as $w_m + b_m$ and w_m / α respectively. The attenuation factor, α of MMC, ERF, EC, log, Root, Airy and IEC techniques were calculated to be 0.9938, 0.9927, 0.9962, 0.9943, 0.9898, 0.9977 and 0.9958 respectively. From (3.31), it can be said that these companding techniques have very less companding noise as α values are close to 1. Hence these techniques with no decompanding operation can also offer a good BER performance.

3.6. Optimum Values for Different Companding Techniques

Companding techniques not only mitigate PAPR but also impact BER performance of the system. Here optimum values for different companding techniques will be selected for better PAPR performance without degrading BER performance. For this, various companding techniques have been simulated by varying their respective parameters to find the optimum values for better BER and PAPR performances. Simulation parameters are defined in Table 3.2.

Table 3.3. Simulation Parameters

Parameter	**Description**
System bandwidth	5 MHz
Channel coding	1/2 rate Convolutional code
Modulation type	16-QAM
N	128
M	512
Subcarriers spacing	9.765625 kHz
Subcarrier mapping	Localized

CP length	20 samples
Channel model	AWGN, Veh-A
Channel estimation	Perfect
Equalization	MMSE

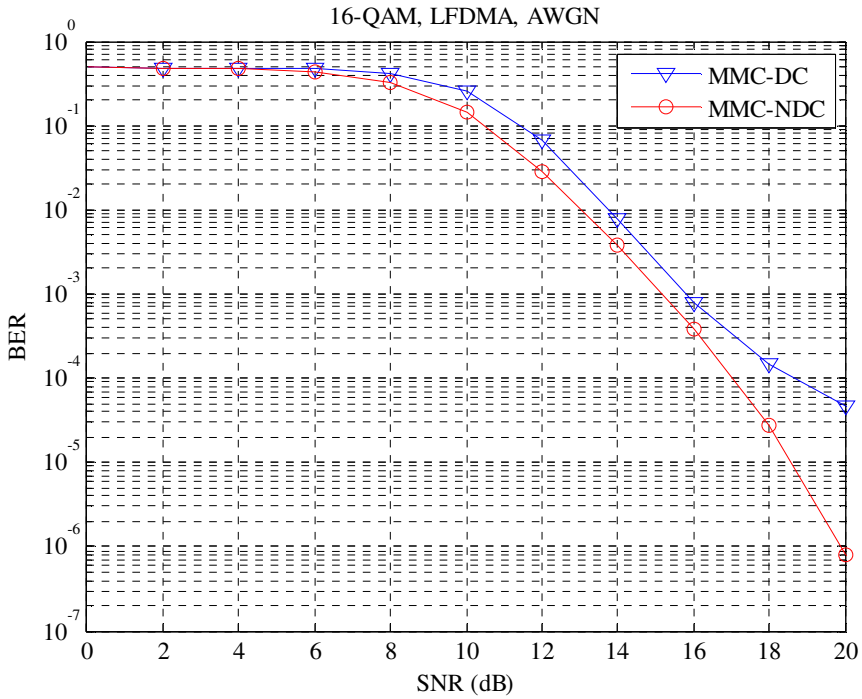

Fig. 3.2. BER curves of MMC with decompanding and no decompanding operations.

Fig. 3.2 presents the BER plot of MMC with decompading (DC) and with no decompanding (NDC) operations for μ=4. We can observe that MMC-NDC outperforms MMC-DC. Hence we consider NDC for the remaining results.

Fig. 3.3 shows complementary cumulative distribution function curves (CCDF) of μ-law companding for different values of 'μ'. It can be noted that PAPR value decreases as 'μ' value is increased. For example, PAPR at CCDF=10^{-4} has been reduced by 2 dB when 'μ' is increased from 1 to 5.

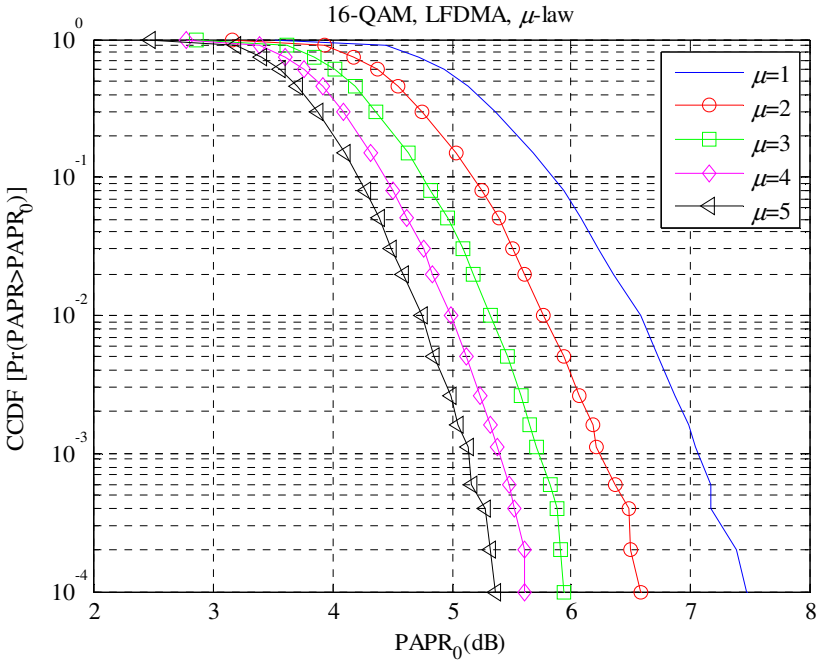

Fig. 3.3. PAPR performance of μ-law companding for different 'μ'.

BER versus 'μ' plot of μ-law companding at different SNR values is illustrated in Fig. 3.4. BER value can be decreased by decreasing 'μ' value. So μ=3 is chosen for a trade-off between BER and PAPR performances.

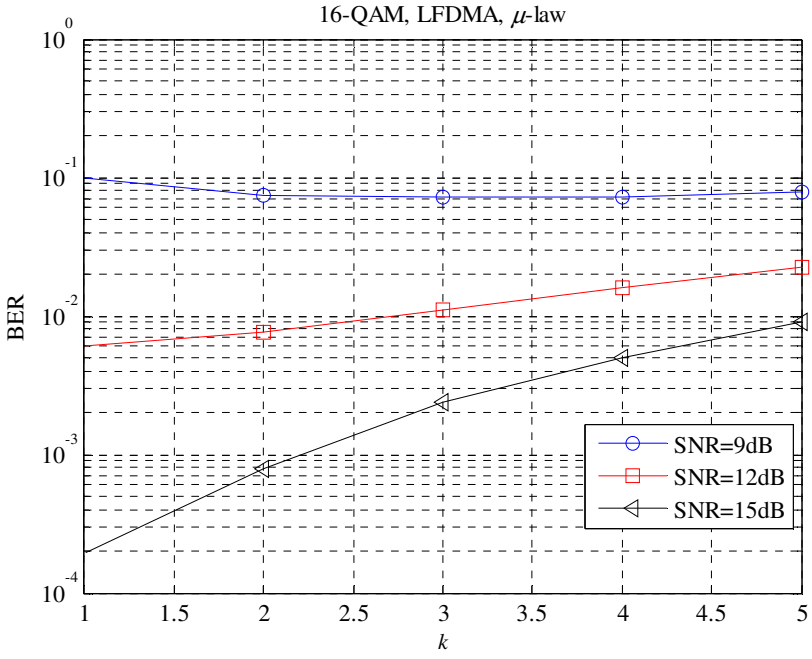

Fig. 3.4. BER vs 'μ' plot of μ-law companding for different SNR.

Fig. 3.5 shows the CCDF curves of MMC for different values of 'μ'. It can be noted that PAPR value decreases as 'μ' value is increased.

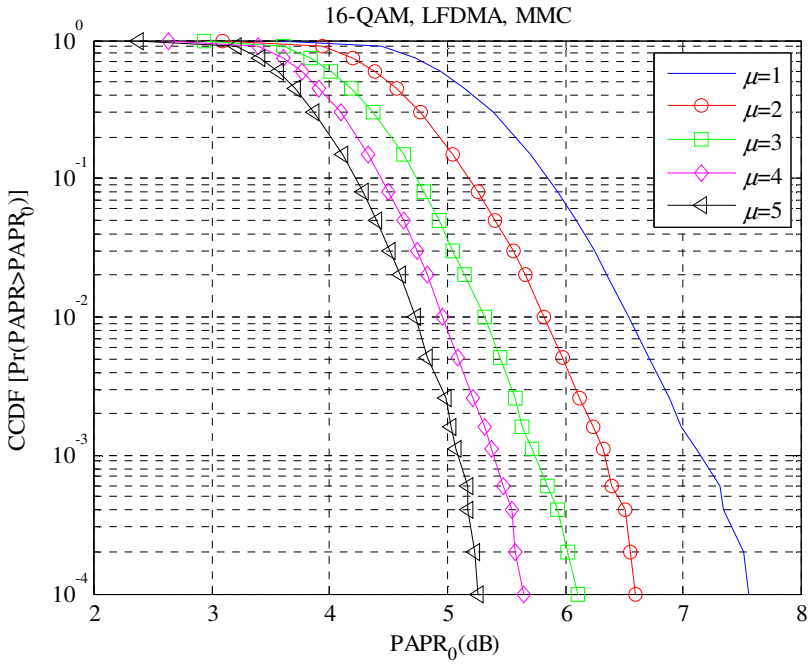

Fig. 3.5. PAPR performance of MMC for different 'μ'.

BER versus 'd' plot of MMC for different values of SNR is illustrated in Fig. 3.6. BER value can be decreased by decreasing 'μ' value. So μ=3 is chosen for a trade-off between BER and PAPR performances.

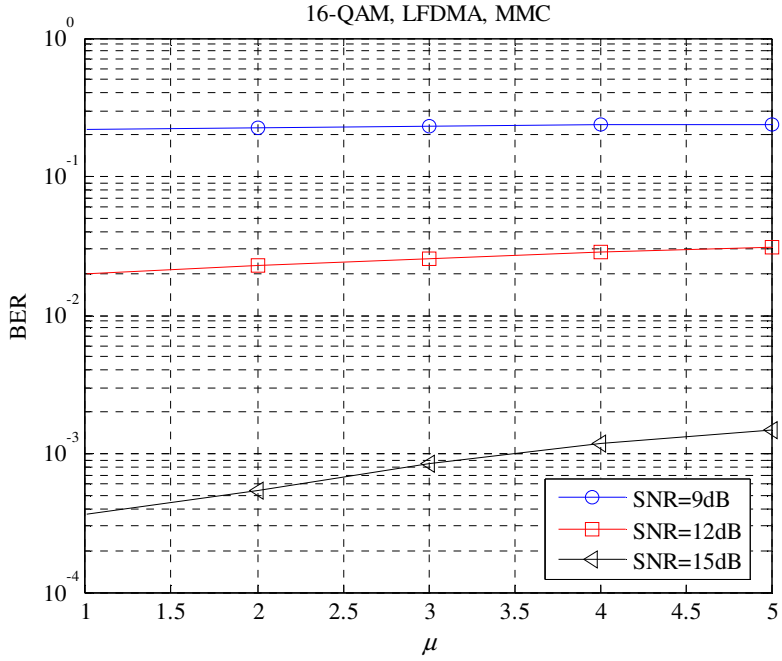

Fig. 3.6. BER vs 'μ' plot of MMC for different SNR.

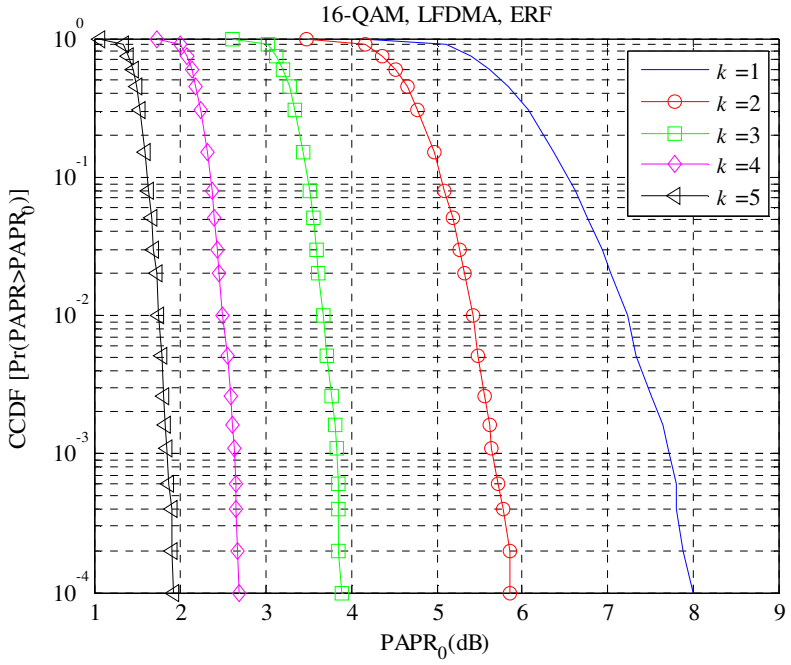

Fig. 3.7. PAPR performance of ERF companding for different '*k*'.

Fig. 3.7 shows CCDF curves of ERF companding for different values of '*k*'. It can be noted that PAPR value decreases as '*k*' value is increased. For example, PAPR at CCDF=10^{-4} has been reduced by 6 dB when '*k*' is increased from 1 to 5.

BER versus '*k*' plot of ERF companding at different SNR values is illustrated in Fig. 3.8. BER value can be decreased by decreasing '*k*' value. So *k*=3 is chosen for a trade-off between BER and PAPR performances.

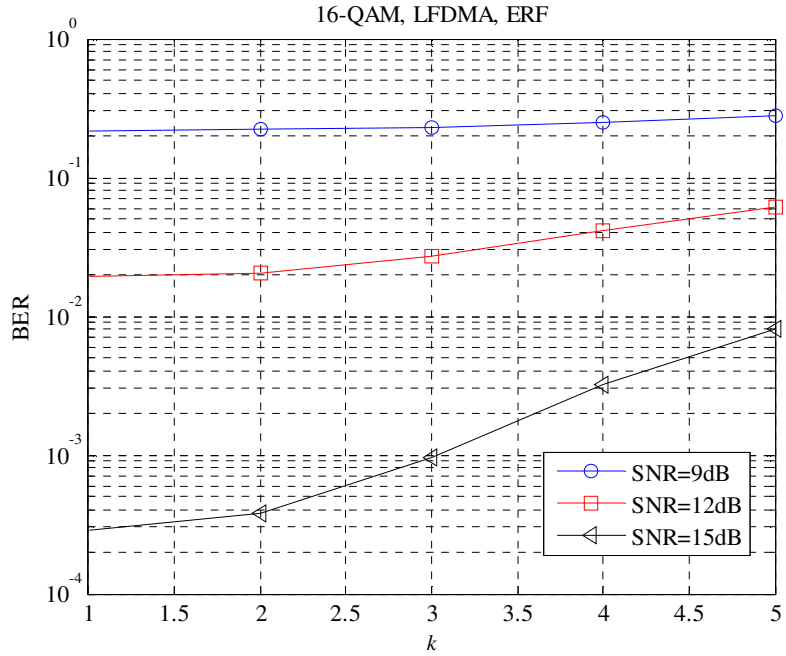

Fig. 3.8. BER vs '*k*' plot of ERF companding for different SNR.

Fig. 3.9 shows the CCDF curves of EC for different values of '*d*'. It can be noted that PAPR value decreases as '*d*' value is increased. PAPR has been reduced by about 1.7 dB when '*d*' is increased from 0.9 to 1.7.

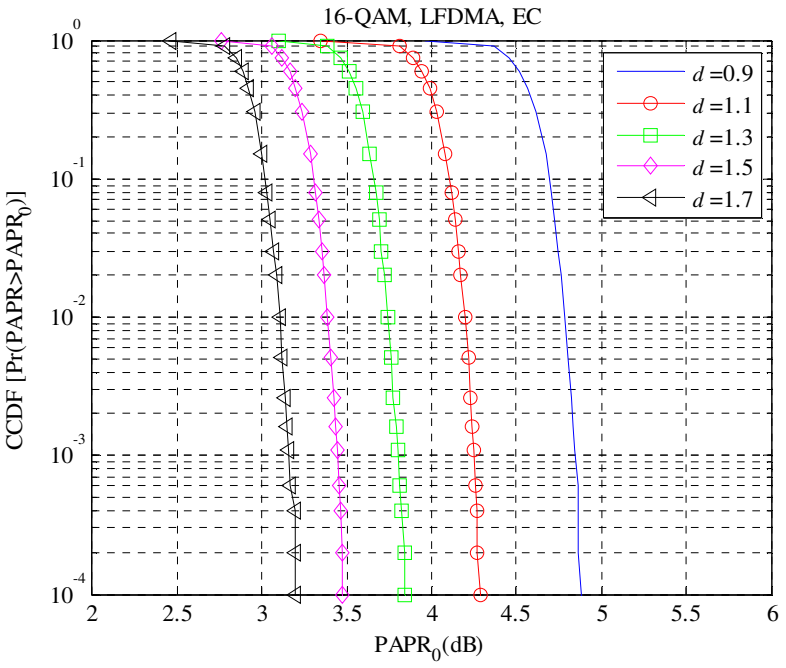

Fig. 3.9. PAPR performance of EC for different '*d*'.

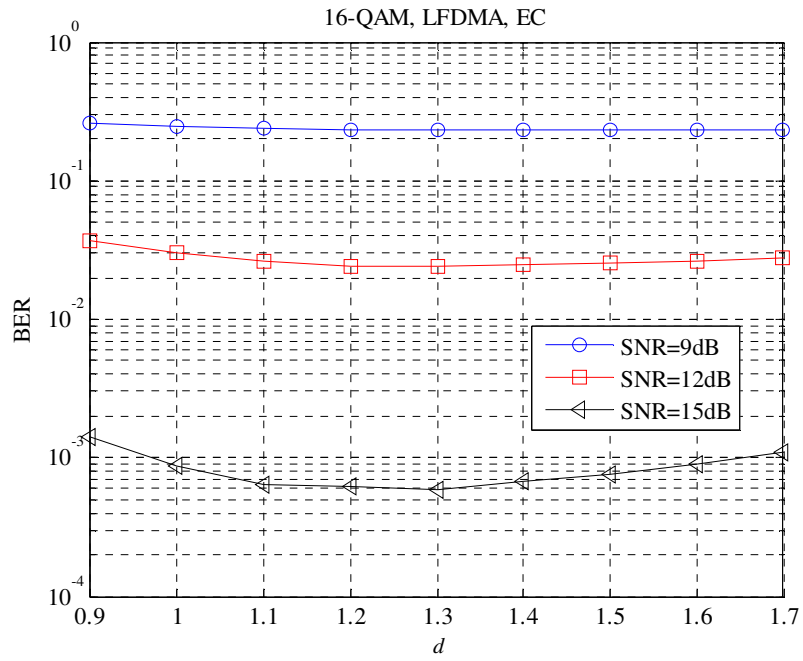

Fig. 3.10. BER vs '*d*' plot of EC for different SNR.

BER versus '*d*' plot of EC for different values of SNR is illustrated in Fig. 3.10. It can be noted that *d*=1.3 is the best pick for minimum BER. Fig. 3.11 shows the CCDF curves of logarithmic companding for different values of '*k*'. It is evident that PAPR value decreases as '*k*' value is increased. PAPR at CCDF=10^{-4} has been reduced by 2.7 dB when '*k*' is increased from 1 to 9.

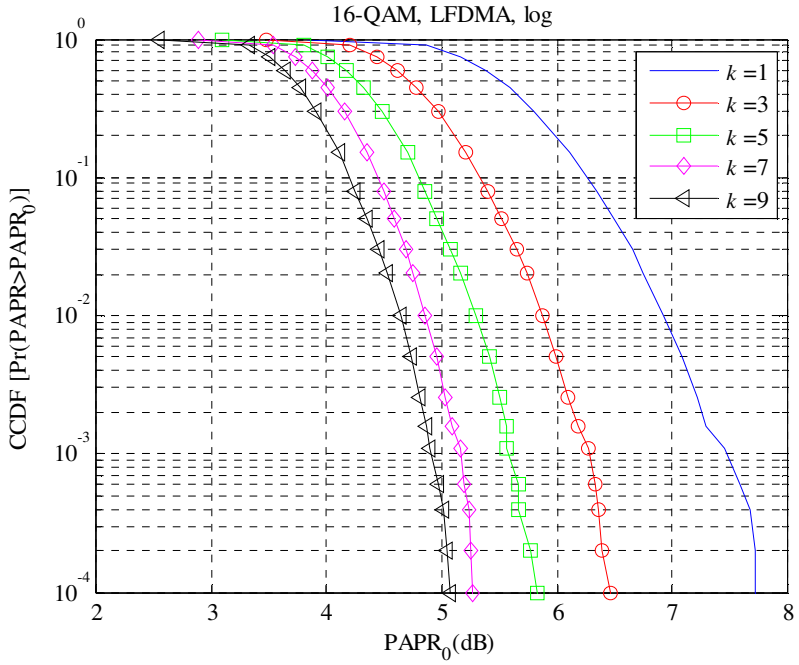

Fig. 3.11. PAPR performance of log companding for different '*k*'.

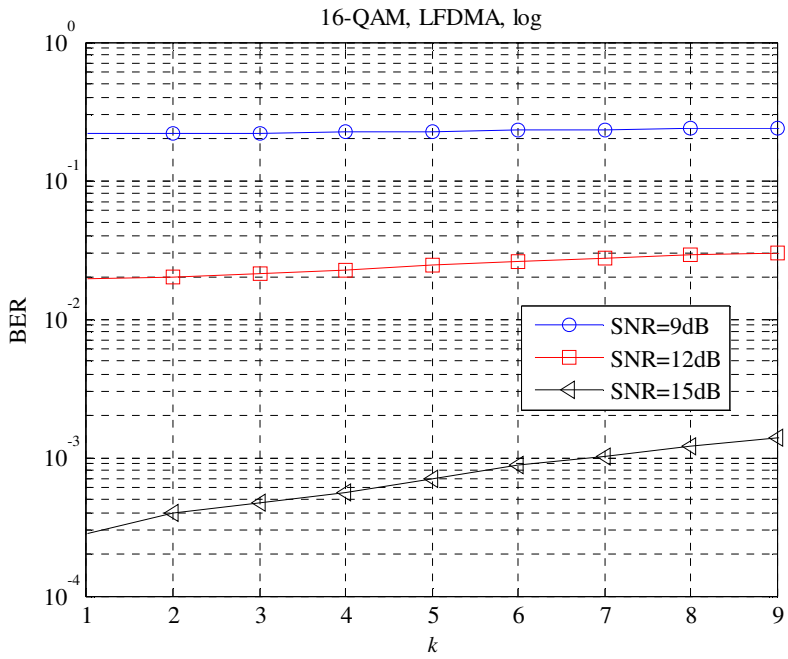

Fig. 3.12. BER vs '*k*' plot of log companding for different SNR.

BER versus '*k*' plot of logarithmic companding at different SNR values is shown in Fig. 3.12. BER value can be decreased by decreasing '*k*' value. So *k*=5 is chosen for a trade-off between PAPR and BER performances.

Fig. 3.13 shows CCDF curves of rooting companding for different values of '*R*'. It can be noted that PAPR value decreases as '*R*' value is decreased. PAPR has been reduced by about 7.1 dB when '*R*' is decreased from 0.9 to 0.1.

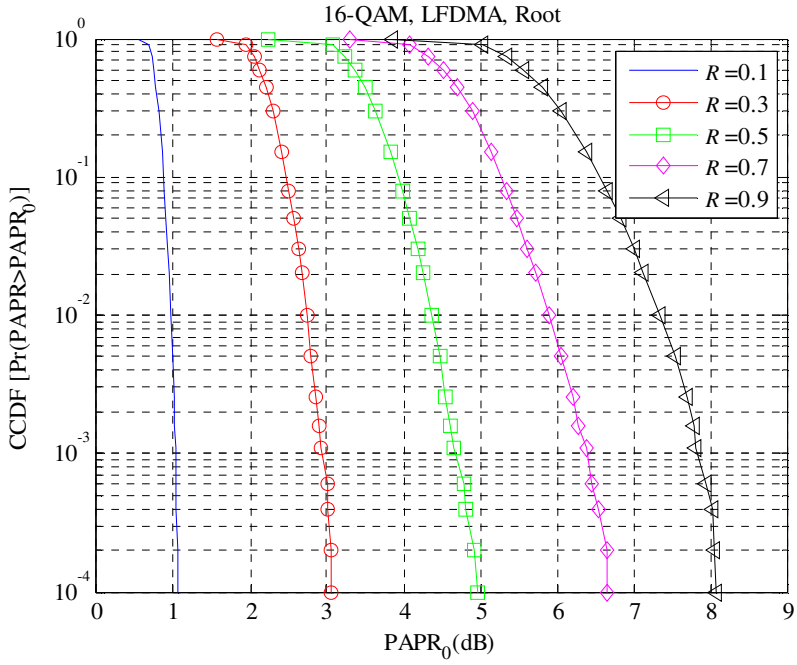

Fig. 3.13. PAPR performance of rooting companding for different '*R*'.

BER versus '*R*' plot of rooting companding at different SNR values is shown in Fig. 3.14. BER value can be decreased by increasing '*R*' value. So *R*=0.6 is chosen for a trade-off between PAPR and BER performances.

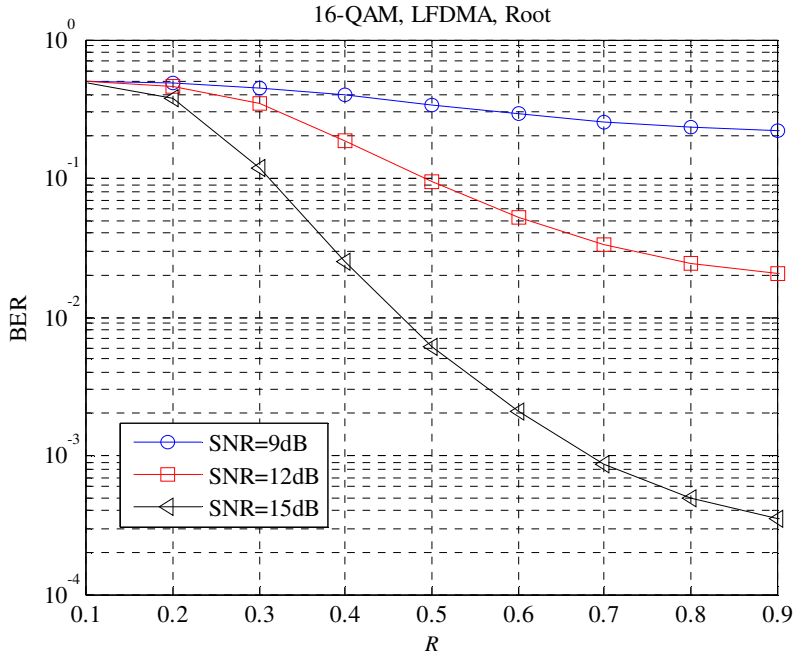

Fig. 3.14. BER vs '*R*' plot of rooting companding for different SNR.

Fig. 3.15 shows CCDF curves of airy companding for different values of '*d*'. It can be noted that PAPR value decreases as '*d*' value is increased. PAPR has been reduced by about 2.5 dB when '*d*' is increased from 1 to 3.

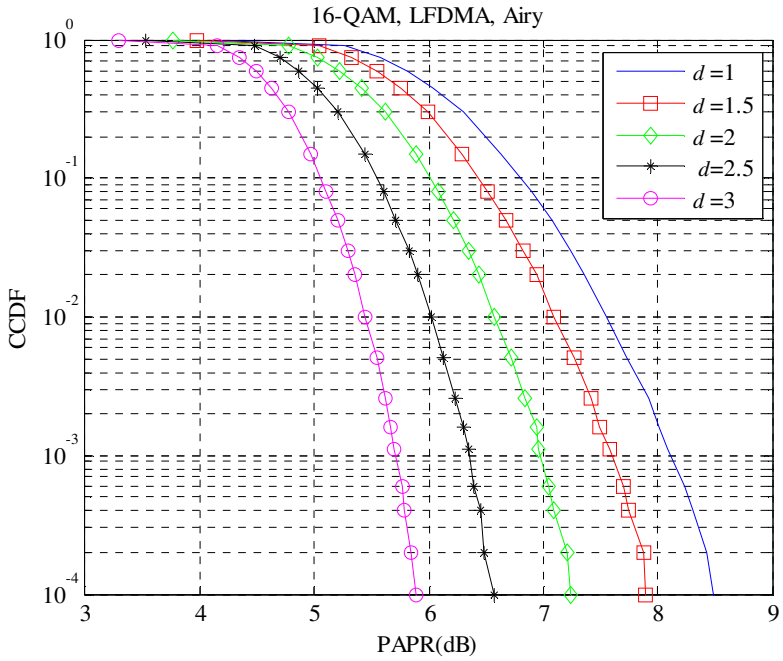

Fig. 3.15. PAPR performance of airy companding for different '*d*'.

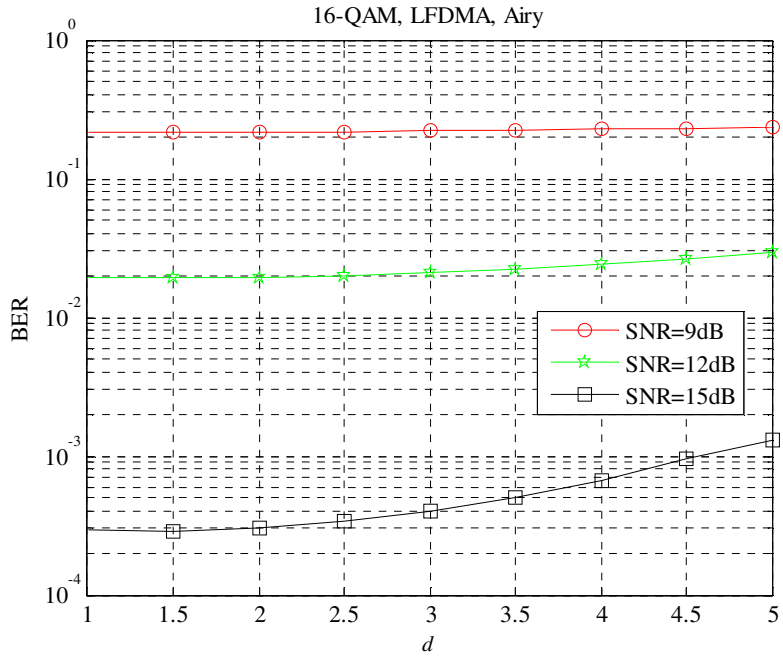

Fig. 3.16. BER vs '*d*' plot of airy companding for different SNR.

BER versus '*d*' plot of airy companding at different SNR values is illustrated in Fig. 3.16. BER value can be decreased by decreasing '*d*' value. So *d*=3 is chosen for a trade-off between BER and PAPR performances.

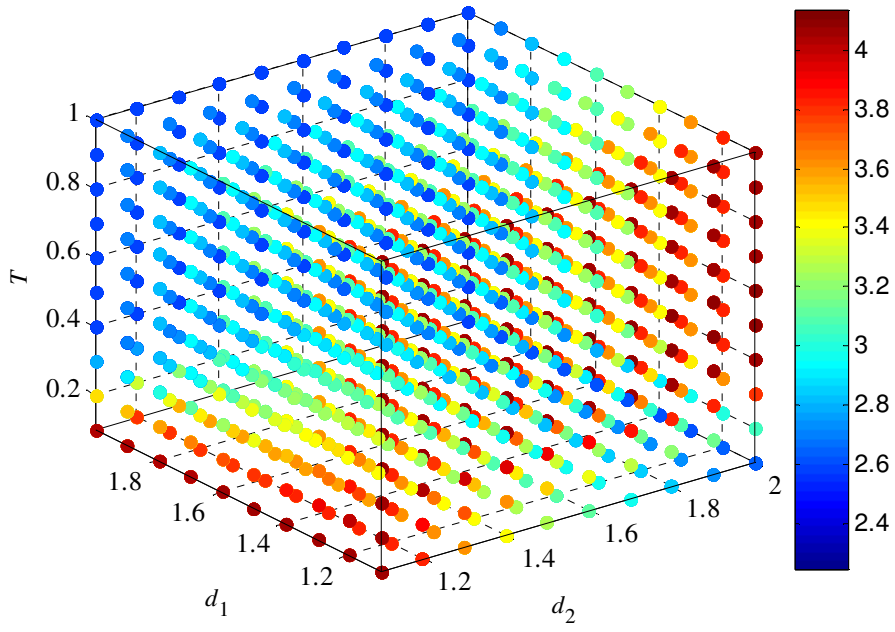

Fig. 3.17. PAPR values of IEC for different $d_1, d_2,$ and *T*.

Figs. 3.17 and 3.18 present the scatter plots of PAPR and BER values of IEC respectively for different $d_1, d_2,$ and *T*. We can notice that PAPR values are high when BER values are low and vice-versa. After extensive simulations, from Fig. 3.17 and 3.18 we found that $d_1 = 1.4, d_2 = 2, T = 0.3$ are the optimum values for better PAPR and BER performances of IEC.

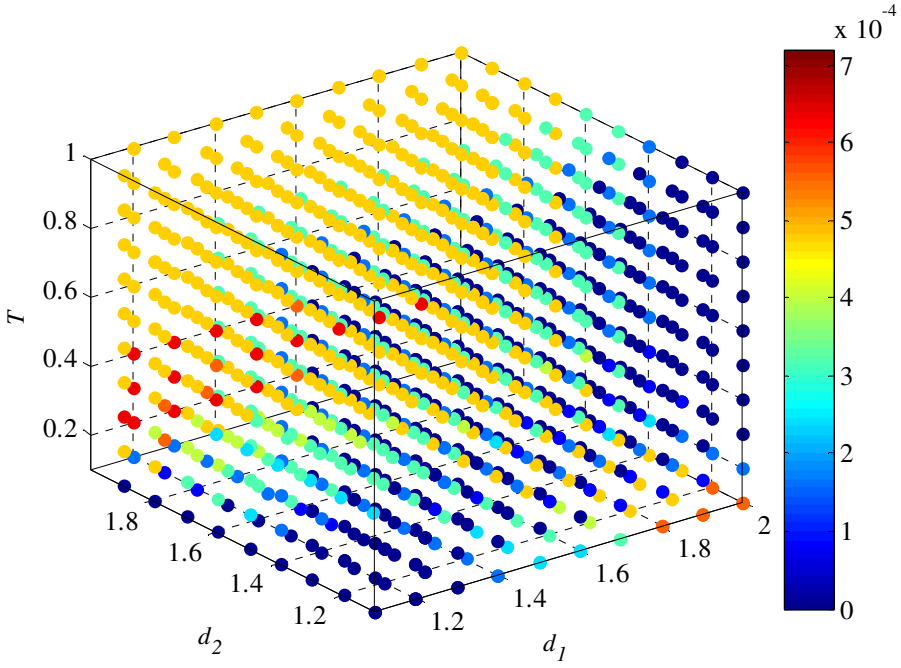

Fig. 3.18. BER values of IEC for different $d_1, d_2,$ and T.

3.7. Simulation Results

Here we compare various companding techniques in terms of PAPR, BER, and Power Spectral Density (PSD). Fig. 3.19 shows CCDF curves of various companding techniques and conventional SC-FDMA system.

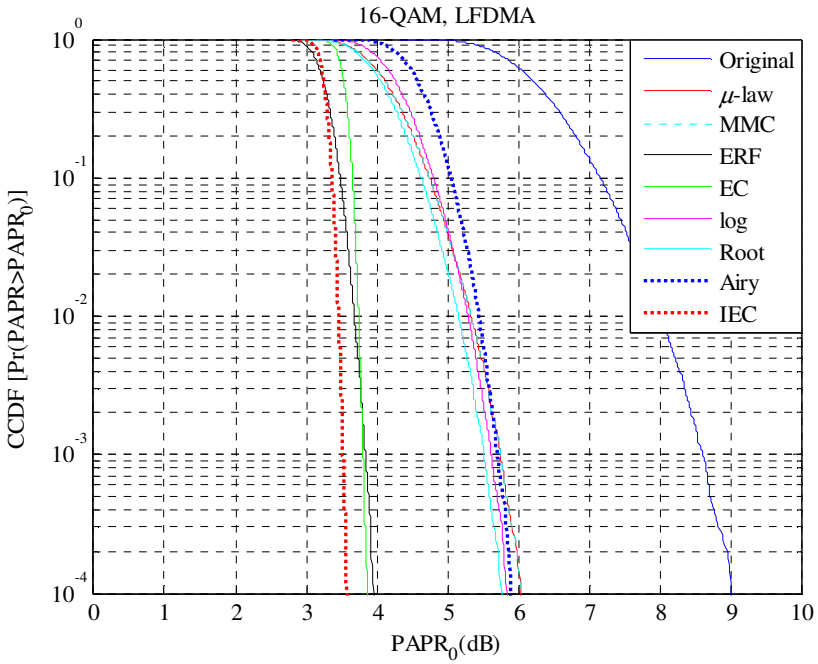

Fig. 3.19. PAPR performance of various companding techniques.

PAPR values at CCDF=10^{-4} are presented in Table 3.3 for original system, and system with various companding techniques. It can be observed that IEC has better PAPR performance when compared to EC and μ-law companding techniques.

Table 3.4. PAPR values at CCDF=10^{-4}

	Original	**μ-law**	**MMC**	**ERF**	**EC**	**log**	**Root**	**Airy**	**IEC**
PAPR (dB)	9.01	6.03	6.03	3.96	3.86	5.85	5.76	5.89	3.58

To ensure that the companding techniques does not increase the average power of the signal, waveforms of the original and companded signals have been presented in Fig. 3.20. The DC line represents the average power level. It can be observed that all the techniques maintain average power same as that of the original signal.

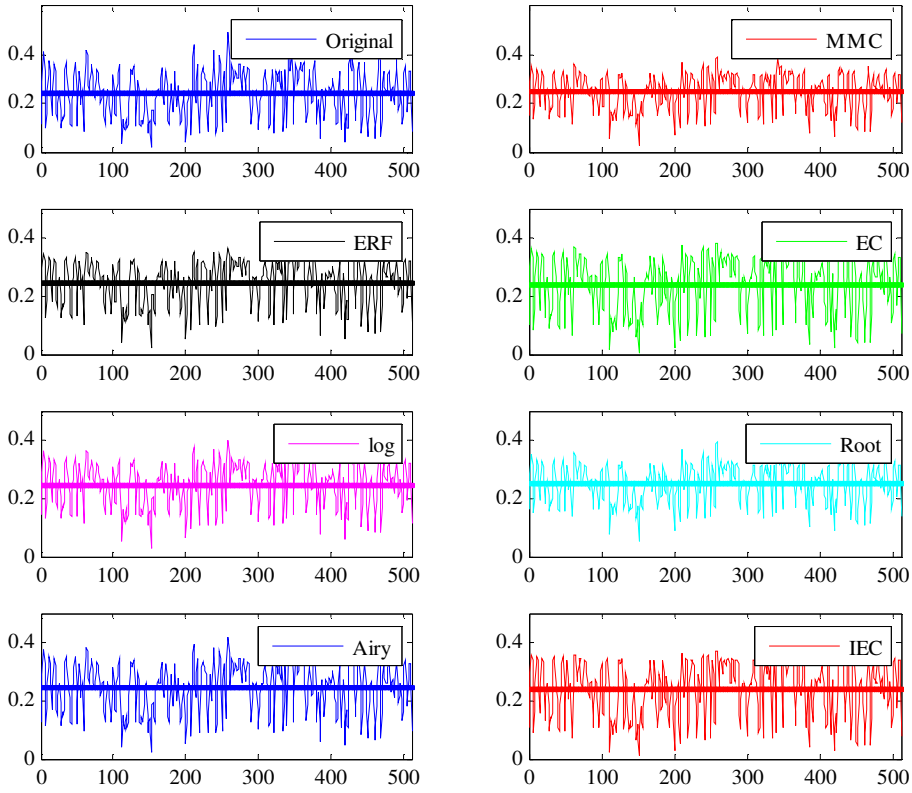

Fig. 3.20. Waveforms of original and companded signals.

Non-linear power amplifier characteristics can be modelled by using Solid State Power Amplifier (SSPA). To study the impact of nonlinear power amplifier on the system, we have considered SSPA with p = 2 and IBO = 5 dB and plotted the PSD results as shown in Fig. 3.21. We have used Welch's method with hamming window and 50% overlap to estimate PSD in MATLAB. The PSD of the original signal has been plotted without considering SSPA. It can be observed that μ-law companding has both in-band and out-of-band distortions and airy companding has PSD characteristics close to that of original signal. Also IEC technique has better PSD performance when compared to that of conventional EC scheme.

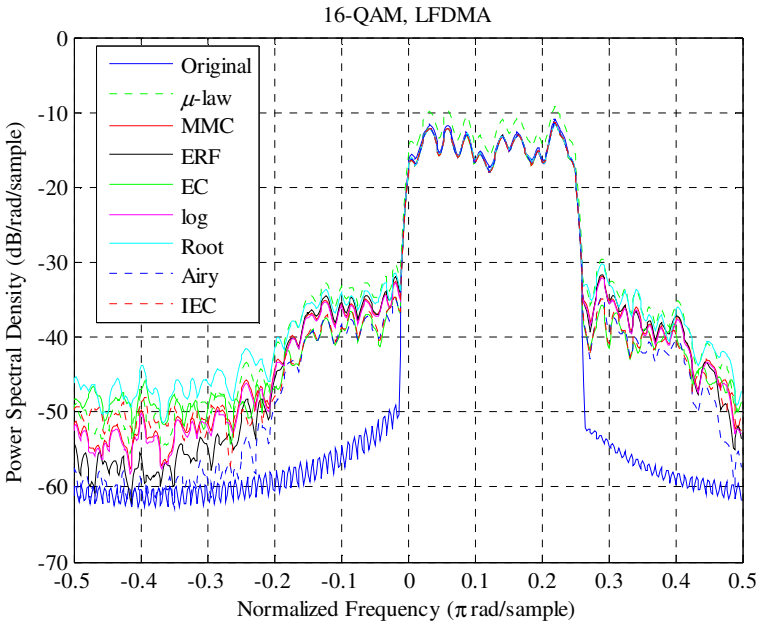

Fig. 3.21. PSDs of original and companded signals.

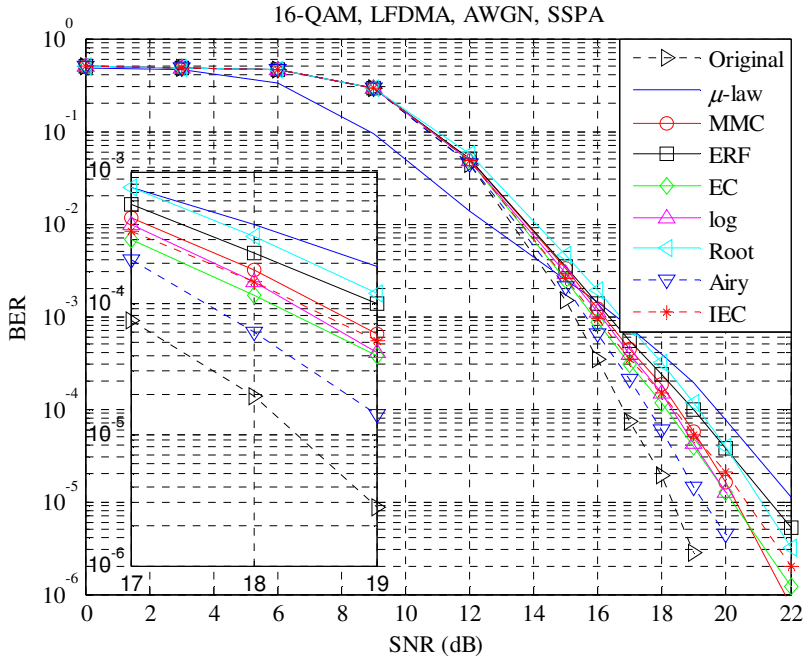

Fig. 3.22. BER curves of original and companded signals over AWGN channel.

Fig. 3.22 presents BER curves of original and companded signals over AWGN channel by considering SSPA. It can be observed that airy companding technique has better BER performance when compared to other techniques.

Fig. 3.23 presents BER curves of original and companded signals over Vehicular-A outdoor channel by considering SSPA. Veh-A channel model corresponds to multipath Rayleigh fading channel with six taps as defined in [103]. It can be observed that all the techniques perform relatively similar over multipath fading environment also. Table 3.4 gives the comparison of SNR values required for a BER of 10^{-4} for various companding techniques.

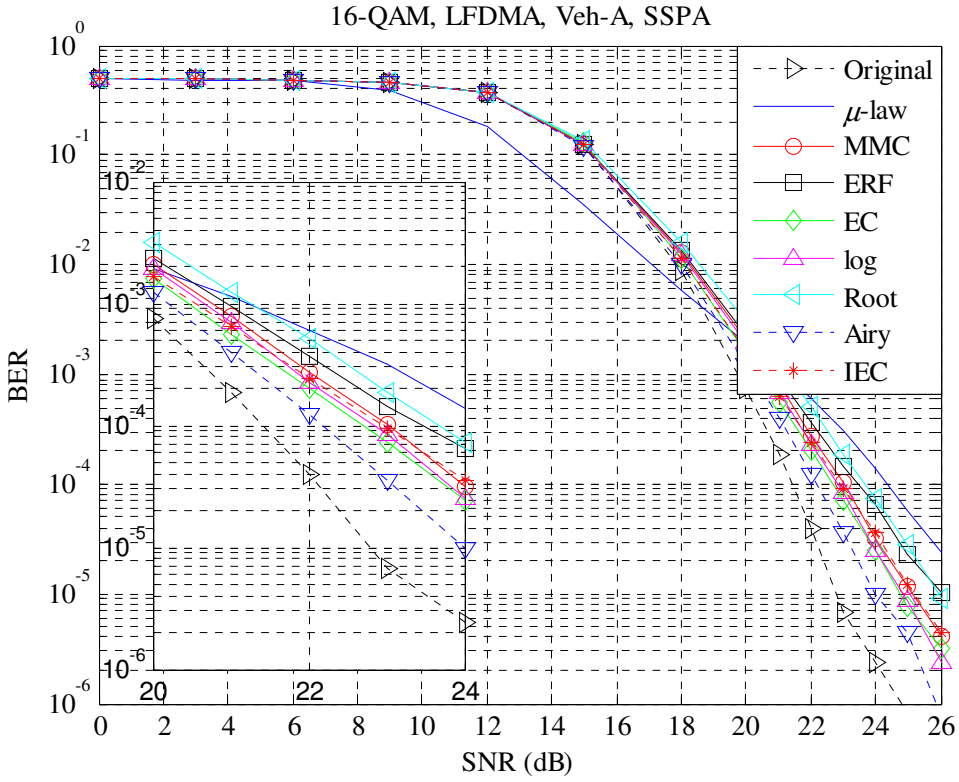

Fig. 3.23. BER curves of original and companded signals over Veh-A channel.

Table 3.5. SNR values at BER=10^{-4}

	Original	***μ*-law**	**MMC**	**ERF**	**EC**	**log**	**Root**	**Airy**	**IEC**
AWGN	16.9	19.8	18.65	18.98	18.19	18.45	19.22	17.73	18.49
Veh-A	21.58	24.47	23.04	23.55	22.78	22.89	23.77	22.25	22.95

Table 3.5 presents the values of PAPR reduction at CCDF = 10^{-4} and additional SNR required to maintain a BER of 10^{-4} over Veh-A channel for various companding schemes when compared to the original signal. IEC provides better PAPR reduction of about 5.43 dB but requires 1.37 dB excess SNR to maintain BER constant. However, IEC outperforms the existing schemes in terms of net gain (PAPR reduction - additional SNR).

Table 3.6. Performance analysis of various techniques

Companding	PAPR Reduction (dB)	Additional SNR (dB)	Net Gain (dB)
μ-law	2.98	2.89	0.09
MMC	2.98	1.46	1.52
ERF	5.05	1.97	3.08
EC	5.15	1.20	3.95
log	3.16	1.31	1.85
Root	3.25	2.19	1.06
Airy	3.12	0.67	2.45
IEC	5.43	1.37	4.06

3.8. Conclusion

In this chapter, the performances of various companding techniques have been studied and analysed. Exponential companding provides better PAPR performance with a PAPR reduction of about 5.15 dB at CCDF=10^{-4}. Then we have proposed an improved exponential companding technique, which offers more flexibility than the conventional exponential companding scheme with a PAPR reduction of about 5.43 dB at CCDF=10^{-4}. Also, the proposed IEC technique has better PSD characteristics than EC scheme. Airy companding offers better PSD and BER performances, with only 0.67 dB increase in SNR to maintain a BER of 10^{-4}. However, it provides a PAPR reduction of 3.12 dB only at CCDF=10^{-4}.

Chapter-4

PAPR Reduction by Approximating the Distribution of SC-FDMA and DCT SC-FDMA Signals

4.1. Introduction

In general companding transform is designed based on the distribution of the signal. The companding transforms discussed in previous chapter have been designed for OFDM systems which have Gaussian distribution. But in [104] authors described that amplitude of single carrier signal does not have Gaussian distribution and it is difficult to derive the exact form of the distribution analytically. In this chapter, the distribution of SC-FDMA signal is approximated by using curve fitting tool and then a companding technique is proposed to transform it into a uniform distribution. Also, the distribution of DCT SC-FDMA signal is approximated by using curve fitting tool and then a companding technique is proposed to transform it into a triangular distribution.

Table 4.1. List of Symbols

Symbol	Description
$f_{\lvert\overline{x}_m\rvert}(x)$	PDF of $\lvert\overline{x}_m\rvert$
$F_{\lvert\overline{x}_m\rvert}(x)$	CDF of $\lvert\overline{x}_m\rvert$
$\Phi(x)$	CDF of standard normal distribution
t_m	Companded signal
$h(x)$	Companding function
c_m	Clipped signal
T	Clipping level threshold

4.2. DFT SC-FDMA System

4.2.1. Approximation of SC-FDMA distribution

The Probability Density Function (PDF) of the magnitude of 16-QAM modulated LFDMA signal, $|\bar{x}_m|$ is plotted using MATLAB simulations. Then curve fitting tool is used to obtain its expression. Fig. 4.1 presents the actual histogram and approximated PDF of LFDMA signal.

The PDF of the magnitude of SC-FDMA signal can be approximated by a sum of Gaussian functions instead of a single Gaussian function as given in equation (4.1).

$$f_{|\bar{x}_m|}(x) = \sum_{i=1}^{4} a_i e^{-\left(\frac{x-b_i}{c_i}\right)^2}, \; x \geq 0 \tag{4.1}$$

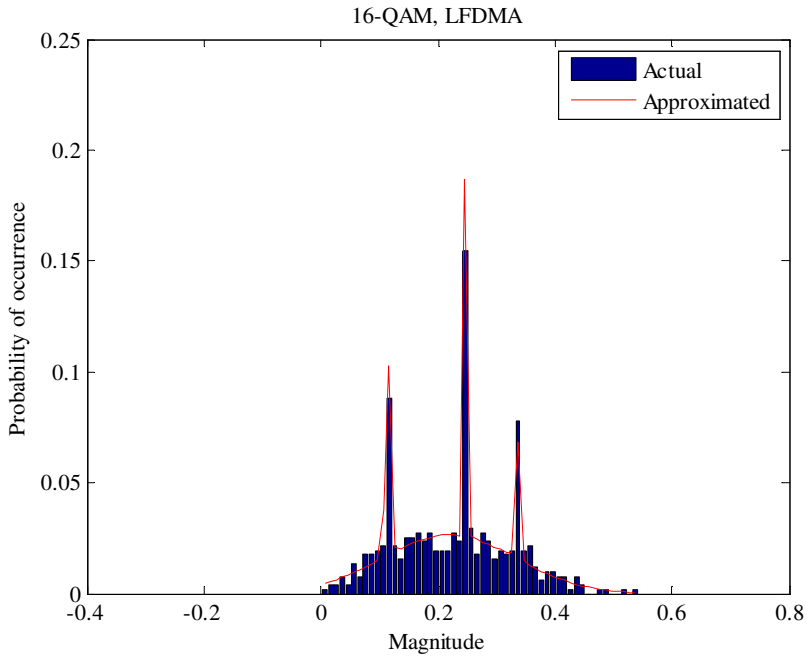

Fig. 4.1. Actual histogram and approximated PDF of LFDMA signal.

The values a_i, b_i and c_i are obtained from curve fitting tool. We have considered 50 samples for curve fitting and the goodness of our approximation is described by the statistics given in Table 4.2.

Table 4.2. Goodness-of-Fit Statistics

Statistic	Value	Ideal value for better fit
The sum of squares due to error (SSE)	0.001157	0
R-square	0.9624	1
Adjusted R-square	0.9512	1
Root mean squared error (RMSE)	0.005592	0

The Cumulative Distribution Function (CDF) is given by

$$\begin{aligned} F_{|\bar{x}_m|}(x) &= P\left\{|\bar{x}_m| \le x\right\} \\ &= \int_{-\infty}^{x} \sum_{i=1}^{4} a_i e^{-\left(\frac{x-b_i}{c_i}\right)^2} dx \end{aligned} \tag{4.2}$$

Let $\frac{x-b_i}{c_i} = \frac{z}{\sqrt{2}}$, then equation (4.2) can be modified as

$$\begin{aligned} F_{|\bar{x}_m|}(x) &= \sum_{i=1}^{4} \int_{-\infty}^{\frac{\sqrt{2}(x-b_i)}{c_i}} a_i e^{-Z^2/2} \frac{c_i}{\sqrt{2}} dz \\ &= \sum_{i=1}^{4} \sqrt{\pi} a_i c_i \Phi\left[\sqrt{2}\left(\frac{x-b_i}{c_i}\right)\right] \\ &= \sum_{i=1}^{4} \frac{\sqrt{\pi} a_i c_i}{2}\left[1 + erf\left(\frac{x-b_i}{c_i}\right)\right], \; x \ge 0 \end{aligned} \tag{4.3}$$

where $\Phi(x) = \frac{1}{\sqrt{2\pi}} \int_{-\infty}^{x} e^{-z^2/2} dz = \frac{1}{2}\left[1 + erf\left(\frac{x}{\sqrt{2}}\right)\right]$ is the CDF of standard normal distribution and erf(.) is error function.

Now the time domain LFDMA signal $\bar{x}_m$ is passed through compander, $h(x)$ to produce t_m.

4.2.2. Proposed Companding Transform

The proposed companding transform is given by

$$t_m = h(\bar{x}_m) \tag{4.4}$$

where t_m is the companded signal of input s_m. Let the d^{th} power of the magnitude of the companded SC-FDMA signal have uniform distribution in the range [0, u], where d is the degree of companding. As all the amplitudes have an equal probability of occurrence, PAPR will tend to reduce. So the d^{th} power of $|t_m|$ should have a CDF given by

$$F_{|t_m|^d}(x) = \frac{x}{u}, \ 0 \le x \le u \tag{4.5}$$

The CDF of companded signal, $|t_m|$ is given by

$$\begin{aligned} F_{|t_m|}(x) &= P\{|t_m| \le x\} \\ &= P\{|t_m|^d \le x^d\} \\ &= \frac{x^d}{u}, \ 0 \le x \le \sqrt[d]{u} \end{aligned} \tag{4.6}$$

The inverse function of $F_{|t_m|}$ is given by

$$F^{-1}_{|t_m|}(x) = \sqrt[d]{ux}, \ 0 \le x \le 1 \tag{4.7}$$

$h(x)$ being a strictly monotonic increasing function, we can write

$$\begin{aligned} F_{|\bar{x}_m|}(x) &= P\{|\bar{x}_m| \le x\} \\ &= P\{h(|\bar{x}_m|) \le h(x)\} \\ &= P\{|t_m| \le h(x)\} \\ &= F_{|t_m|}(h(x)) \end{aligned} \tag{4.8}$$

As companding function does not change the phase of input signal, $h(x)$ can be written as

$$\begin{aligned} h(x) &= F^{-1}_{|t_m|}\left(F_{|\bar{x}_m|}(x)\right) \\ &= \text{sgn}(x)\sqrt[d]{u\sum_{i=1}^{4}\frac{\sqrt{\pi}a_i c_i}{2}\left[1 + erf\left(\frac{|x| - b_i}{c_i}\right)\right]} \end{aligned} \tag{4.9}$$

where sgn(.) is the sign function. To maintain average power level of t_m same as that of $\bar{x}_m$, we let

$$E\left[\left|\bar{x}_m\right|^2\right] = E\left[\left|t_m\right|^2\right]$$
$$= E\left[\left(u\sum_{i=1}^{4}\frac{\sqrt{\pi}a_i c_i}{2}\left[1+erf\left(\frac{\left|\bar{x}_m\right|-b_i}{c_i}\right)\right]\right)^{2/d}\right] \tag{4.10}$$

Now u is given by

$$u = \left(\frac{E\left[\left|\bar{x}_m\right|^2\right]}{E\left[\left(\sum_{i=1}^{4}\frac{\sqrt{\pi}a_i c_i}{2}\left[1+erf\left(\frac{\left|\bar{x}_m\right|-b_i}{c_i}\right)\right]\right)^{2/d}\right]}\right)^{d/2} \tag{4.11}$$

After adding a CP to t_m, it is transmitted over the channel. At the receiver side, CP is removed and r_m is passed through M-point DFT without any decompanding function. Then subcarrier de-mapping, Frequency Domain Equalization, N-point IDFT, demodulation and decoding processes are performed to detect the transmitted data.

4.2.3. Hybrid Companding and Clipping Technique

SC-FDMA system with hybrid companding and clipping technique is shown in Fig. 4.2. The companded signal is clipped at the transmitter side while the received side remains unaffected. The companded signal t_m is clipped to a predefined threshold value by using a soft limiter as [7]

$$c_m = \begin{cases} t_m, & if\ \left|t_m\right| \le T \\ Te^{j\angle t_m}, & if\ \left|t_m\right| > T \end{cases} \tag{4.12}$$

where c_m is the clipped signal and T is the threshold at which signal is clipped.

The clipping ratio (CR) is given by

$$\text{CR} = \frac{T}{\sqrt{P_{av}}} \tag{4.13}$$

where P_{av} is average power of the original signal before clipping. As the hybrid technique comprises of companding followed by clipping, PAPR can be improved further.

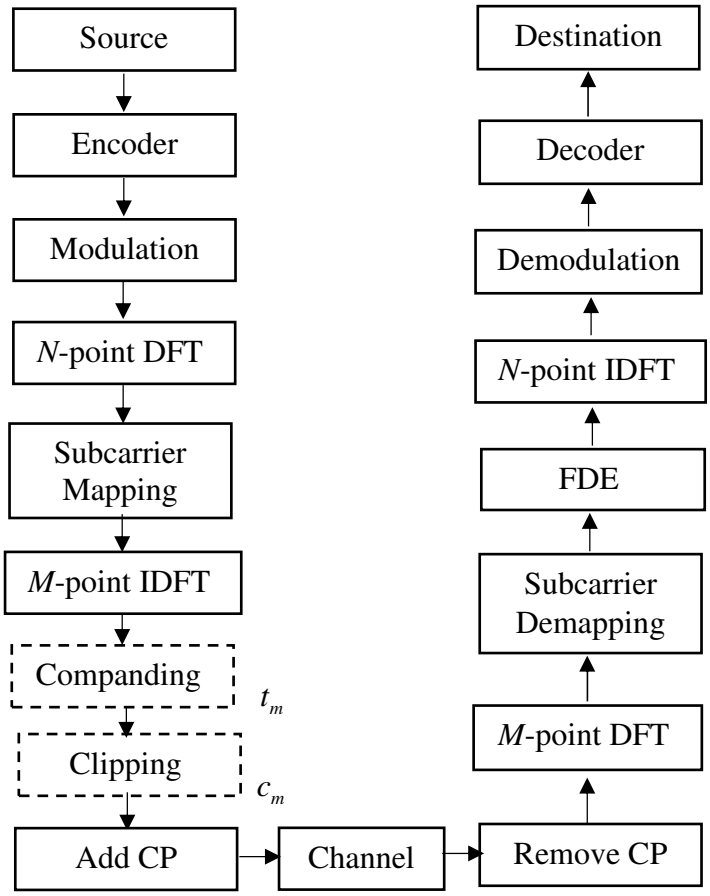

Fig. 4.2. SC-FDMA system with hybrid companding and clipping technique.

The hybrid system existing in [105] uses clipping in the first stage and companding in the second stage. As clipping is used in the first stage, the information will be lost as the signal will be clipped to a predefined threshold. The companding in the second stage compresses and expands the clipped signal. However our proposed hybrid system uses companding in the first stage and clipping in the second stage. As companding is used in the first stage most of the signal peaks are compressed. Now clipping in the second stage does not cause much information loss as there will not be many peaks available due to companding operation.

4.2.4. Performance Evaluation

To evaluate the performance of proposed companding technique, we have considered SC-FDMA system as shown in Fig. 4.2 and set the parameters as listed in Table 4.3. As PAPR problem is severe for higher order modulations, we have considered 16-QAM as the modulation technique over QPSK.

Table 4.3. Simulation Parameters

Parameter	Description
System bandwidth	5 MHz
Channel coding	1/2 rate Convolutional code
Modulation type	16-QAM
N	128
M	512
Subcarriers spacing	9.765625 kHz
Subcarrier mapping	Localized
CP length	20 samples
Channel model	AWGN, Veh-A
Channel estimation	Perfect
Equalization	MMSE

To study the effect of *d* on PAPR performance, CCDF curves of proposed companding technique for different values of *d* are presented in Fig. 4.3. It can be observed that PAPR can be reduced by increasing *d* values.

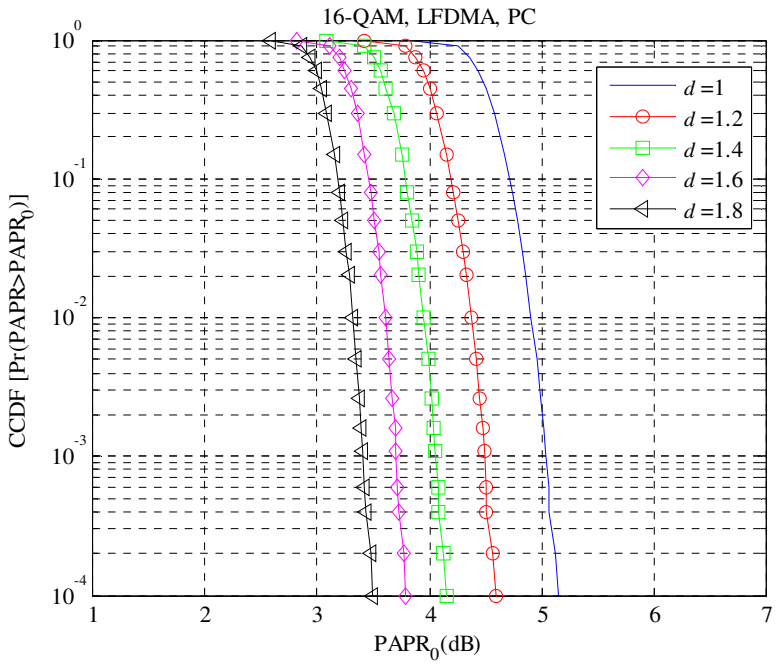

Fig. 4.3. CCDF curves of proposed companding technique for different values of *d*.

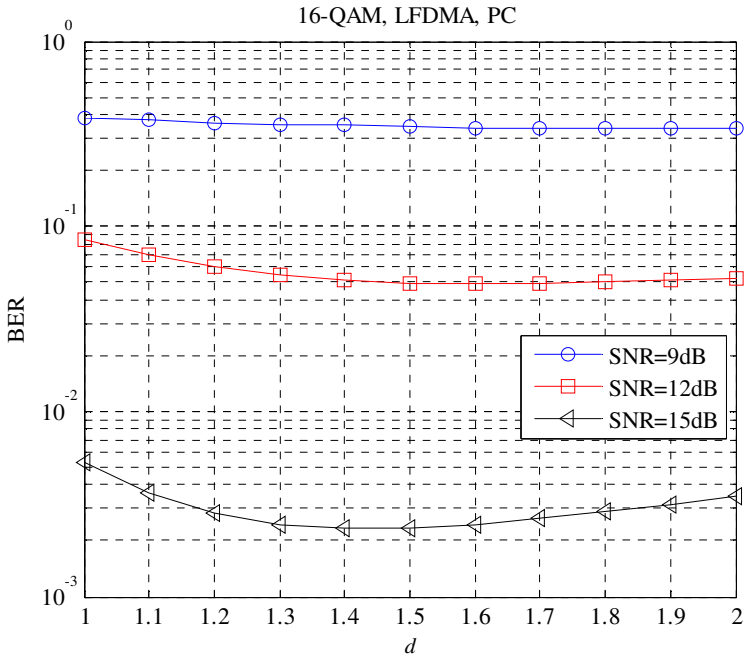

Fig. 4.4. BER vs *d* plot of proposed companding technique for different SNR values.

To find the optimum value of *d* that achieves the minimum BER, BER vs *d* plot of proposed companding technique for different SNR values is presented in Fig. 4.4. It can be observed that $d = 1.5$ is the best choice for better BER performance.

This can also be analysed from Fig. 4.5 which shows the transformation profile of proposed companding technique. In Fig. 4.5 when $d = 1$, $h(x)$ compresses x in the range 0 to 0.1 instead of expanding. PAPR can be reduced when smaller values are expanded and larger values are compressed. Hence PAPR reduction will be minimum when $d = 1$ and PAPR can be reduced by increasing the value of *d*.

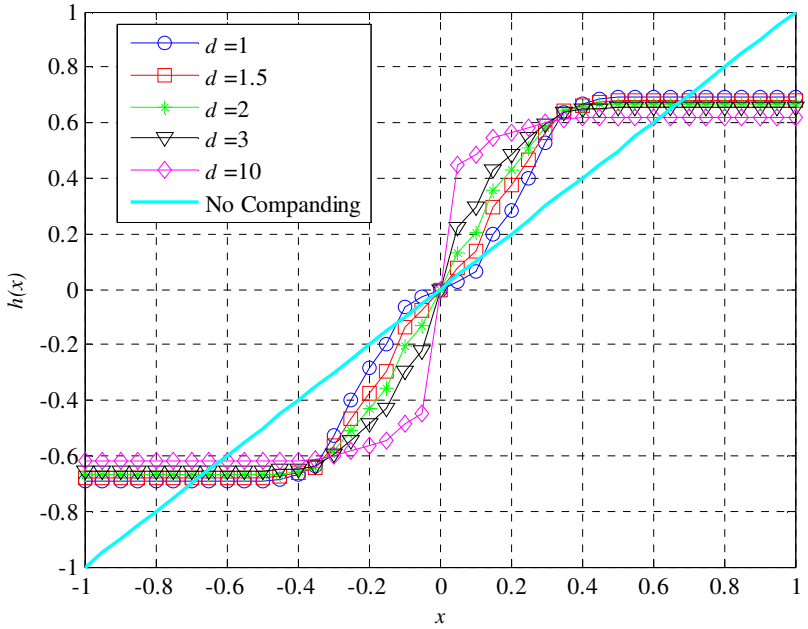

Fig. 4.5. Transformation profile of proposed companding technique.

When coming to BER performance it can be observed that when d = 1.5 the profile is closer to the ideal profile (No companding). Hence it provides better BER performance. As d increases or decreases beyond 1.5 the profile moves farther from ideal profile hence increasing BER. So as a trade-off between PAPR and BER performances we chose d = 1.5 as optimum value for proposed companding technique.

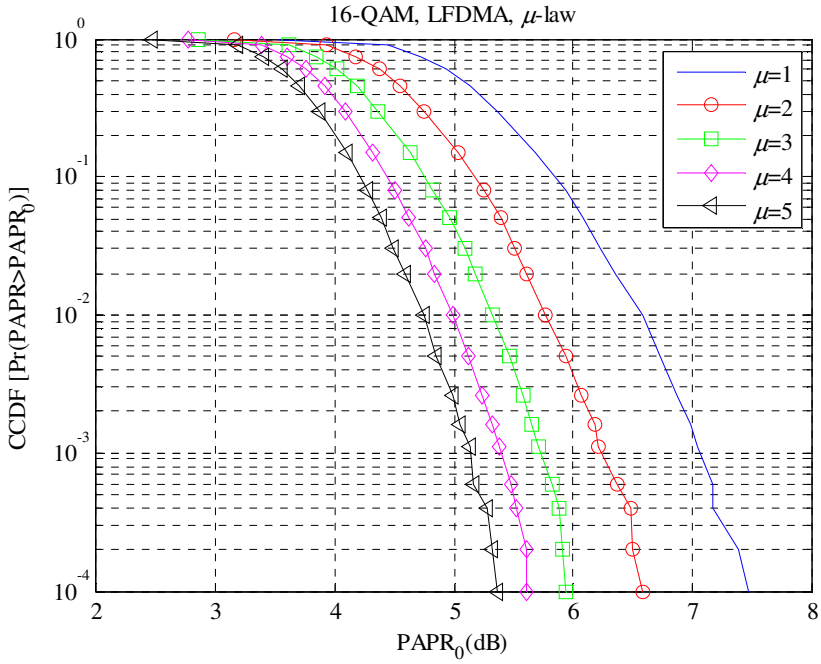

Fig. 4.6. PAPR performance of μ-law companding for different 'μ'.

Fig. 4.6 shows CCDF of μ-law companding for different values of 'μ'. It can be noted that PAPR value decreases as 'μ' value is increased. BER versus 'μ' plot of μ-law companding at different SNR values is illustrated in Fig. 4.7. BER value can be decreased by decreasing 'μ' value. So μ=1 is chosen for a trade-off between BER and PAPR performances.

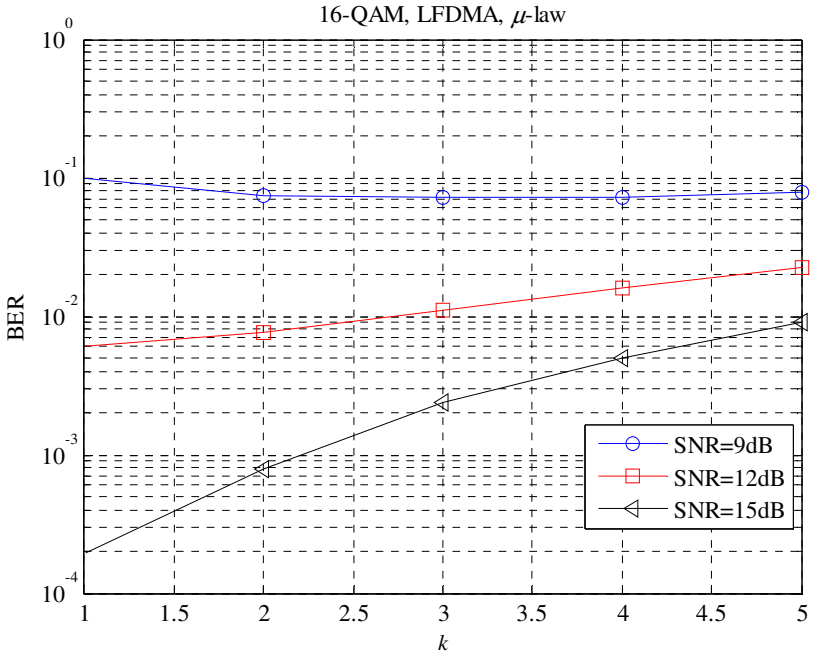

Fig. 4.7. BER vs 'μ' plot of μ-law companding for different SNR.

To make sure that the proposed companding technique does not increase the average power of the signal we have plotted waveforms of the original SC-FDMA signal, μ-law companded signal, and signal companded by the proposed technique in Fig. 4.8. From the figure, it can be observed that μ law companding increases the average power of the signal but proposed companding technique does not increase the average power of companded signal.

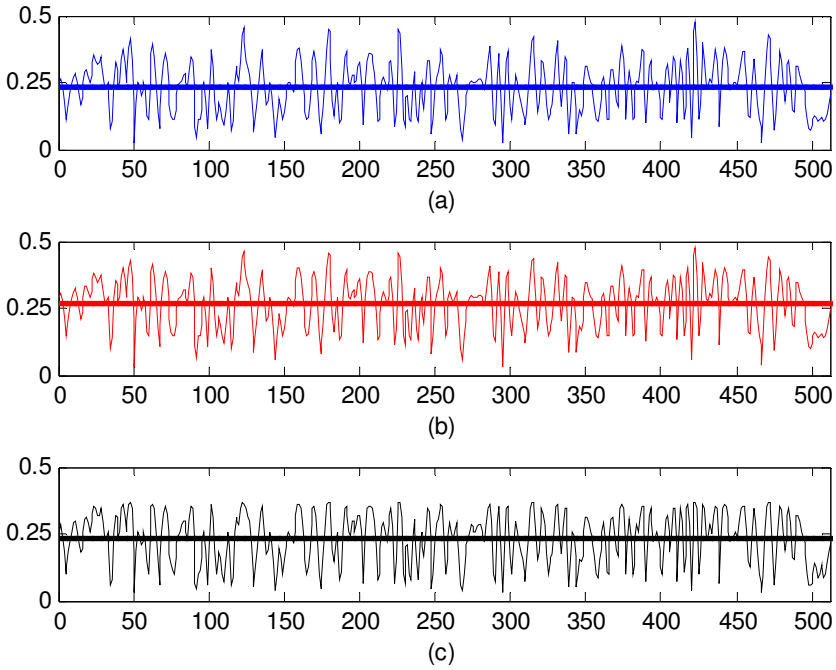

Fig. 4.8. Waveforms of original and companded signals (a) Original SC-FDMA signal (b) μ-law companded signal (c) Signal companded by proposed technique.

To find the optimum value of clipping ratio for hybrid system, BER vs CR curve has been presented in Fig. 4.9. From this plot we can say that BER can be reduced by increasing the clipping ratio. It can be noticed that, for CR values higher than 1.45, BER performance remains almost unchanged.

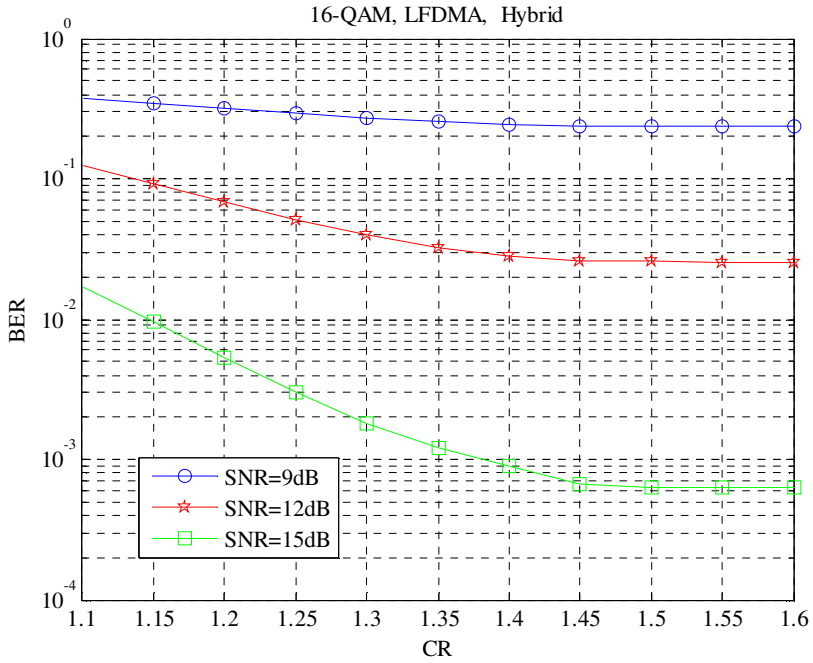

Fig. 4.9. BER vs CR curve of proposed hybrid technique.

Waveforms of companded and clipped companded signals are plotted in Fig. 4.10. As seen in the figure, there is more information loss when CR = 1.4. Hence BER performance has been degraded when CR=1.4. But when CR=1.45 the information loss is very less. Due to these minute changes in the peaks of clipped signal the BER has not been effected significantly.

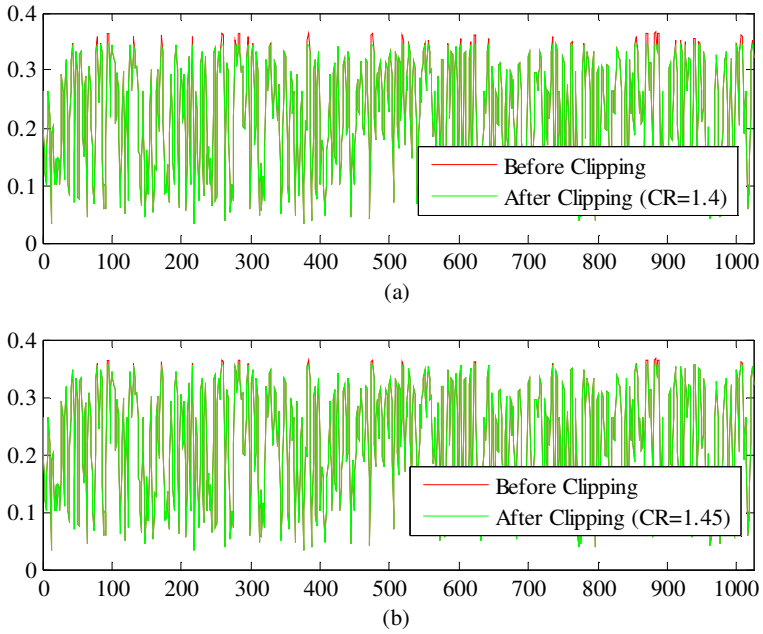

Fig. 4.10. Waveforms before and after clipping.

CCDF curves of original SC-FDMA signal, μ-law companded signal, signal companded by using proposed technique and hybrid technique are shown in Fig. 4.11. We can observe that the proposed companding technique provides better PAPR reduction when compared to μ-law companding technique. When the companded signal is clipped by hybrid technique, PAPR has been further improved. Hybrid technique with lower clipping ratio provides better PAPR reduction as the signal will be clipped to smaller amplitudes thus leading to lower PAPR. Table 4.4 gives a comparison of PAPR values of various companding techniques at CCDF = 10^{-4}.

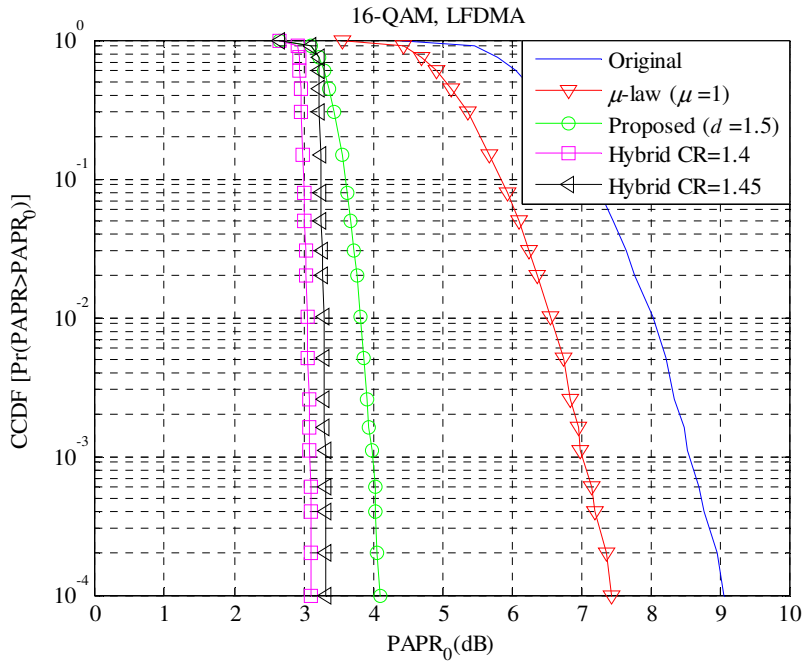

Fig. 4.11. CCDF curves of original and companded signals.

Table 4.4. PAPR values at CCDF=10^{-4}

	Original	**μ-law**	**Proposed Companding**	**Hybrid (CR=1.4)**	**Hybrid (CR=1.45)**
PAPR (dB)	9.07	7.45	4.07	3.11	3.33

BER performance curves of original and companded signals over AWGN channel in the presence of SSPA are shown in Fig. 4.12. BER performance of the proposed companding technique has been slightly degraded when compared to the original system. BER performance of hybrid technique is closer to that of proposed companding when CR=1.45 but slightly degraded when CR = 1.4.

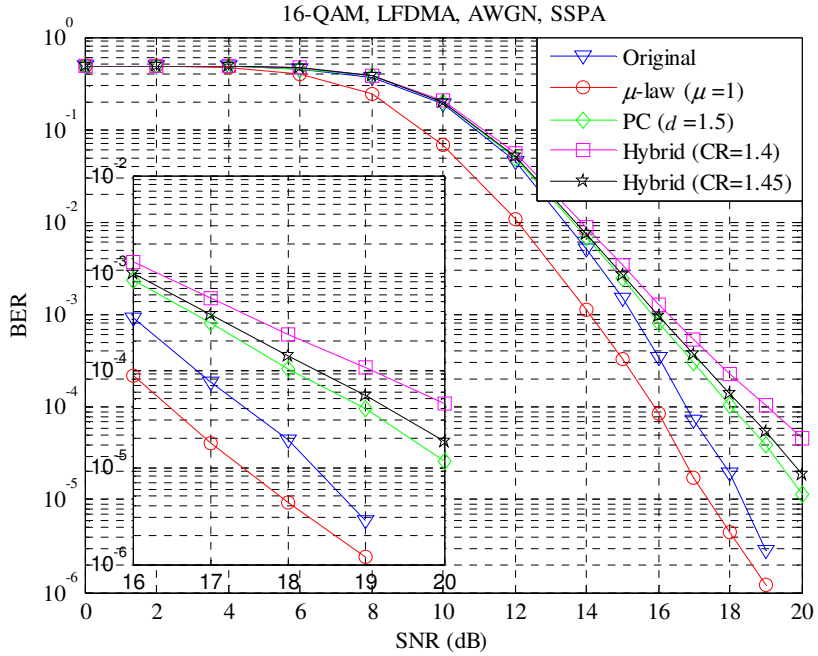

Fig. 4.12. BER curves of original and companded signals with SSPA over AWGN channel.

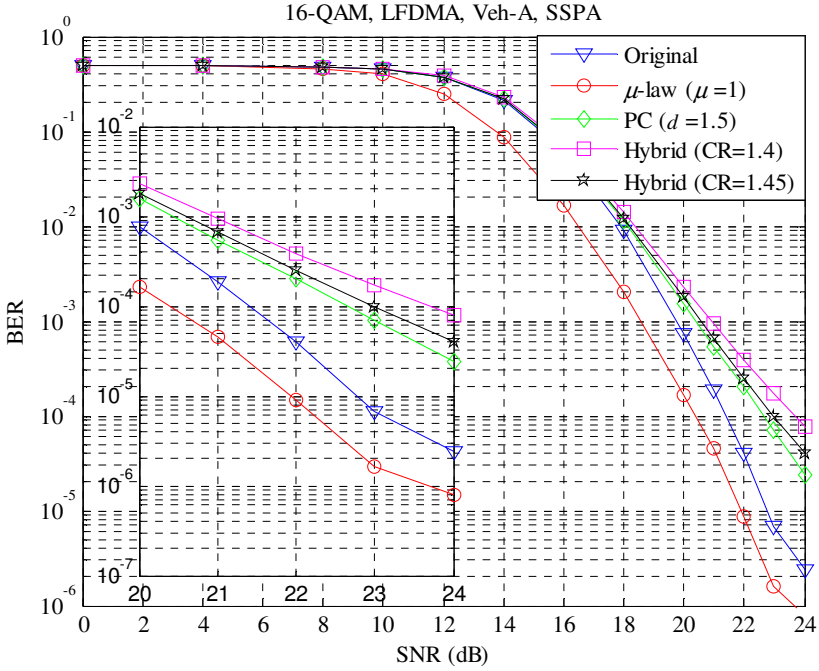

Fig. 4.13. BER curves of original and companded signals with SSPA over Veh-A channel.

BER curves of the original and companded signals over Vehicular-A outdoor channel with SSPA are shown in Fig. 4.13. It can be observed that the proposed companding technique is robust to multipath fading environment also. Table 4.5 gives the comparison of SNR values required for a BER of 10^{-4} for various companding techniques.

Table 4.5. SNR values at BER=10^{-4}

	Original	**μ-law**	**Proposed Companding**	**Hybrid (CR=1.4)**	**Hybrid (CR=1.45)**
AWGN	16.9	15.94	18	19.07	18.45
Veh-A	21.58	20.55	22.57	23.76	22.98

Table 4.6 presents the values of PAPR reduction at CCDF = 10^{-4} and additional SNR required to maintain a BER of 10^{-4} over Veh-A channel for various companding schemes when compared to the original signal. Proposed companding provides a PAPR reduction of about 5 dB but require 0.99 dB excess SNR to maintain BER constant. μ-law companding has better BER performance than proposed companding but provides a PAPR reduction of 1.62 dB only. Hybrid system with CR=1.45 has better net gain (PAPR reduction - additional SNR).

Table 4.6. Performance analysis of various techniques

Companding	**PAPR Reduction (dB)**	**Additional SNR (dB)**	**Net Gain (dB)**
μ-law	1.62	-1.03	2.65
Proposed	5	0.99	4.01
Hybrid (CR=1.4)	5.96	2.18	3.78
Hybrid (CR=1.45)	5.74	1.4	4.34

4.3. DCT SC-FDMA System

In [70] authors presented sinusoidal transforms as an alternative to DFT for OFDM. This enabled authors in [17] to propose a new SC-FDMA system based on the DCT Type-II. DCT's energy compaction property enables it to pack most of the signal energy into the first few samples, reducing inter-symbol interference (ISI) due to relatively small amplitudes at high frequency indices [106], [107]. This results in a lower bit error rate (BER) when compared to DFT. Also, it uses only real arithmetic instead of complex arithmetic used in DFT. In [103] authors concluded that DCT SC-FDMA system outperforms DFT SC-FDMA system in terms of BER performance. But, DCT SC-FDMA system has slightly higher PAPR than DFT SC-FDMA system.

Table 4.7. List of Symbols

Symbol	Description
$x(n)$	Modulated symbols
N	Input block size
$X(k)$	DFT of $x(n)$
$S(l)$	Frequency-domain samples after the subcarriers mapping
M	Number of subcarriers
$s(m)$	IDFT of $S(l)$
$f_{\lvert s_m \rvert}(x)$	PDF of $\lvert s(m) \rvert$
$F_{\lvert s_m \rvert}(x)$	CDF of $\lvert s(m) \rvert$
y_m	Companded signal
$h(x)$	Companding function
r_m	Received signal
c_m	Clipped signal
A	Clipping level threshold

4.4. DCT SC-FDMA System with Companding and Clipping

The proposed DCT SC-FDMA system with companding and clipping is illustrated in Fig. 4.14.

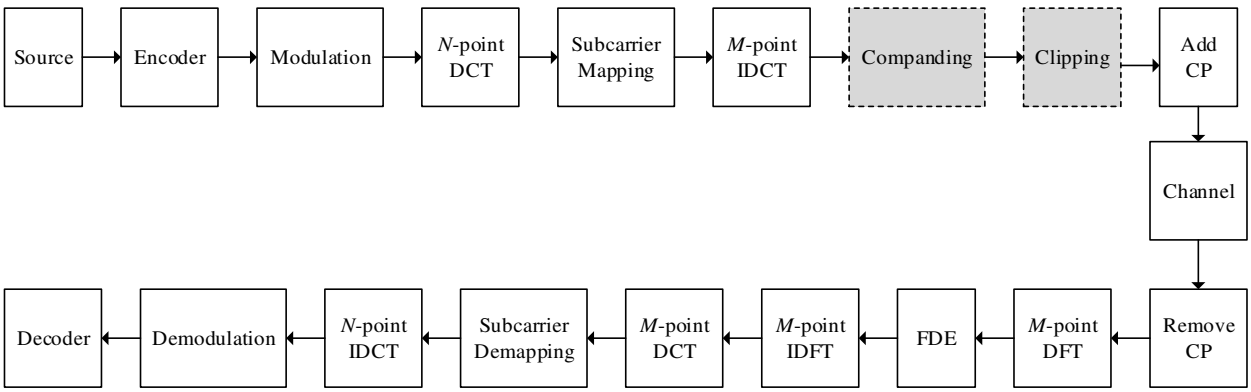

Fig. 4.14. Proposed DCT SC-FDMA System with Companding followed by Clipping.

After encoding, the modulated symbols are grouped into N symbol blocks, and are sent through N-point DCT to produce

$$X(k)=\sqrt{\frac{2}{N}}\beta(k)\sum_{n=0}^{N-1}x(n)\cos\left(\frac{\pi k(2n+1)}{2N}\right),k=0,1,...,N-1 \tag{4.14}$$

where $x(n),(n=0,1,...,N-1)$ are the modulated symbols and $\beta(k)$ is given by

$$\beta(k)=\begin{cases}\frac{1}{\sqrt{2}} & k=0\\ 1 & k=1,2,....N-1\end{cases} \tag{4.15}$$

These N symbols are then mapped to M subcarriers ($M>N$, $M=Q.N$) by using either localized or interleaved mapping. In localized mapping, these N symbols are transmitted over adjacent subcarriers. After subcarrier mapping, $S(l)$ is given by

$$S(l)=\begin{cases}X(l), & 0\le l\le N-1\\ 0 & N\le l\le M-1\end{cases} \tag{4.16}$$

Now $S(l)$ are sent through M-point IDCT to produce time domain signal given by

$$\mathrm{s}(m)=\sqrt{\frac{2}{M}}\sum_{l=0}^{M-1}S(l)\beta(l)\cos\left(\frac{\pi l(2m+1)}{2M}\right),m=0,1,...,M-1 \tag{4.17}$$

Let $m = Qn + q$, where $0\le n\le N-1$ and $0\le q\le Q-1$. Then the DCT LFDMA time domain signal is given by

$$s(m)=s(Qn+q)=\sqrt{\frac{2}{QN}}\sum_{k=0}^{N-1}X(k)\beta(k)\cos\left(\frac{\pi k(2Qn+2q+1)}{2QN}\right) \tag{4.18}$$

By substituting equation (4.14) in (4.18) we get

$$s(m)=\frac{1}{\sqrt{Q}}\sqrt{\frac{2}{N}}\sum_{k=0}^{N-1}\left(\beta^2(k)\sum_{p=0}^{N-1}x(p)\cos\left(\frac{\pi k(2p+1)}{2N}\right)\right)\cos\left(\frac{\pi k(2Qn+2q+1)}{2M}\right) \tag{4.19}$$

As the time-domain DCT LFDMA symbols in equation (4.19) are sum of all the input time-domain symbols with different real weights, PAPR might be increased. Now a companding transform is applied to reduce PAPR of this time domain signal. To design the companding transform, we need the distribution of DCT SC-FDMA signal. So first we approximate its distribution.

4.4.1. Approximation of DCT SC-FDMA Distribution

The PDF of the magnitude of 16-QAM modulated DCT LFDMA signal, $|s(m)|$ is plotted by using MATLAB simulations. Then curve fitting tool is used to obtain its expression. Fig. 4.15 presents the actual histogram and approximated PDF of DCT LFDMA. The PDF of DCT LFDMA signal magnitude can be approximated as given below.

$$f_{|s_m|}(x) = \sum_{i=1}^{3} a_i e^{-\left(\frac{x-b_i}{c_i}\right)^2}, \quad x \geq 0 \tag{4.20}$$

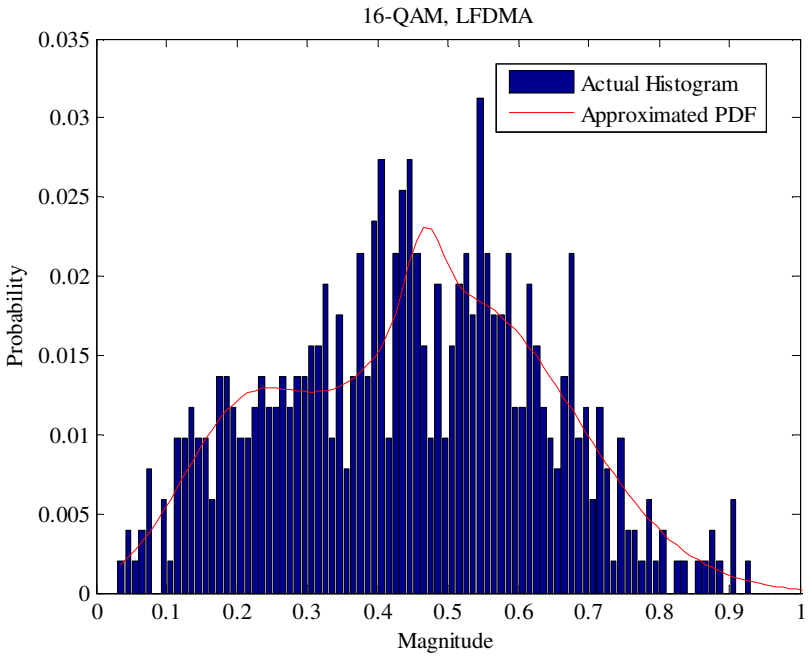

Fig. 4.15. Actual histogram and approximated PDF of DCT LFDMA signal.

Curve fitting tool provides the values of a_i, b_i and c_i by considered 100 samples and the goodness statistics of our approximation are illustrated in Table 4.8.

Table 4.8. Goodness-of-Fit Statistics

Statistic	Value
Sum of squares due to error (SSE)	0.001429
R-square	0.8479
Adjusted R-square	0.8241
Root mean squared error (RMSE)	0.003621

The Cumulative Distribution Function is given by

$$\begin{aligned} F_{|s_m|}(x) &= P\{|s_m| \le x\} \\ &= \int_{-\infty}^{x} \sum_{i=1}^{3} a_i e^{-\left(\frac{x-b_i}{c_i}\right)^2} dx \end{aligned} \tag{4.21}$$

Let $\frac{x-b_i}{c_i} = \frac{z}{\sqrt{2}}$ then equation (4.21) can be modified as

$$\begin{aligned} F_{|s_m|}(x) &= \sum_{i=1}^{3} \int_{-\infty}^{\frac{\sqrt{2}(x-b_i)}{c_i}} a_i e^{-Z^2/2} \frac{c_i}{\sqrt{2}} dz \\ &= \sum_{i=1}^{3} \sqrt{\pi} a_i c_i \Phi\left[\sqrt{2}\left(\frac{x-b_i}{c_i}\right)\right] \\ &= \sum_{i=1}^{3} \frac{\sqrt{\pi} a_i c_i}{2}\left[1 + erf\left(\frac{x-b_i}{c_i}\right)\right], \; x \ge 0 \end{aligned} \tag{4.22}$$

where $\Phi(z) = \frac{1}{\sqrt{2\pi}} \int_{-\infty}^{z} e^{-z^2/2} dz = \frac{1}{2}\left[1 + erf\left(\frac{x}{\sqrt{2}}\right)\right]$ is the CDF of standard normal distribution and erf(.) is error function.

4.4.2. Proposed Companding Transform

The proposed companding transform is given by

$$y_m = h(s_m) \tag{4.23}$$

where y_m is the companded signal of input s_m. Let the d^{th} power of $|y_m|$ have a triangular distribution in the range [0, c] as shown in Fig. 4.16, while d being the degree of companding.

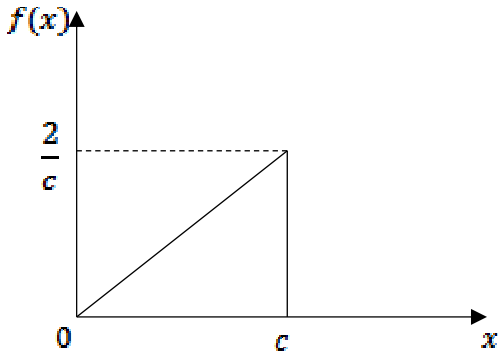

Fig. 4.16. PDF of proposed triangular distribution.

So the PDF of the proposed distribution is

$$f_{|y_m|^d}(x) = \frac{2x}{c^2},\ 0 \le x \le c \tag{4.24}$$

Then the CDF of $|y_m|^d$ is

$$F_{|y_m|^d}(x) = \frac{x^2}{c^2},\ 0 \le x \le c \tag{4.25}$$

Then CDF of $|y_m|$ can be described as

$$\begin{aligned} F_{|y_m|}(x) &= P\{|y_m| \le x\} \\ &= P\{|y_m|^d \le x^d\} \\ &= \frac{x^{2d}}{c^2},\ 0 \le x \le \sqrt[d]{c} \end{aligned} \tag{4.26}$$

The inverse of $F_{|y_m|}$ can be written as

$$F^{-1}_{|y_m|}(x) = \left(c^2 x\right)^{\frac{1}{2d}},\ 0 \le x \le 1 \tag{4.27}$$

As $h(x)$ is a strictly monotonically increasing function

$$\begin{aligned} F_{|s_m|}(x) &= P\{|s_m| \le x\} \\ &= P\{h(|s_m|) \le h(x)\} \\ &= P\{|y_m| \le h(x)\} \\ &= F_{|y_m|}(h(x)) \end{aligned} \tag{4.28}$$

As $h(x)$ does not alter the input signal's phase, it is formulated as

$$\begin{aligned} &F_{|y_m|}(x) = P\{|y_m| \le x\} \\ &h(x) = F^{-1}_{|y_m|}\left(F_{|s_m|}(x)\right) \\ &\quad = \mathrm{sgn}(x)\left(c^2 \sum_{i=1}^{3} \frac{\sqrt{\pi} a_i c_i}{2}\left[1 + erf\left(\frac{|x| - b_i}{c_i}\right)\right]\right)^{\frac{1}{2d}} \end{aligned} \tag{4.29}$$

where sgn(.) is the sign function. To maintain the average power of y_m at the same level of s_m,

$$
\begin{aligned}
E\left[\left|s_m\right|^2\right] &= E\left[\left|y_m\right|^2\right] \\
&= E\left[\left|h(s_m)\right|^2\right] \\
&= E\left[\left(c^2\sum_{i=1}^{3}\frac{\sqrt{\pi}a_i c_i}{2}\left[1+erf\left(\frac{\left|s_m\right|-b_i}{c_i}\right)\right]\right)^{1/d}\right]
\end{aligned}
\tag{4.30}
$$

Hence c can be derived as

$$
c=\left(\frac{E\left[\left|s_m\right|^2\right]}{E\left[\left(\sum_{i=1}^{3}\frac{\sqrt{\pi}a_i c_i}{2}\left[1+erf\left(\frac{\left|s_m\right|-b_i}{c_i}\right)\right]\right)^{1/d}\right]}\right)^{d/2}
\tag{4.31}
$$

Now s_m is sent through $h(x)$ to give y_m. Then the signal y_m is clipped to a specific threshold, A as [7]

$$
c_m=\begin{cases} y_m, & if\ \left|y_m\right|\le A \\ Ae^{j\psi_m}, & if\ \left|y_m\right|>A \end{cases}
\tag{4.32}
$$

where c_m is the clipped signal and $\psi_m = \arg[\, y_m\,]$. Clipping ratio (CR) is defined as

$$
\mathrm{CR}=\frac{A}{\sqrt{P_{av}}}
\tag{4.33}
$$

where P_{av} is average power of input signal. As the clipping is done after companding, PAPR can be reduced further. As the companded signal does not have many peaks, the following clipping stage does not degrade BER performance significantly by cautiously choosing CR. Now cyclic prefix (CP) is appended to c_m and transmitted via wireless channel.

At the receiver side, after removing the CP, the resulting signal, r_m is sent through M-point DFT to perform Frequency Domain Equalization (FDE) and then transformed back to time domain by using M-point IDFT. Now the corresponding DCT SC-FDMA demodulation operations will be carried out to detect the transmitted data.

4.4.3. Performance Evaluation

Performance of the proposed companding transform is evaluated by considering DCT SC-FDMA system as illustrated in Fig. 4.14 with N=128, M=512, 16-QAM modulation, and

localized subcarrier mapping. The CP length is 20 samples, and 1/2 rate convolutional channel coding is used. We have used perfect channel estimation with MMSE equalization.

To study the influence of *d* on the performance of PAPR, Fig. 4.17 presents the CCDF curves of proposed companding transform for different values of *d*. By increasing value of *d*, PAPR can be reduced.

From BER vs *d* plot of proposed companding transform as presented in Fig. 4.18 it is clear that $d = 0.7$ provides minimum BER. Considering both CCDF and BER plots, $d = 0.7$ is chosen for a trade-off between the BER and PAPR performances. Hence we use $d = 0.7$ for the rest of the simulations.

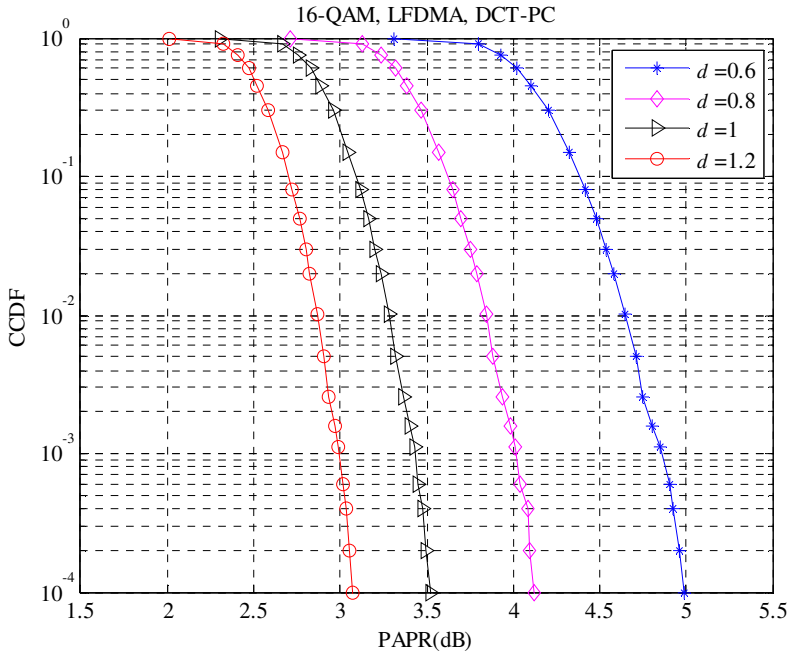

Fig. 4.17. CCDF curves of proposed companding transform for different '*d*'.

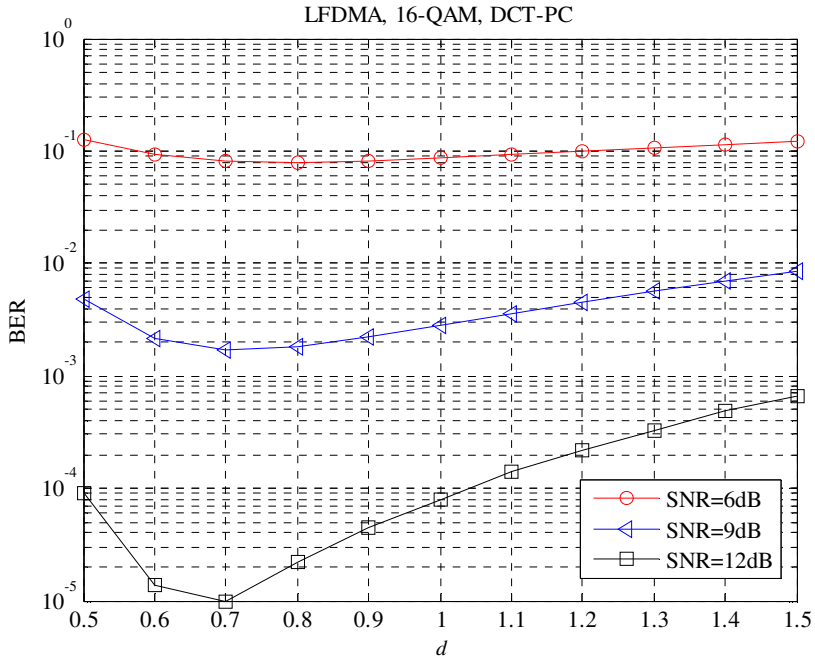

Fig. 4.18. BER vs *d* plot of proposed companding transform.

Fig. 4.19 shows BER vs *d* plot of absolute exponential companding [93] transform for different values of SNR. It can be observed that d = 1.1 provides minimum BER. Fig. 4.20 shows BER vs μ plot of μ-law companding [108] for different values of SNR. It can be observed that μ = 1 provides minimum BER.

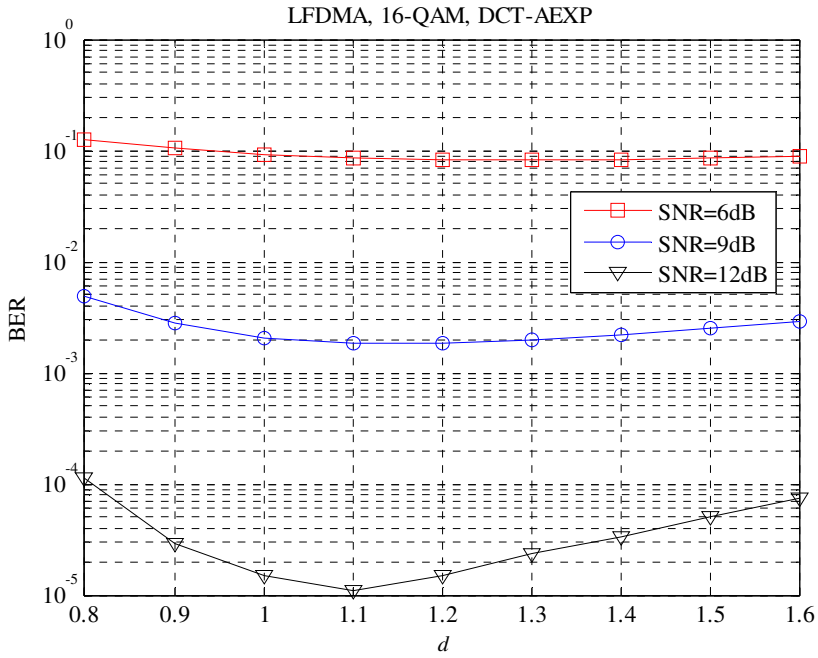

Fig. 4.19. BER vs *d* plot of absolute exponential companding.

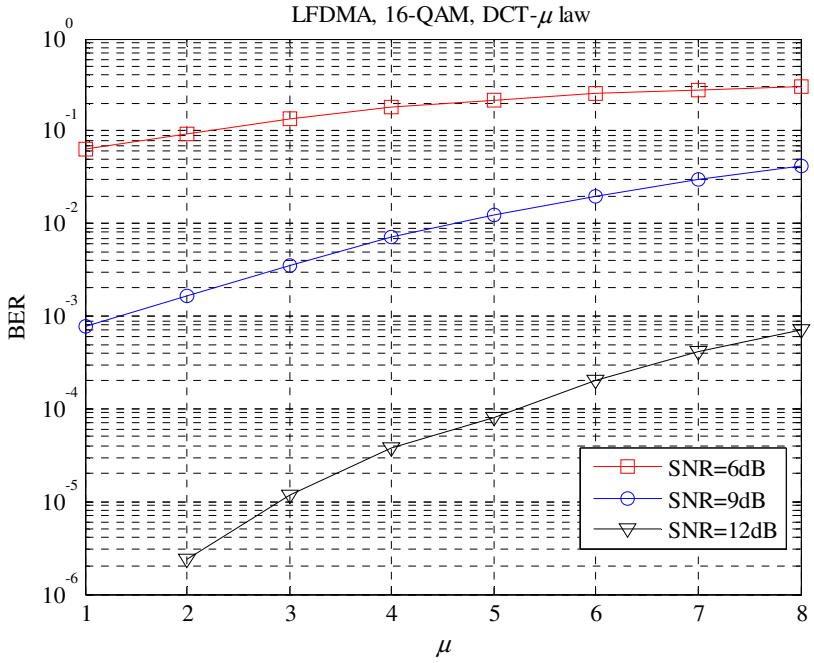

Fig. 4.20. BER vs μ plot of μ-law companding.

The magnitudes of DCT LFDMA signal, μ law companded signal, and signal companded by the proposed transform are plotted in Fig. 4.21. It can be observed that proposed companding transform maintains the average power while μ law companding increases the average power.

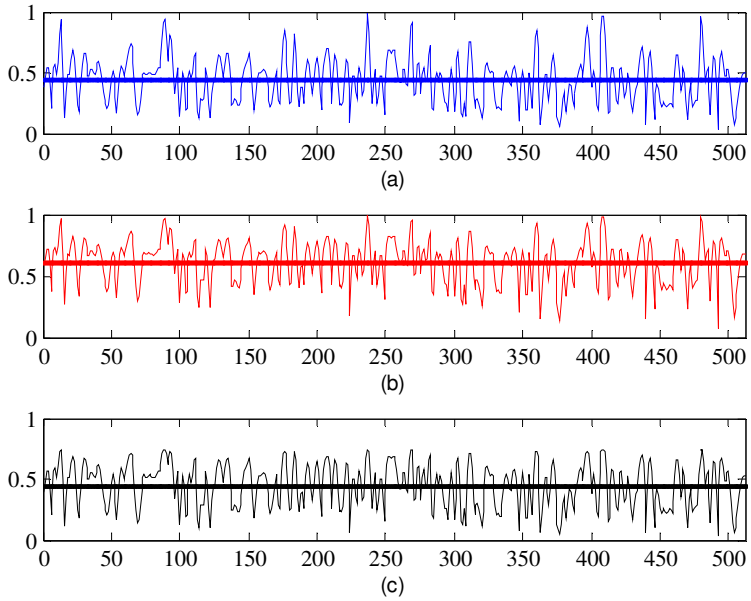

Fig. 4.21. Magnitude of (a) DCT LFDMA signal (b) μ-law companded signal (c) Signal companded by proposed transform.

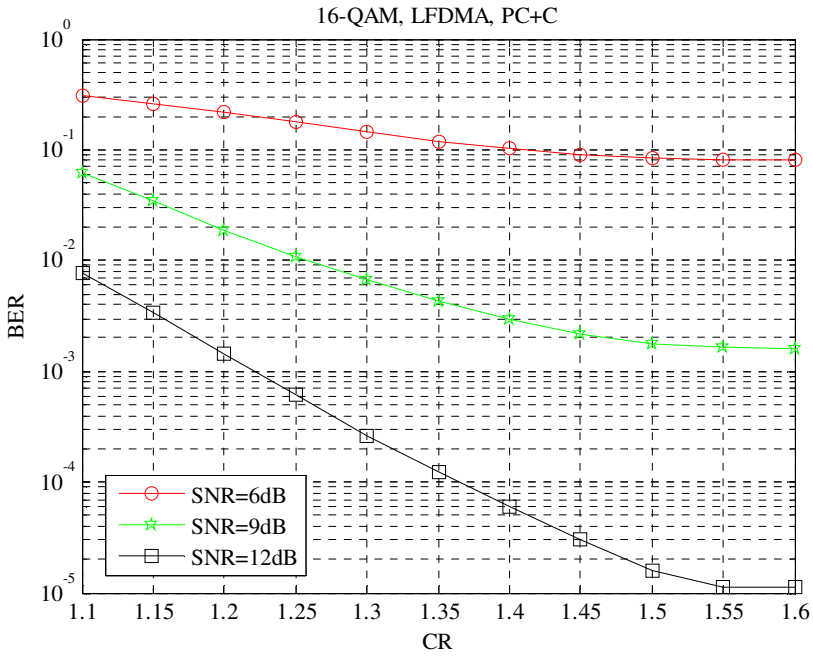

Fig. 4.22. BER versus CR plot of proposed companding + clipping for different values of SNR.

BER vs CR plot of proposed companding transform + clipping for different values of SNR is shown in Fig. 4.22. It can be observed that CR values greater than 1.5 doesn't degrade the BER performance. So we consider CR=1.45 and 1.5 for the rest of the simulations.

Companded and clipped signal magnitudes are presented in Fig. 4.23. When CR = 1.45 the information loss is more there by degrading BER performance. However when CR=1.5, clipping does not degrade BER significantly.

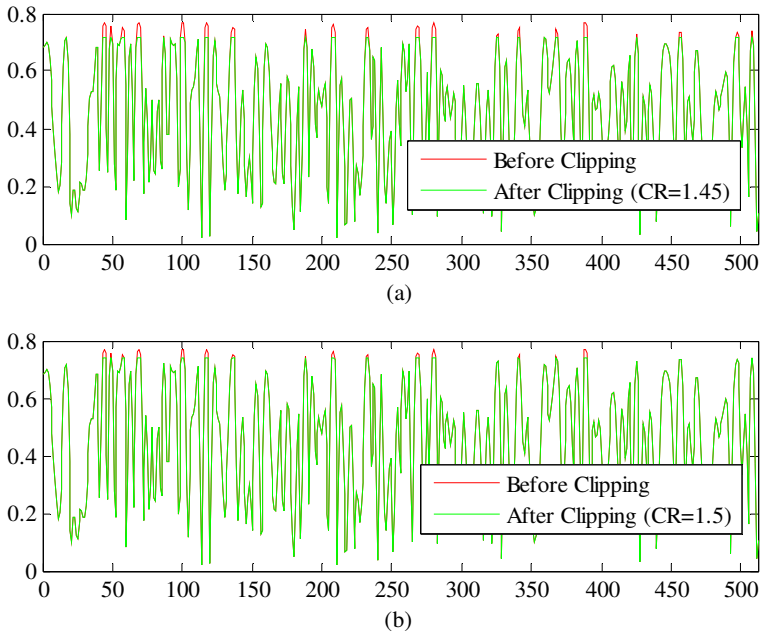

Fig. 4.23. Companded and clipped signal magnitudes when (a) CR = 1.45 (b) CR=1.5.

CCDF plot of various companding transforms is presented in Fig. 4.24. DCT with proposed companding transform (DCT-PC) has low PAPR than DCT-μ, DCT SC-FDMA and DFT SC-FDMA systems. When the companding operation is followed by clipping, PAPR is reduced further. DCT with proposed companding followed by clipping (DCT-PC+C) provides low PAPR when the clipping ratio is low. PAPR values of various companding transforms at CCDF = 10^{-4} are given in Table 4.9.

From Table 4.9 it can be observed that DCT-PC provides a PAPR reduction of about 4.44 dB at CCDF=10^{-4}, while DCT-AEXP provides about 4.71 dB when compared to the DFT SC-FDMA system. DCT-PC+C reduces PAPR by about 5.54 dB and 5.34 dB when CR = 1.45 and 1.5 respectively.

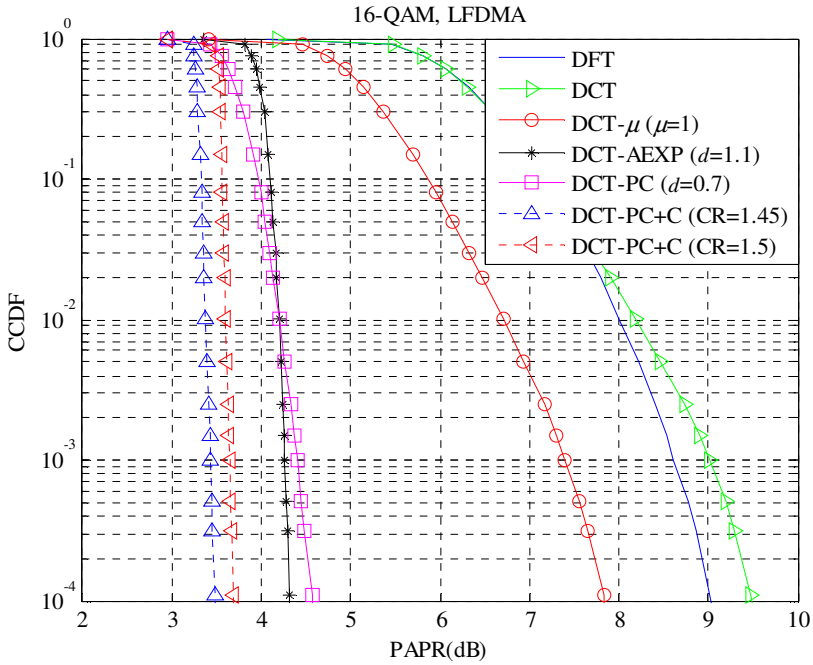

Fig. 4.24. CCDF plot of various companding transforms.

Table 4.9. PAPR values at CCDF=10^{-4}

	DFT	**DCT**	**DCT-μ (μ =1)**	**DCT-AEXP (d =1.1)**	**DCT-PC (d =0.7)**	**DCT-PC+C (CR=1.45)**	**DCT-PC+C (CR=1.5)**
PAPR (dB) at CCDF=10^{-4}	9.02	9.50	7.83	4.31	4.58	3.48	3.68

BER plot of various companding transforms over AWGN channel considering Solid State Power Amplifier (SSPA) with IBO=5 dB and p=2 is presented in Fig. 4.25. Proposed DCT-PC system's performance is slightly degraded than DCT system but has better performance than DCT-AEXP system. The proposed DCT-PC+C system's performance is close to that of DCT-PC system when CR=1.5 but degraded when CR=1.45.

BER plot of various companding transforms over Vehicular-A outdoor channel with SSPA is shown in Fig. 4.26. It can be observed that the proposed companding technique is robust to multipath fading environment also. SNR values at a BER of 10^{-5} for various companding techniques are displayed in Table 4.10.

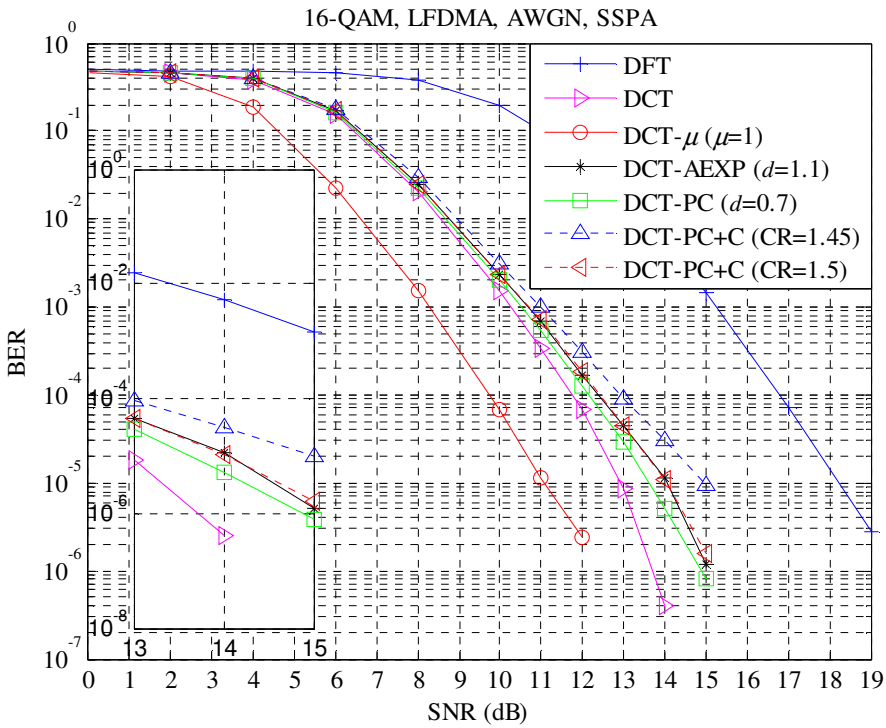

Fig. 4.25. BER plot of various companding transforms with SSPA over AWGN channel.

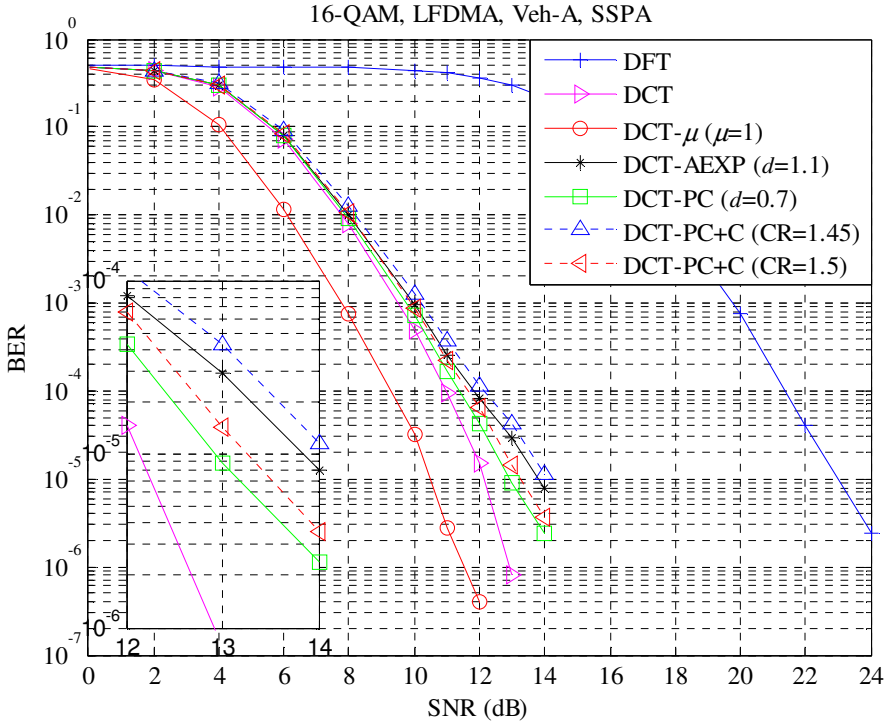

Fig. 4.26. BER plot of various companding transforms with SSPA over Veh-A outdoor channel.

Table 4.10. SNR at BER=10^{-5}

	DFT	**DCT**	**DCT-μ (μ =1)**	**DCT-AEXP (d =1.1)**	**DCT-PC (d =0.7)**	**DCT-PC+C (CR=1.45)**	**DCT-PC+C (CR=1.5)**
AWGN	18.80	12.97	11.17	14.12	13.8	14.98	14.09
Veh-A	23.60	12.34	10.75	13.91	12.96	14.41	13.41

Table 4.11 presents the values of PAPR reduction at CCDF = 10^{-4} and additional SNR required to maintain a BER of 10^{-5} over Veh-A channel for various companding schemes when compared to the DCT SC-FDMA system. DCT-PC provides a PAPR reduction of about 4.92 dB but require 0.62 dB excess SNR to maintain BER constant. DCT-PC has better net gain than DCT-AEXP. Hybrid system with CR=1.5 has better net gain (PAPR reduction - additional SNR).

Table 4.11. Performance analysis of various techniques

Companding	**PAPR Reduction (dB)**	**Additional SNR (dB)**	**Net Gain (dB)**
μ-law	1.67	-1.59	3.26
AEXP	5.19	1.57	3.62
PC	4.92	0.62	4.3
PC+C (CR=1.45)	6.02	2.07	3.95
PC+C (CR=1.5)	5.82	1.07	4.75

The power spectral density (PSD) plot of various techniques is presented in Fig. 4.27. It can be observed that the proposed companding (PC) technique causes lower spectrum side lobes when compared to the absolute exponential (AEXP) companding technique and μ-law causes in-band distortion.

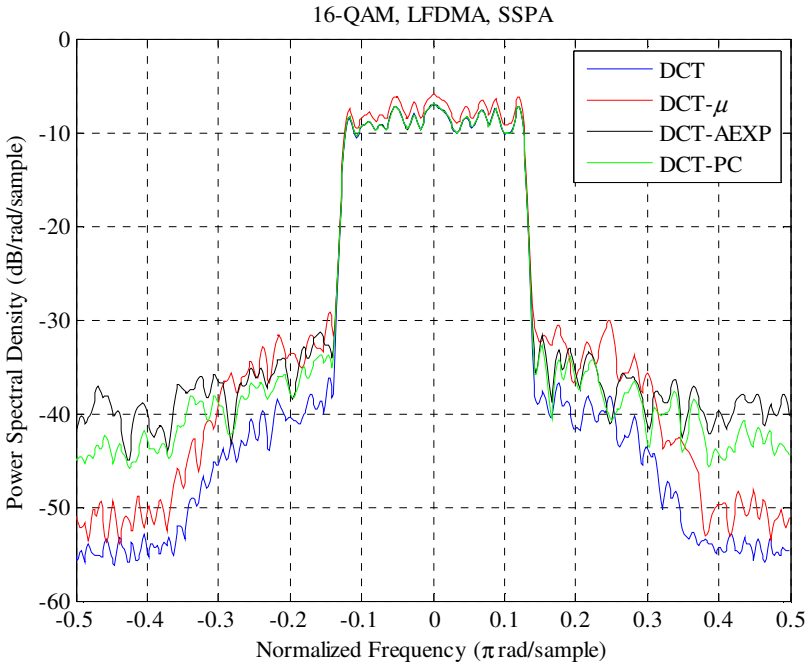

Fig. 4.27. PSD plot of various techniques with SSPA.

4.5. Conclusion

In this chapter, we have approximated the distributions of DFT and DCT SC-FDMA signals by using curve fitting and proposed companding transforms based on their distributions. Proposed techniques provide better PAPR reduction when compared to μ-law companding with a slight degradation in BER performance. Hybrid techniques further improve the PAPR, with similar BER performance as that of proposed techniques by carefully choosing clipping ratio.

Chapter-5

Performance Analysis of Walsh Hadamard Transform based SC-FDMA System

5.1. Introduction

In [18], a new transceiver design for SC-FDMA system based on Discrete Wavelet Transform (DWT) has been proposed. DWT based SC-FDMA system has superior BER and PAPR performances when compared to DFT SC-FDMA system. Hence we can conclude that DCT SC-FDMA system and DWT SC-FDMA system has superior BER performance when compared to the conventional DFT based SC-FDMA system.

In this chapter we propose a new transceiver for SC-FDMA system based on Walsh Hadamard Transform (WHT). WHT is the most well-known non-sinusoidal orthogonal transform which can be computed using real additions and subtractions [109]. It has gained prominence in various digital signal processing applications, as its hardware implementation is simple. We study performance of different ordered WHT systems over AWGN and multipath fading environments and derive the time domain symbols for different ordered WHT systems. We then use exponential companding technique in WHT SC-FDMA system to further reduce its PAPR without degrading BER performance.

5.2. Walsh Hadamard Transform

Walsh Hadamard Transform of a sequence is given by

$$\mathbf{X}_N = \frac{1}{N}\mathbf{H}_N\mathbf{x}_N \tag{5.1}$$

where $\mathbf{H}_N$ is a Hadamard matrix of order N and $\mathbf{x}_N = [x_1\ x_2\ ....\ x_N]^T$ is an $N\times1$ matrix. The Hadamard matrix of order N (where $N = 2^n$, n is a positive integer) can be defined recursively by using

$$\mathbf{H}_N = \begin{bmatrix} \mathbf{H}_{N/2} & \mathbf{H}_{N/2} \\ \mathbf{H}_{N/2} & -\mathbf{H}_{N/2} \end{bmatrix}, \text{where}$$

$$\mathbf{H}_1 = [1], \mathbf{H}_2 = \begin{bmatrix} 1 & 1 \\ 1 & -1 \end{bmatrix}, \mathbf{H}_4 = \begin{bmatrix} 1 & 1 & 1 & 1 \\ 1 & -1 & 1 & -1 \\ 1 & 1 & -1 & -1 \\ 1 & -1 & -1 & 1 \end{bmatrix} \tag{5.2}$$

The WHT can alternatively be defined as

$$X(u) = \frac{1}{N}\sum_{m=0}^{N-1} x(m)(-1)^{\langle m,u\rangle}, u = 0,1,...,N-1 \tag{5.3}$$

where

$$\langle m,u\rangle = \sum_{s=0}^{n-1} u_s m_s;\ n = \log_2 N \tag{5.4}$$

The terms u_s and m_s are the coefficients of the binary representations of u and m respectively. The IWHT is defined as

$$x(m) = \sum_{u=0}^{N-1} X(u)(-1)^{\langle m,u\rangle}, m = 0,1,...,N-1 \tag{5.5}$$

5.2.1. Types of ordering in WHT

There are three different ordering schemes to compute Walsh Hadamard Transform namely Hadamard, Sequency, and Dyadic [110]. The Hadamard-ordered or Natural-ordered Hadamard matrix of order 8 is defined by using a recursive relation in (5.2) as

$$\left(\mathbf{H}_8\right)_h = \begin{bmatrix} 1 & 1 & 1 & 1 & 1 & 1 & 1 & 1 \\ 1 & -1 & 1 & -1 & 1 & -1 & 1 & -1 \\ 1 & 1 & -1 & -1 & 1 & 1 & -1 & -1 \\ 1 & -1 & -1 & 1 & 1 & -1 & -1 & 1 \\ 1 & 1 & 1 & 1 & -1 & -1 & -1 & -1 \\ 1 & -1 & 1 & -1 & -1 & 1 & -1 & 1 \\ 1 & 1 & -1 & -1 & -1 & -1 & 1 & 1 \\ 1 & -1 & -1 & 1 & -1 & 1 & 1 & -1 \end{bmatrix} \begin{matrix} 0 \\ 7 \\ 3 \\ 4 \\ 1 \\ 6 \\ 2 \\ 5 \end{matrix} \quad (5.6)$$

# of sign changes

It is called natural order as $\mathbf{H}$ is not ordered based on the number of sign changes in each row. If $\mathbf{H}$ is ordered with number of sign changes, then we have sequency-ordered matrix as

$$\left(\mathbf{H}_8\right)_s = \begin{bmatrix} 1 & 1 & 1 & 1 & 1 & 1 & 1 & 1 \\ 1 & 1 & 1 & 1 & -1 & -1 & -1 & -1 \\ 1 & 1 & -1 & -1 & -1 & -1 & 1 & 1 \\ 1 & 1 & -1 & -1 & 1 & 1 & -1 & -1 \\ 1 & -1 & -1 & 1 & -1 & -1 & -1 & 1 \\ 1 & -1 & -1 & 1 & -1 & 1 & 1 & -1 \\ 1 & -1 & 1 & -1 & -1 & 1 & -1 & 1 \\ 1 & -1 & 1 & -1 & 1 & -1 & 1 & -1 \end{bmatrix} \begin{matrix} 0 \\ 1 \\ 2 \\ 3 \\ 4 \\ 5 \\ 6 \\ 7 \end{matrix} \quad (5.7)$$

# of sign changes

Dyadic ordered matrix can be ordered by using Gray code. The relation between sequency-ordered and dyadic-ordered Walsh functions is given in Table 5.1. Here $b(i)$ represents the Gray code-to-binary conversion of i.

Table 5.1. Relation between sequency-ordered and dyadic-ordered Walsh functions

***i* (decimal)**	***i* (binary)**	***b*(*i*) (binary)**	***b*(*i*) (decimal)**
0	000	000	0
1	001	001	1
2	010	011	3
3	011	010	2
4	100	111	7
5	101	110	6
6	110	100	4
7	111	101	5

So the Dyadic ordered matrix arranges the sign changes as 0,1,3,2,7,6,4,5 as defined in (5.8)

$$\left(\mathbf{H}_8\right)_d = \begin{bmatrix} 1 & 1 & 1 & 1 & 1 & 1 & 1 & 1 \\ 1 & 1 & 1 & 1 & -1 & -1 & -1 & -1 \\ 1 & 1 & -1 & -1 & 1 & 1 & -1 & -1 \\ 1 & 1 & -1 & -1 & -1 & -1 & 1 & 1 \\ 1 & -1 & 1 & -1 & 1 & -1 & 1 & -1 \\ 1 & -1 & 1 & -1 & -1 & 1 & -1 & 1 \\ 1 & -1 & -1 & 1 & 1 & -1 & -1 & 1 \\ 1 & -1 & -1 & 1 & -1 & 1 & 1 & -1 \end{bmatrix} \begin{matrix} 0 \\ 1 \\ 3 \\ 2 \\ 7 \\ 6 \\ 4 \\ 5 \end{matrix} \quad \begin{matrix} \\ \\ \\ \\ \\ \\ \\ \#\text{of sign changes} \end{matrix} \tag{5.8}$$

5.3. WHT based SC-FDMA System Model with Exponential Companding

The proposed WHT based SC-FDMA transceiver with exponential companding is depicted in Fig. 5.1. Input symbols are encoded and mapped to the complex symbols by any of the modulation techniques (BPSK, QPSK, or M-QAM) and passed through *N*-point WHT to obtain $\mathbf{X}_N$. The resultant *N* symbols are mapped to *M* subcarriers ($M=Q\times N$, $M>N$).

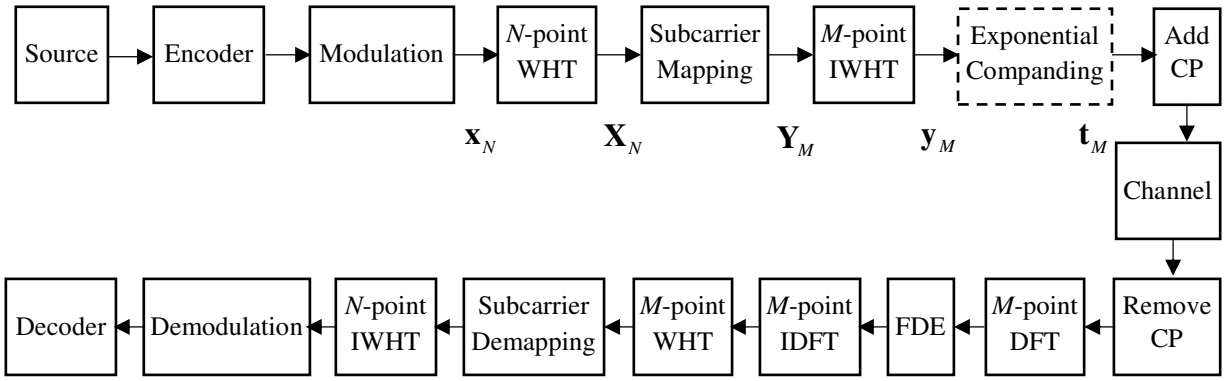

Fig. 5.1. WHT SC-FDMA System with Exponential Companding.

For subcarrier mapping there are two choices namely, Localized FDMA (LFDMA) and Interleaved FDMA (IFDMA). In LFDMA, the symbols are mapped over consecutive subcarriers and in IFDMA the symbols are spread equidistantly over entire bandwidth with zeros in between. $\mathbf{X}_N$ are mapped to $\mathbf{Y}_M$ (where $M = Q\times N$) as

$$\mathbf{Y}_M = \mathbf{M}\mathbf{X}_N \tag{5.9}$$

For localized mapping

$$\mathbf{M} = \left[\mathbf{I}_N ; 0_{(M-N)\times N} \right] \tag{5.10}$$

For interleaved mapping

$$\mathbf{M} = \left[\mathbf{u}_1^T ; 0_{(Q-1)\times N}, \mathbf{u}_2^T ; 0_{(Q-1)\times N}, ..., \mathbf{u}_N^T ; 0_{(Q-1)\times N} \right] \tag{5.11}$$

where $\mathbf{I}_N$ is an $N \times N$ identity matrix, $0_{(Q-1)\times N}$ is $(Q\text{-}1)\times N$ all-zero matrix and $\mathbf{u}_l (l = 1, 2, ..., N)$ is unit column vector of length N, with all-zero entries except at l. After subcarrier mapping, $\mathbf{Y}_M$ are sent through M-point IWHT to produce time domain signal as given by

$$\begin{aligned} \mathbf{y}_M &= M\mathbf{H}_M^{-1}\mathbf{Y}_M \\ \mathbf{y}_M &= \frac{M}{N}\mathbf{H}_M^{-1}\mathbf{M}\mathbf{H}_N\mathbf{x}_N \end{aligned} \tag{5.12}$$

where

$\mathbf{x}_N$ is an $N \times 1$ matrix of modulated symbols

$\mathbf{H}_N$ is an $N \times N$ WHT matrix

$\mathbf{M}$ is an $M \times N$ matrix describing the subcarrier mapping

$\mathbf{H}_M^{-1}$ is an $M \times M$ IWHT matrix

5.3.1. Time Domain Symbols

Considering Hadamard ordered WHT with N=2, M=4, Q=2 and modulated symbols $\mathbf{x}_N = \left[x_1 \;\; x_2 \right]^T$ we have

$$\mathbf{X}_N = \frac{1}{N}\mathbf{H}_N\mathbf{x}_N = \frac{1}{2}\begin{bmatrix} 1 & 1 \\ 1 & -1 \end{bmatrix}\begin{bmatrix} x_1 \\ x_2 \end{bmatrix} = \begin{bmatrix} (x_1 + x_2)/2 \\ (x_1 - x_2)/2 \end{bmatrix} \tag{5.13}$$

For localized mapping

$$\mathbf{Y}_M = \mathbf{M}\mathbf{X}_N = \begin{bmatrix} 1 & 0 \\ 0 & 1 \\ 0 & 0 \\ 0 & 0 \end{bmatrix}\begin{bmatrix} (x_1 + x_2)/2 \\ (x_1 - x_2)/2 \end{bmatrix} = \begin{bmatrix} (x_1 + x_2)/2 \\ (x_1 - x_2)/2 \\ 0 \\ 0 \end{bmatrix} \tag{5.14}$$

$$\mathbf{y}_M = M\mathbf{H}_M^{-1}\mathbf{Y}_M = 4\begin{bmatrix} 1 & 1 & 1 & 1 \\ 1 & -1 & 1 & -1 \\ 1 & 1 & -1 & -1 \\ 1 & -1 & -1 & 1 \end{bmatrix}^{-1}\begin{bmatrix} (x_1+x_2)/2 \\ (x_1-x_2)/2 \\ 0 \\ 0 \end{bmatrix} = \begin{bmatrix} x_1 \\ x_2 \\ x_1 \\ x_2 \end{bmatrix} \tag{5.15}$$

$$\mathbf{y}_M = 4\begin{bmatrix} 1/4 & 1/4 & 1/4 & 1/4 \\ 1/4 & -1/4 & 1/4 & -1/4 \\ 1/4 & 1/4 & -1/4 & -1/4 \\ 1/4 & -1/4 & -1/4 & 1/4 \end{bmatrix}\begin{bmatrix} (x_1+x_2)/2 \\ (x_1-x_2)/2 \\ 0 \\ 0 \end{bmatrix} = \begin{bmatrix} x_1 \\ x_2 \\ x_1 \\ x_2 \end{bmatrix} \tag{5.16}$$

Hence for localized mapping $\mathbf{y}_M = \left[x_1\ x_2 \ldots x_N\ x_1\ x_2 \ldots x_N \ldots . x_1\ x_2 \ldots x_N\right]^T$ i.e. $\mathbf{x}_N$ will be repeated Q times. As the resulting WHT LFDMA symbols simply consists of modulated symbols in contrast to that of DFT LFDMA symbols which consists of sum of modulated symbols with different complex-weights, the PAPR of WHT LFDMA system will be less when compared to DFT LFDMA system. For interleaved mapping

$$\mathbf{Y}_M = \mathbf{M}\mathbf{X}_N = \begin{bmatrix} 1 & 0 \\ 0 & 0 \\ 0 & 1 \\ 0 & 0 \end{bmatrix}\begin{bmatrix} (x_1+x_2)/2 \\ (x_1-x_2)/2 \end{bmatrix} = \begin{bmatrix} (x_1+x_2)/2 \\ 0 \\ (x_1-x_2)/2 \\ 0 \end{bmatrix} \tag{5.17}$$

$$\mathbf{y}_M = M\mathbf{H}_M^{-1}\mathbf{Y}_M = 4\begin{bmatrix} 1 & 1 & 1 & 1 \\ 1 & -1 & 1 & -1 \\ 1 & 1 & -1 & -1 \\ 1 & -1 & -1 & 1 \end{bmatrix}^{-1}\begin{bmatrix} (x_1+x_2)/2 \\ 0 \\ (x_1-x_2)/2 \\ 0 \end{bmatrix} = \begin{bmatrix} x_1 \\ x_1 \\ x_2 \\ x_2 \end{bmatrix} \tag{5.18}$$

Hence for interleaved mapping $\mathbf{y}_M = \left[x_1\ x_1 \ldots x_1\ x_2\ x_2 \ldots x_2 \ldots . x_N\ x_N \ldots x_N\right]^T$ i.e. x_1 will be repeated Q times then x_2 will be repeated Q times and so on x_N will be repeated Q times. As the resulting WHT IFDMA symbols simply consists of modulated symbols similar to the DFT IFDMA symbols, the PAPR of WHT IFDMA system will be same as that of DFT IFDMA system.

For Sequency ordered WHT we have

$$\left(\mathbf{H}_4\right)_s = \begin{bmatrix} 1 & 1 & 1 & 1 \\ 1 & 1 & -1 & -1 \\ 1 & -1 & -1 & 1 \\ 1 & -1 & 1 & -1 \end{bmatrix} \begin{matrix} 0 \\ 1 \\ 2 \\ 3 \end{matrix} \qquad (5.19)$$

# of sign changes

For localized mapping

$$\mathbf{y}_M = M\mathbf{H}_M^{-1}\mathbf{Y}_M = 4\begin{bmatrix} 1 & 1 & 1 & 1 \\ 1 & 1 & -1 & -1 \\ 1 & -1 & -1 & 1 \\ 1 & -1 & 1 & -1 \end{bmatrix}^{-1} \begin{bmatrix} (x_1 + x_2)/2 \\ (x_1 - x_2)/2 \\ 0 \\ 0 \end{bmatrix} = \begin{bmatrix} x_1 \\ x_1 \\ x_2 \\ x_2 \end{bmatrix} \qquad (5.20)$$

Hence for Sequency ordered WHT, the time domain signal for localized mapping is given by $\mathbf{y}_M = \left[x_1 \; x_1 \ldots x_1 \; x_2 \; x_2 \ldots x_2 \ldots . \; x_N \; x_N \ldots x_N\right]^T$ i.e. x_1 will be repeated Q times then x_2 will be repeated Q times and so on x_N will be repeated Q times. For interleaved mapping

$$\mathbf{y}_M = M\mathbf{H}_M^{-1}\mathbf{Y}_M = 4\begin{bmatrix} 1 & 1 & 1 & 1 \\ 1 & 1 & -1 & -1 \\ 1 & -1 & -1 & 1 \\ 1 & -1 & 1 & -1 \end{bmatrix}^{-1} \begin{bmatrix} (x_1 + x_2)/2 \\ 0 \\ (x_1 - x_2)/2 \\ 0 \end{bmatrix} = \begin{bmatrix} x_1 \\ x_2 \\ x_2 \\ x_1 \end{bmatrix} \qquad (5.21)$$

Hence for Sequency ordered WHT, the time domain signal for interleaved mapping is given by $\mathbf{y}_M = \left[x_1 \; x_2 \ldots x_N \; x_N \; x_{N-1} \ldots x_1 \ldots . \; x_1 \; x_2 \ldots x_N\right]^T$.

For Dyadic ordered WHT we have

$$\left(\mathbf{H}_4\right)_d = \begin{bmatrix} 1 & 1 & 1 & 1 \\ 1 & 1 & -1 & -1 \\ 1 & -1 & 1 & -1 \\ 1 & -1 & -1 & 1 \end{bmatrix} \begin{matrix} 0 \\ 1 \\ 3 \\ 2 \end{matrix} \qquad (5.22)$$

# of sign changes

For localized mapping

$$\mathbf{y}_M = M\mathbf{H}_M^{-1}\mathbf{Y}_M = 4\begin{bmatrix} 1 & 1 & 1 & 1 \\ 1 & 1 & -1 & -1 \\ 1 & -1 & 1 & -1 \\ 1 & -1 & -1 & 1 \end{bmatrix}^{-1}\begin{bmatrix} (x_1+x_2)/2 \\ (x_1-x_2)/2 \\ 0 \\ 0 \end{bmatrix} = \begin{bmatrix} x_1 \\ x_1 \\ x_2 \\ x_2 \end{bmatrix} \tag{5.23}$$

Hence for Dyadic ordered WHT, the time domain signal for localized mapping is given by $\mathbf{y}_M = \left[x_1\ x_1 \ldots x_1\ x_2\ x_2 \ldots x_2 \ldots . x_N\ x_N \ldots x_N\right]^T$ i.e. x_1 will be repeated Q times then x_2 will be repeated Q times and so on x_N will be repeated Q times. For interleaved mapping

$$\mathbf{y}_M = M\mathbf{H}_M^{-1}\mathbf{Y}_M = 4\begin{bmatrix} 1 & 1 & 1 & 1 \\ 1 & 1 & -1 & -1 \\ 1 & -1 & 1 & -1 \\ 1 & -1 & -1 & 1 \end{bmatrix}^{-1}\begin{bmatrix} (x_1+x_2)/2 \\ 0 \\ (x_1-x_2)/2 \\ 0 \end{bmatrix} = \begin{bmatrix} x_1 \\ x_2 \\ x_1 \\ x_2 \end{bmatrix} \tag{5.24}$$

Hence for Dyadic ordered WHT, the time domain signal for interleaved mapping is given by $\mathbf{y}_M = \left[x_1\ x_2 \ldots x_N\ x_1\ x_2 \ldots x_N \ldots . x_1\ x_2 \ldots x_N\right]^T$ i.e. $\mathbf{x}_N$ will be repeated Q times. As all the time domain signals are simply the repetition of modulated symbols, PAPR of Hadamard, Sequency, and Dyadic ordered WHT systems remain the same. Also, it can be observed that H-WHT with localized mapping and D-WHT with interleaved mapping have the same time domain signals. Similarly, H-WHT with interleaved mapping, S-WHT and D-WHT with localized mapping have the same time domain signals. Hence they tend to offer similar BER performance.

Now, $\mathbf{y}_M$ is passed through exponential compander to produce $\mathbf{t}_M$ where $\mathbf{t}_M = \left[t_1\ t_2 \ldots t_M\right]^T$. The companding operation can be described as

$$t_m = h(y_m) \tag{5.25}$$

where y_m is the original signal, t_m is the companded signal and $h(\cdot)$ is the companding function. Exponential companding function [99] is given by

$$h(x) = \mathrm{sgn}(x)\sqrt[d]{A\left[1-\exp\left(-\frac{|x|^2}{\sigma^2}\right)\right]} \tag{5.26}$$

where '*d*' controls the amount of companding and *A* keeps the average power of output signal same as that of input signal.

$$A = \left(\frac{E\left[|x|^2 \right]}{E\left[\sqrt[d]{\left[1 - \exp\left(-\frac{|x|^2}{\sigma^2} \right) \right]^2} \right]} \right)^{\frac{d}{2}} \tag{5.27}$$

Now cyclic prefix (CP) is added to t_m and transmitted over the wireless channel. We do not use any decompanding operation at the receiver side. CP is removed at the receiver side and passed through *M*-point DFT for frequency domain equalization (FDE) and then inverted back to the time domain by *M*-point IDFT. Then the corresponding inverse operations like *M*-point WHT, subcarrier demapping, *N*-point IWHT, demodulation, and decoding operations are performed to retrieve the source data.

5.3.2. Complexity Evaluation

The fast WHT algorithm in [109] has similar computational complexity as that of fast DFT [111] algorithm. Just as the discrete Fourier transform, fast WHT requires $N \log_2 N$ arithmetic operations for an *N*-point sequence. Hence, WHT based SC-FDMA transmitter has comparative complexity as that of DFT based transmitter. The receiver's complexity is a little higher than that of the DFT based receiver, as it uses additional DFT and IDFT blocks for frequency domain equalization. But as the receiver is a base station in case of uplink communications, slightly higher complexity can be acceptable owing to the supremacy of WHT based SC-FDMA system.

5.4. Performance Evaluation

The efficiency of the proposed system presented in Fig. 5.1 has been evaluated with the parameters as given in Table 5.2.

Table 5.2. Simulation Parameters

Parameter	Description
Modulation type	16-QAM
Channel coding	1/2 rate Convolutional code
N	128
M	512
System bandwidth	5 MHz
Subcarriers spacing	9.765625 kHz
Subcarrier mapping	Localized, Interleaved
CP length	20 samples
Channel model	AWGN, Veh-A
Equalization	MMSE

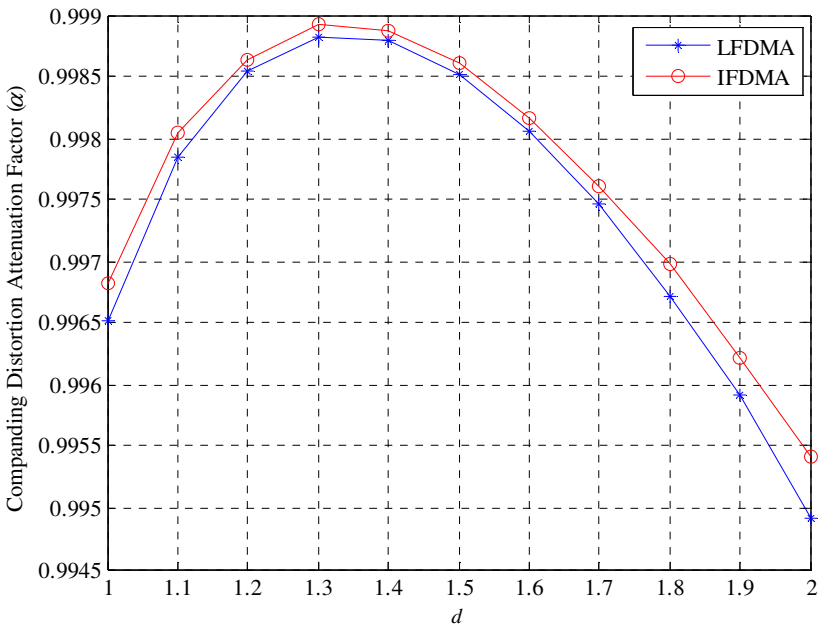

Fig. 5.2. Companding distortion attenuation factor of exponential companding scheme.

Fig. 5.2 presents attenuation factor α vs d plot for exponential companding scheme. From equation (3.31) as α tends to one, power of companding noise will reduce and hence the BER performance of the system will be better. The values of α for the proposed LFDMA and IFDMA systems were evaluated to be 0.9988 and 0.9989 (close to 1) respectively for d = 1.3. Hence, the proposed method offers very low companding noise when d = 1.3.

Figs. 5.3 and 5.4 present the CCDF curves of Hadamard ordered WHT with exponential companding for various *d* values with localized and interleaved mapping respectively. It can be observed that as *d* value increases PAPR has been reduced, in both the cases.

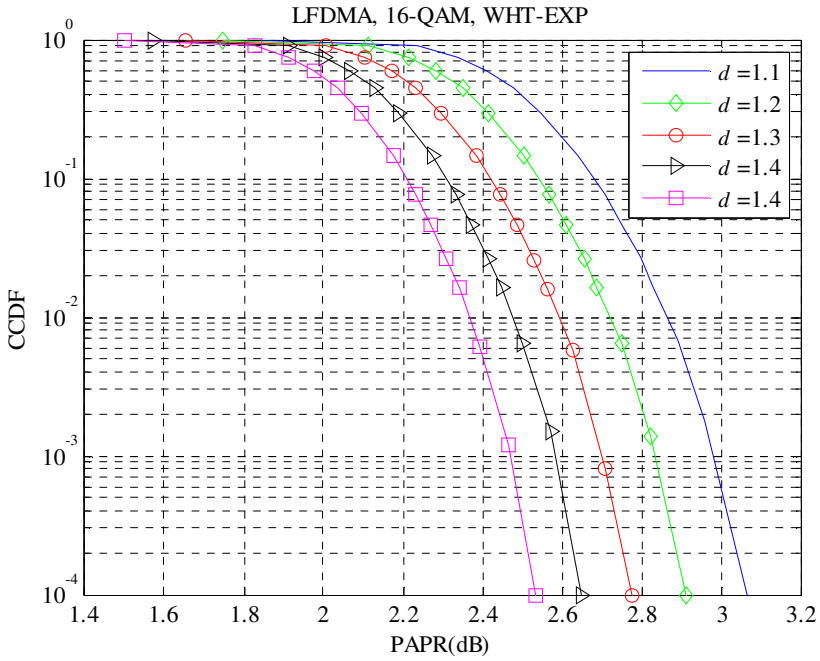

Fig. 5.3. CCDF curves of proposed system with LFDMA for different '*d*'.

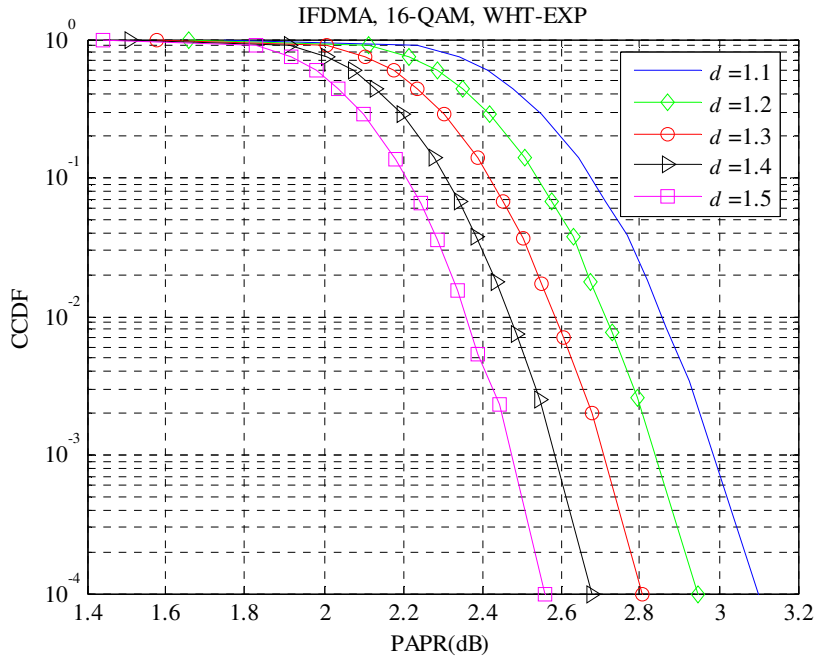

Fig. 5.4. CCDF curves of proposed system with IFDMA for different '*d*'.

BER vs *d* plots of the proposed LFDMA and IFDMA systems for various SNRs are illustrated in Figs. 5.5 and 5.6, respectively. It can be noticed that d = 1.3 is the optimum value, which is also evident from Fig. 5.2 that companding noise is minimum when d = 1.3. So d =1.3 has been chosen for a trade-off between PAPR and BER performances.

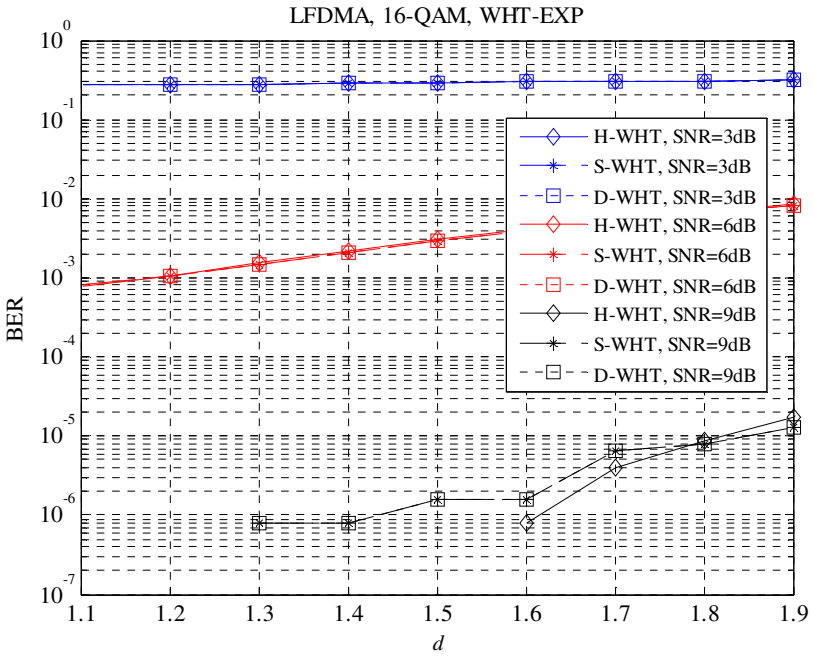

Fig. 5.5. BER vs *d* curves of proposed LFDMA system for different SNR.

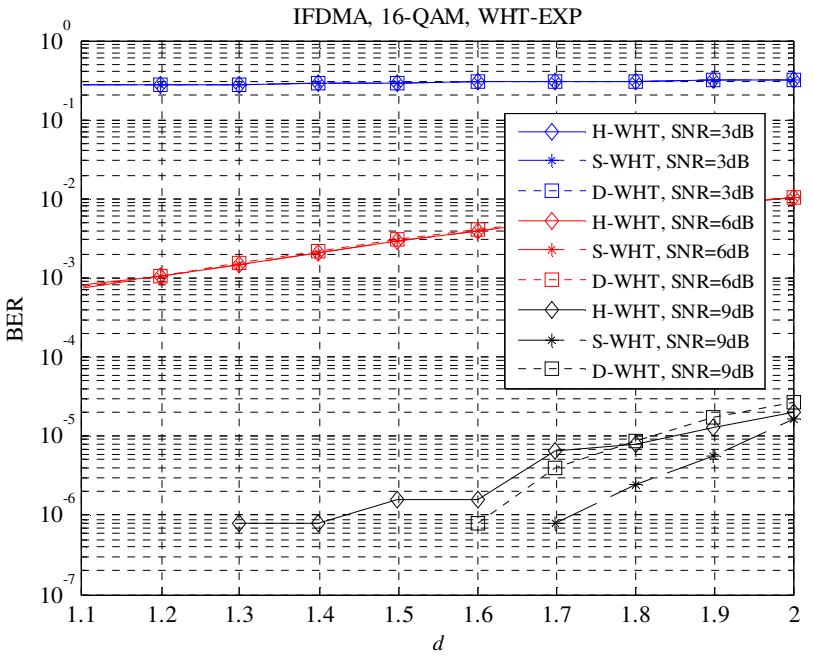

Fig. 5.6. BER vs *d* curves of proposed IFDMA system for different SNR.

CCDF curves of DFT, DCT, Discrete Sine Transform (DST) and WHT based SC-FDMA systems for localized and interleaved mapping techniques are shown in Figs. 5.7 and 5.8 respectively. For localized mapping, we can observe that DCT based system has high PAPR and DST based system has low PAPR when compared to DFT based system. The proposed WHT based system has low PAPR when compared to DFT, DCT, and DST based systems. We can also observe that Hadamard, Sequency, and Dyadic ordered WHT systems provide same PAPR as discussed in section 5.3.1. When exponential companding is used in WHT based system, PAPR has been further improved.

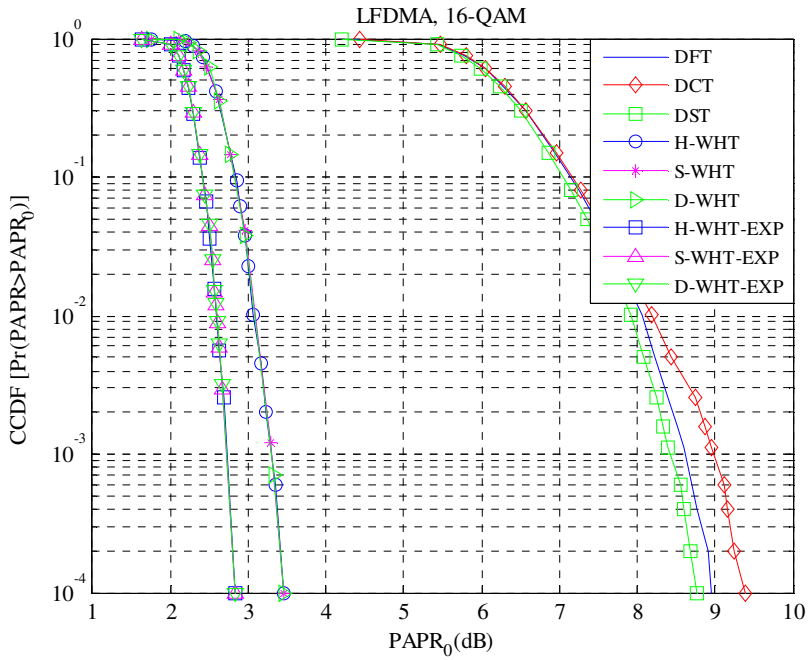

Fig. 5.7. CCDF curves of different systems with localized mapping.

For interleaved mapping we can observe that DFT, DCT and WHT based systems provide same PAPR. From Figs. 5.7 and 5.8, we can also conclude that WHT based system provides same PAPR for both localized and interleaved mapping methods. Table 5.3 summarizes the values of PAPR for different systems at CCDF=10^{-4}.

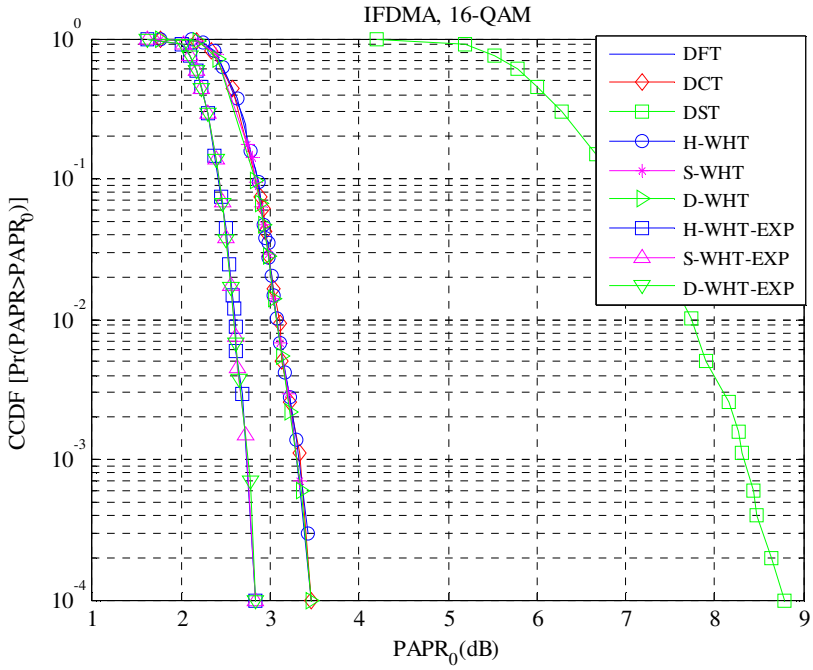

Fig. 5.8. CCDF curves of different systems with interleaved mapping.

Table 5.3. PAPR values in dB at CCDF=10^{-4}

	DFT	**DCT**	**DST**	**H-WHT**	**S-WHT**	**D-WHT**	**H-WHT-EXP**	**S-WHT-EXP**	**D-WHT-EXP**
LFDMA	8.96	9.39	8.77	3.45	3.45	3.45	2.84	2.84	2.84
IFDMA	3.45	3.45	8.79	3.45	3.45	3.45	2.84	2.84	2.84

From Table 5.3 it can be noticed that the proposed WHT based system reduces PAPR by about 5.51 dB at CCDF=10^{-4}, while WHT-EXP reduces by about 6.12 dB when compared to the DFT based system when localized mapping is used.

The effect of input block size on the PAPR performance of proposed H-WHT-EXP based SC-FDMA system with M=512 is presented in Fig. 5.9. It can be noticed that PAPR reduces as block size N increases. As a result, improvements in the PAPR performance can be achieved by increasing the input block size.

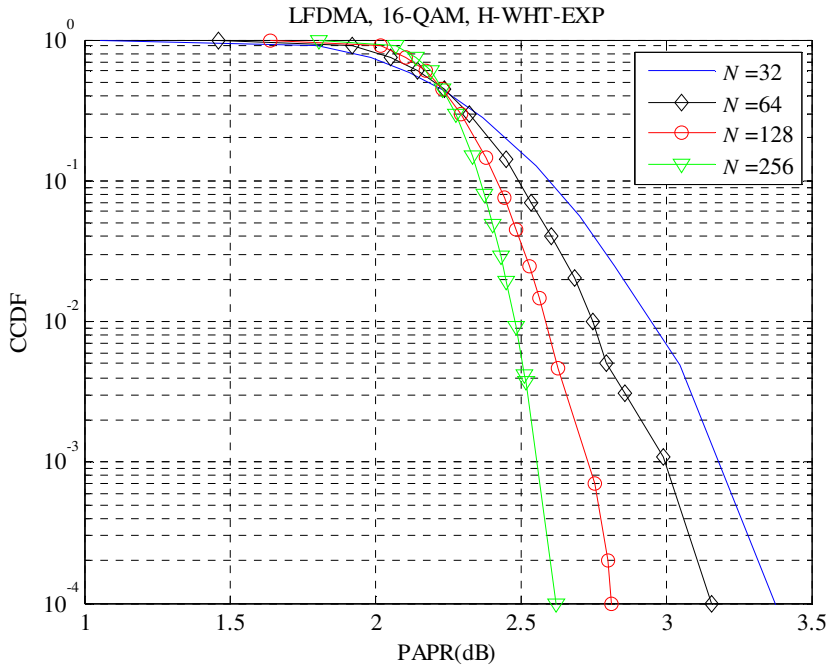

Fig. 5.9. CCDF curves of H-WHT-EXP system with different input block sizes.

The effect of output block size on the PAPR performance of proposed H-WHT-EXP based SC-FDMA system with N=128 is presented in Fig. 5.10. It can be observed that as block size M increases, PAPR increases negligibly.

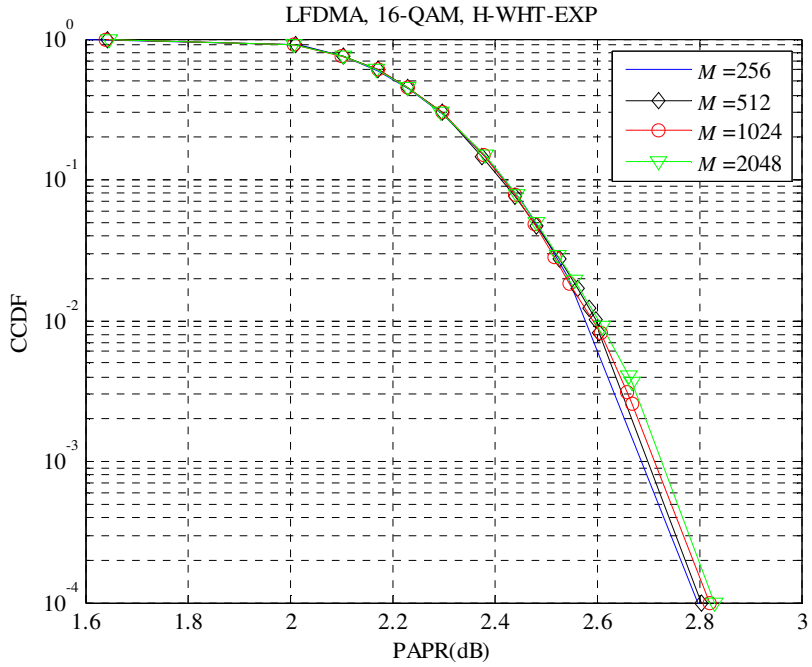

Fig. 5.10. CCDF curves of H-WHT-EXP system with different output block sizes.

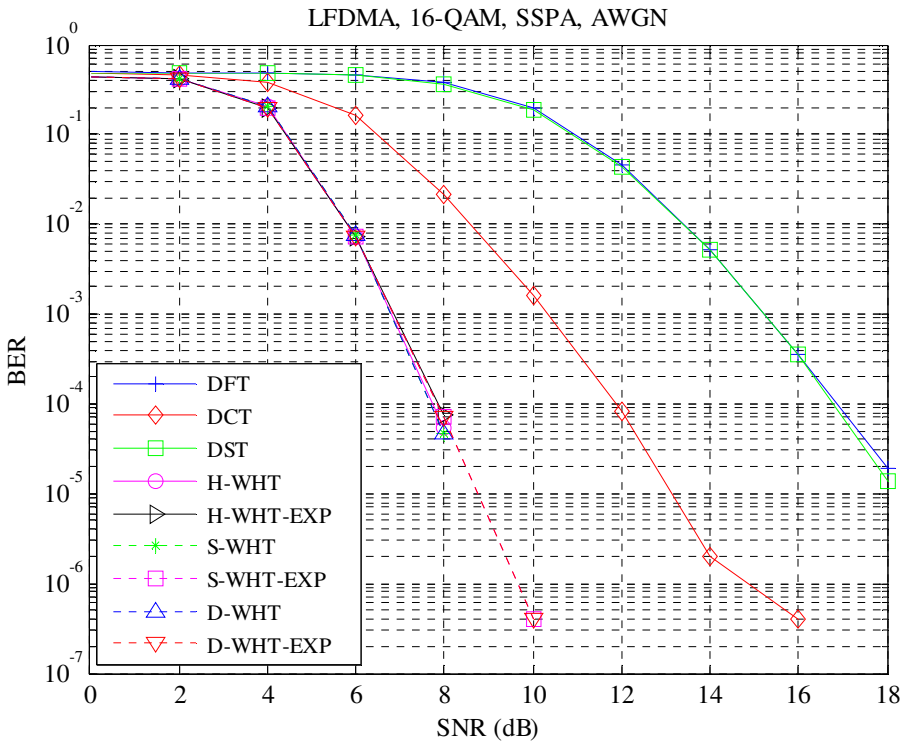

Fig. 5.11. BER curves of various LFDMA systems over AWGN channel with SSPA.

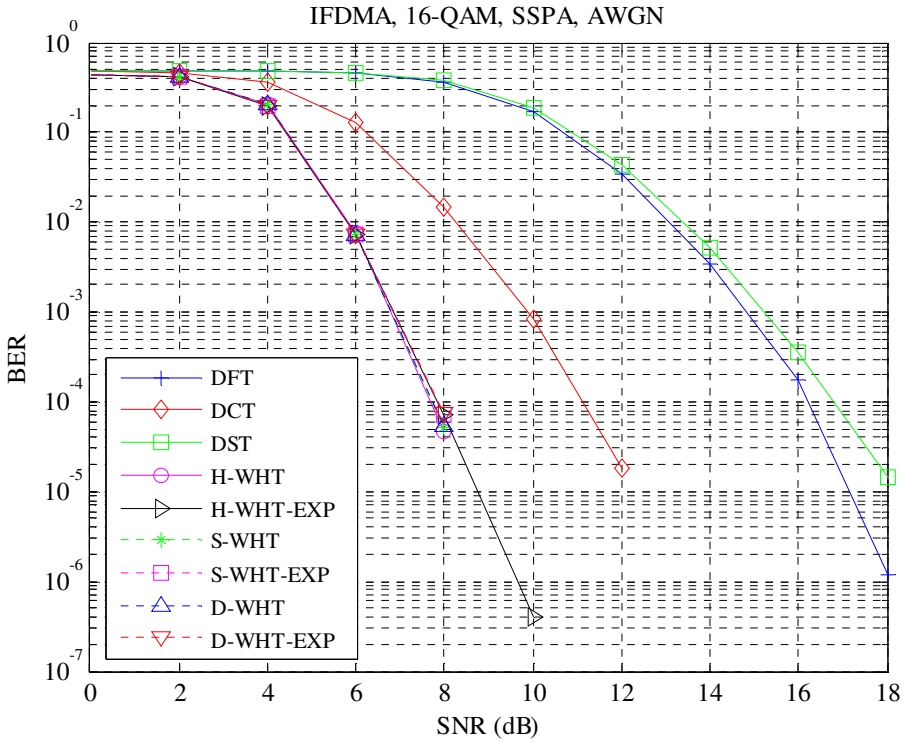

Fig. 5.12. BER curves of various IFDMA systems over AWGN channel with SSPA.

BER performance curves of DFT, DCT, DST and WHT based SC-FDMA systems over AWGN channel for localized and interleaved mapping techniques considering SSPA with IBO=5 dB and p=2 are shown in Figs. 5.11 and 5.12 respectively. It can be observed that all the Hadamard, Sequency and Dyadic ordered WHT systems perform similarly. When exponential companding is used in WHT based system, there is a slight degradation in BER performance which is almost negligible.

BER performance curves of different systems over Vehicular-A channel for localized and interleaved mapping techniques considering SSPA are shown in Figs. 5.13 and 5.14 respectively. It can be observed that Sequency and Dyadic ordered WHT based systems provide better BER performance with localized mapping, whereas Hadamard ordered WHT based system provide better BER performance with interleaved mapping. Also as stated in section 5.3.1 H-WHT with localized mapping and D-WHT with interleaved mapping have same BER performance. H-WHT with interleaved mapping and S-WHT, D-WHT with localized mapping have same BER performance. Table 5.4 shows the required SNR values to attain a BER of 10^{-4} for different systems.

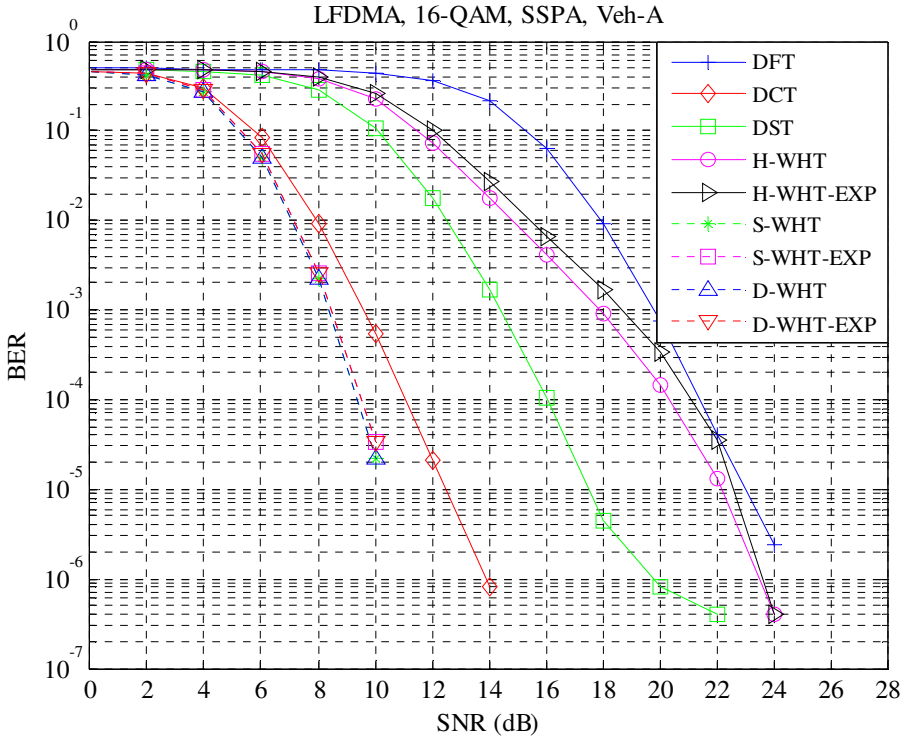

Fig. 5.13. BER curves of various LFDMA systems over Veh-A channel with SSPA.

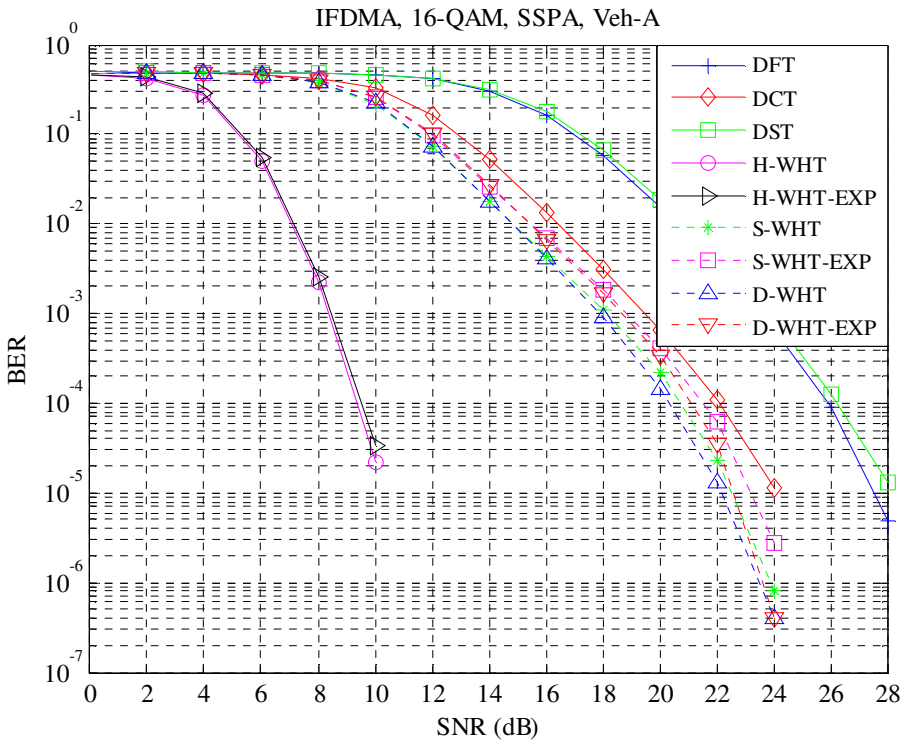

Fig. 5.14. BER curves of various IFDMA systems over Veh-A channel with SSPA.

Table 5.4. SNR in dB required for BER=10^{-4}

	DFT	**DCT**	**DST**	**H-WHT**	**H-WHT-EXP**	**S-WHT**	**S-WHT-EXP**	**D-WHT**	**D-WHT-EXP**
AWGN LFDMA	17.51	11.98	17.50	7.98	7.99	7.98	7.99	7.98	7.99
AWGN IFDMA	16.86	11.79	17.49	7.98	7.99	7.98	7.99	7.98	7.99
Veh-A LFDMA	21.83	11.70	16.13	20.71	21.58	9.93	9.95	9.93	9.95
Veh-A IFDMA	25.96	22.23	26.46	9.93	9.95	21.21	21.78	20.71	21.58

5.5. Conclusion

In this chapter, an SC-FDMA transceiver based on Walsh Hadamard Transform which offers low PAPR and enhanced BER performance when compared to conventional DFT based SC-FDMA system has been proposed. Time domain symbols for Hadamard, Sequency and Dyadic ordered WHT systems have been derived for both localized and interleaved subcarrier

mapping schemes. Complexity of the proposed system is similar to the conventional system at transmitter side, while receiver complexity is slightly high. Hadamard ordered system performs good in case of interleaved mapping and Sequency, Dyadic ordered systems perform good in case of localized mapping when multipath fading environment is considered. Moreover, all the time domain signals are simply the repetition of modulated symbols, and hence PAPR of Hadamard, Sequency and Dyadic ordered WHT systems remain same.

Chapter-6

Verification of Proposed Techniques by Considering a Real Time Indoor Channel using WARP Hardware

6.1. Experimental Setup

WARP v3 hardware developed by Mango Communications is used to implement the experiments. WARPLab framework [112] allows physical layer algorithms to be prototyped by combining the ease of MATLAB with the capabilities of WARP. The WARPLab framework allows MATLAB to control the WARP nodes and perform signal processing operations. WARP repository [113] contains the necessary MATLAB m-code and FPGA code functions required for interaction between MATLAB workspace and WARP nodes. A WARP node comprises of two identical RF interfaces: RF A and RF B. Each RF interface has a transceiver operating at 2.4/5GHz with an RF bandwidth of 40MHz. RF A is used to transmit samples and RF B is used to receive the samples.

Basic WARPLab setup where a WARP node and host PC are connected via an ethernet switch is used to verify the experiments. The baseband samples were constructed in MATLAB and the WARPLab framework downloads the samples from the MATLAB workspace to the FPGA buffers. A trigger signal is sent from host PC to the WARP node so that samples can be transmitted from RF A to RF B. The baseband samples are up-converted to RF signal at the transmitter side and down-converted at the receiver side. These down-converted samples are then stored in buffers before loading them to the MATLAB workspace. These are then processed on the host PC by using MATLAB.

The experimental setup of WARP v3 board is depicted in Fig. 6.1. We have considered 1000 SC-FDMA symbols with N=128, M=512, and CP with 32 samples. Initially

random data is modulated by using 16-QAM modulation, and corresponding operations of SC-FDMA modulator are performed before adding CP. Then, pilot symbols are added and passed through square-root raised cosine filter with a roll off factor of 0.3. Later a preamble is added and the baseband signal is up converted to 5MHz before transmitting it over the air. The received signal is down converted to baseband signal and is correlated with the reference signal to detect the preamble sequence. The channel is estimated by using pilot symbols and corresponding operations of SC-FDMA demodulator are performed.

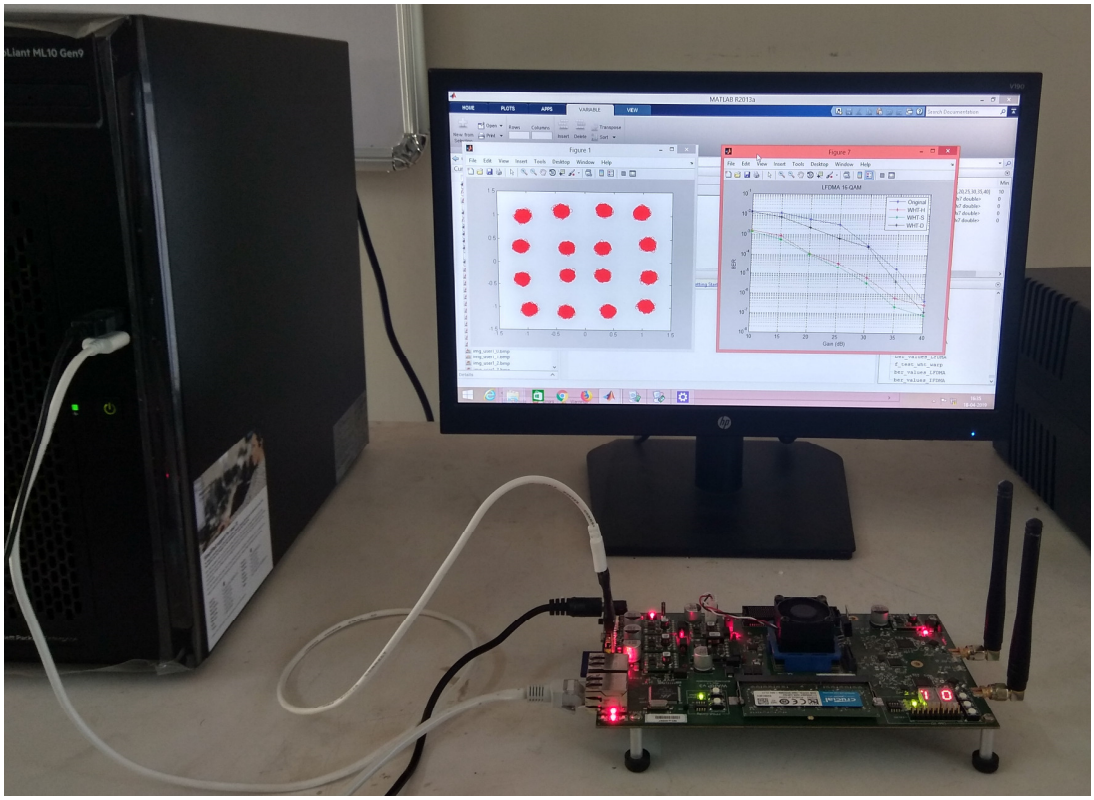

Fig. 6.1. Experimental Setup using WARP v3 board.

Fig. 6.2 presents BER vs transmit amplifier gain curves of DFT SC-FDMA system and DFT SC-FDMA system with μ-law companding, exponential companding and improved exponential companding techniques. It can be observed that the performances are relatively similar to the simulation case.

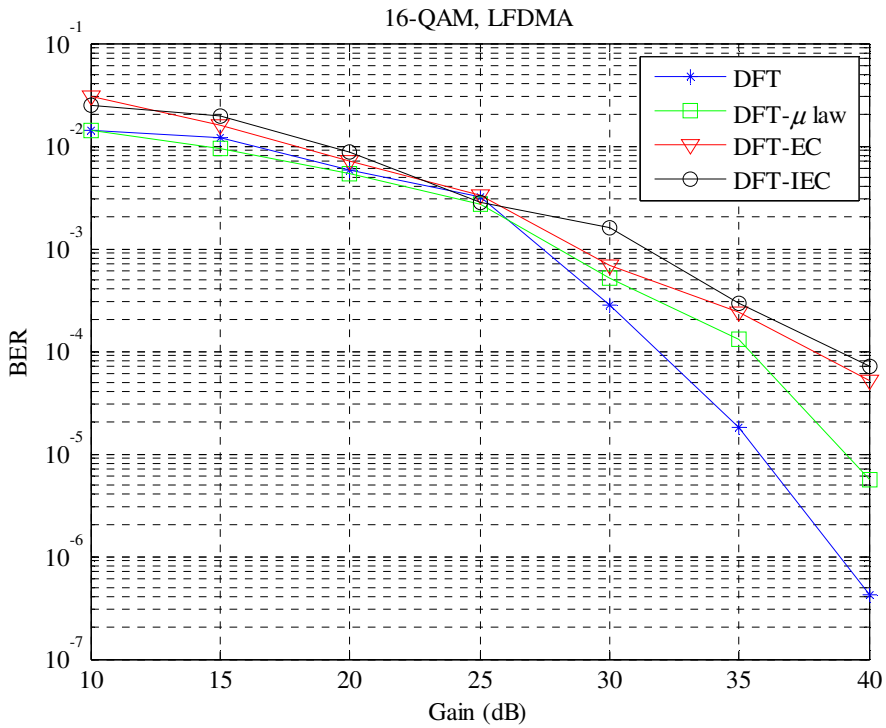

Fig. 6.2. BER curves of original and companded signals over real time channel.

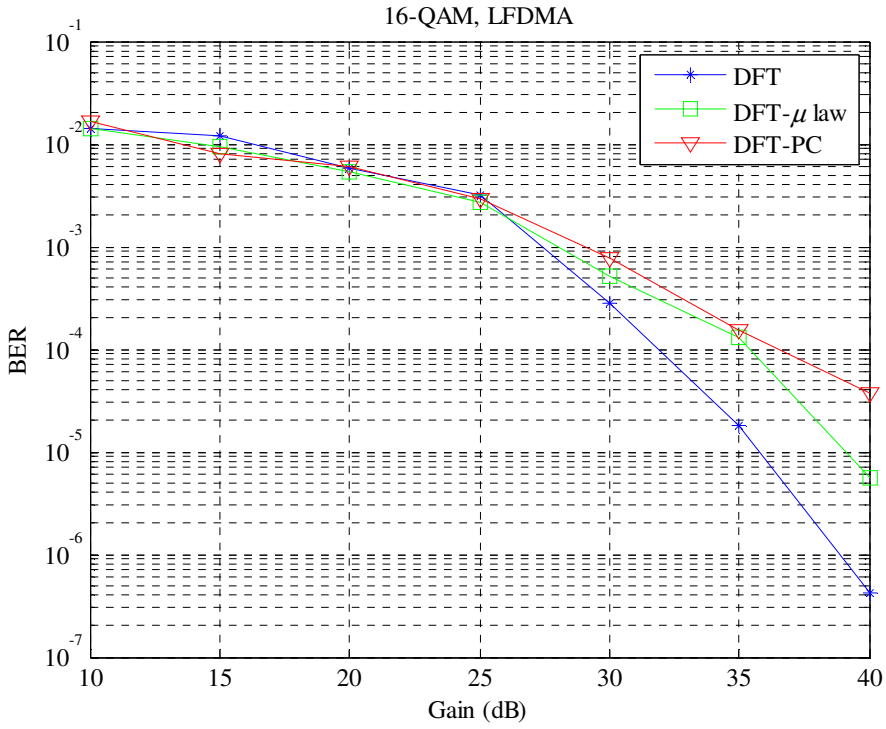

Fig. 6.3. BER curves of original and companded signals over real time channel.

Fig. 6.3 presents BER vs transmit amplifier gain curves of DFT SC-FDMA system and DFT SC-FDMA system with μ-law companding and proposed companding by approximating the

distribution of SC-FDMA signal. It can be observed that the performances are relatively similar to the simulation case.

Fig. 6.4 presents BER vs transmit amplifier gain curves of DCT SC-FDMA system and DCT SC-FDMA system with μ-law companding, absolute exponential companding and proposed companding by approximating the distribution of DCT SC-FDMA signal. It can be observed that DCT-PC has better performance than DCT-AEXP in real-time scenario.

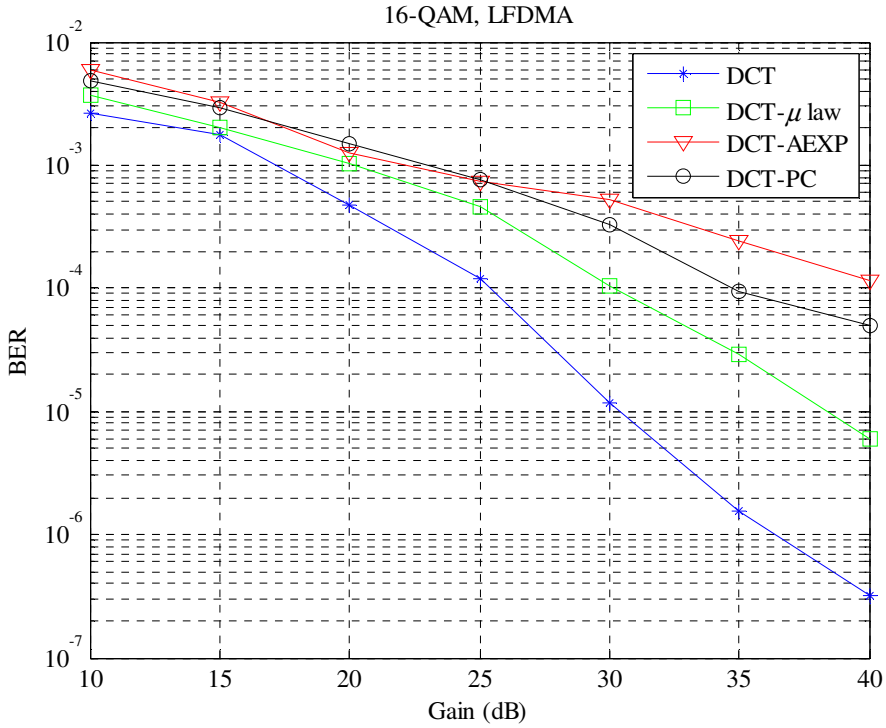

Fig. 6.4. BER curves of DCT SC-FDMA system and companded signals over real time channel.

BER vs transmit amplifier gain curves of proposed WHT based system and conventional system over real time channel for localized and interleaved mapping techniques are presented in Figs. 6.5 and 6.6 respectively. It can be observed that all the Hadamard, Sequency and Dyadic ordered WHT based SC-FDMA systems perform either better or maintain the performance of the conventional SC-FDMA system but does not degrade the performance. Sequency ordered WHT based system provide better BER performance with localized mapping, whereas Hadamard ordered WHT based system provide better BER performance with interleaved mapping.

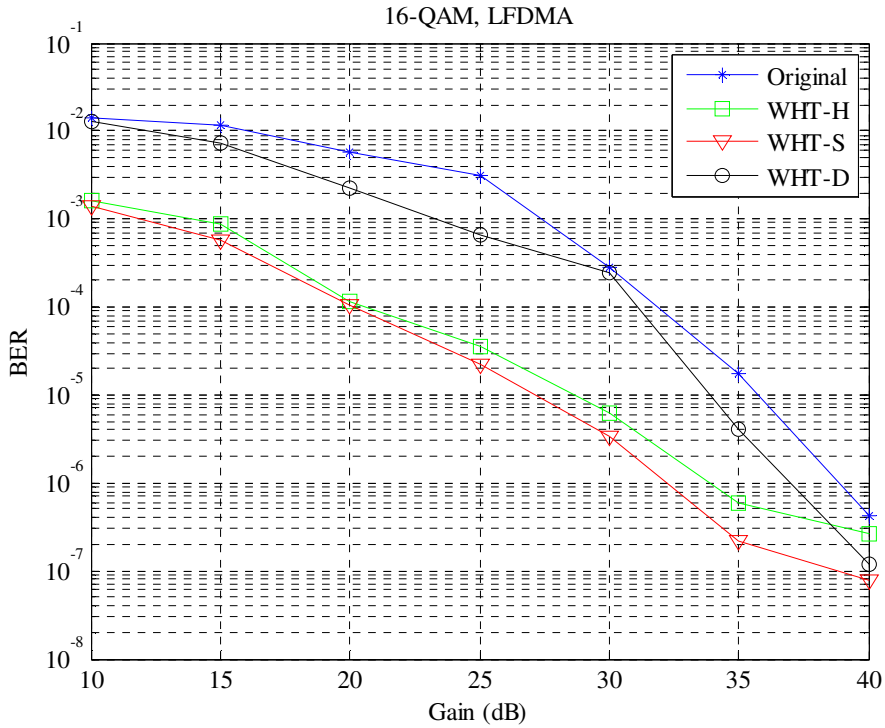

Fig. 6.5. BER curves of original and WHT based LFDMA systems over real time channel.

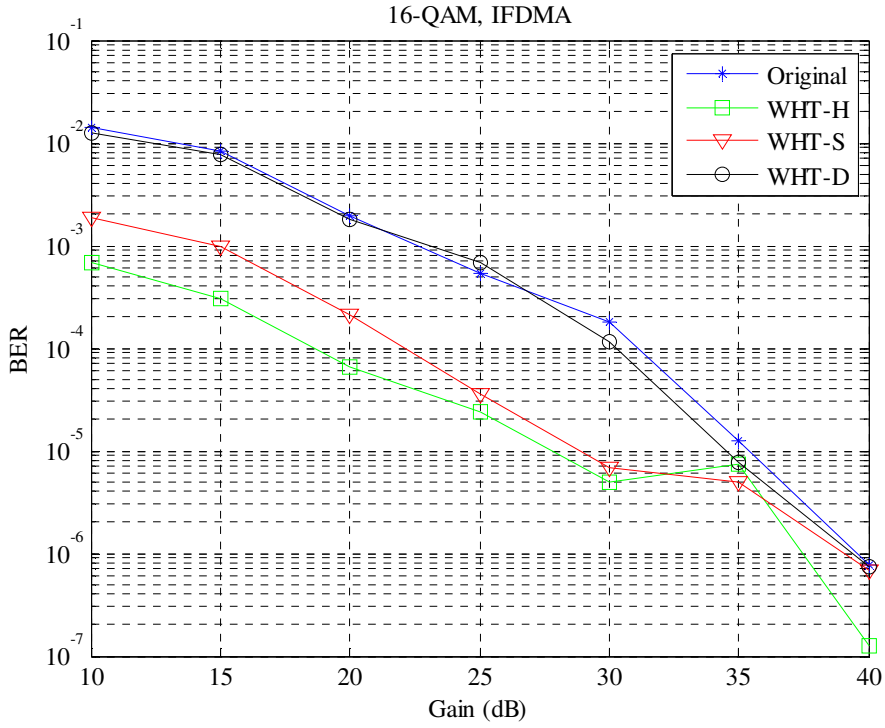

Fig. 6.6. BER curves of original and WHT based IFDMA systems over real time channel.

6.2. Conclusion

In this chapter we have verified the proposed techniques by considering a real time indoor channel using WARPLab implementation. All the proposed techniques have relatively similar performance in real time scenario also.

Chapter-7

Conclusions and Future Scope

7.1. Conclusions

In this thesis, the research has been oriented mainly into the PAPR reduction of the SC-FDMA signals. It contains seven chapters, including this as the last chapter.

In **Chapter 1**, introduction, background, and motivation factor for carrying out this work has been described.

In **Chapter 2**, the overview of the traditional SC-FDMA system, introduction to PAPR, nonlinearities of power amplifiers, problems associated with high PAPR, and literature review of various PAPR reduction techniques have been provided.

In **Chapter 3**, the performances of various companding techniques have been analysed. Exponential companding provides better PAPR performance with a PAPR reduction of about 5.15 dB at CCDF=10^{-4}. Then, an improved exponential companding technique with two different companding levels that can offer more flexibility than the conventional exponential companding technique has been proposed, with a PAPR reduction of about 5.43 dB at CCDF=10^{-4}. Airy companding offers better PSD and BER performances, with only 0.67 dB increase in SNR to maintain a BER of 10^{-4}. However, it provides a PAPR reduction of 3.12 dB only at CCDF=10^{-4}.

In **Chapter 4**, the distribution of the SC-FDMA signal is approximated using a curve fitting tool. Then a companding technique that transforms the SC-FDMA signal into uniform distribution is proposed to reduce the PAPR without increasing the average power of the signal. The proposed technique provides superior PAPR reduction when compared to μ-law

companding with a slight degradation in BER performance. The proposed technique provides a PAPR reduction of 5 dB with a 0.99 dB increase in SNR to maintain a BER of 10^{-4} when compared to the DFT system without companding. The hybrid technique further improves the PAPR, with similar BER performance as that of the proposed technique by carefully choosing the clipping ratio. Also, the distribution of the DCT SC-FDMA signal is approximated, and a companding technique that transforms the DCT SC-FDMA signal into triangular distribution is proposed to reduce the PAPR without increasing the average power of the signal. The proposed technique provides a PAPR reduction of 4.92 dB with a 0.62 dB increase in SNR to maintain a BER of 10^{-5} when compared to the DCT system without companding.

In **Chapter 5**, an SC-FDMA transceiver based on Walsh Hadamard Transform is proposed, which offers low PAPR and enhanced BER performance when compared to conventional DFT based SC-FDMA system. The time-domain symbols for Hadamard, Sequency, and Dyadic ordered WHT systems have been derived for both localized and interleaved subcarrier mapping techniques. The complexity of the proposed system is similar to the conventional system at the transmitter side, while receiver complexity is slightly high. Hadamard ordered system perform well in case of interleaved mapping and Sequency, Dyadic ordered systems perform well in case of localized mapping when multipath fading environment is considered. Moreover, all the time domain signals are simply the repetition of modulated symbols, and hence PAPR of Hadamard, Sequency, and Dyadic ordered WHT systems remain the same.

In **Chapter 6**, the proposed techniques have been verified by considering a real-time indoor channel using WARPLab implementation. Proposed techniques have relatively similar performance in real-time scenario also.

Applications: SC-FDMA system is currently being used in the uplink communications of the third-generation partnership project (3GPP) long term evolution (LTE) standard. Also SC-FDMA is a candidate for 5G communications [114]. Hence the proposed techniques can be used in 4G and 5G systems for uplink communications. Also, the proposed WHT based SC-FDMA system would be a good candidate for 5G systems instead of traditional DFT based system due to its better PAPR and BER performances.

7.2. Future Scope

In this thesis, different PAPR reduction techniques are investigated for SC-FDMA signals. Based on this work, many future research works may be performed. Some of these are outlined below:

- Joint ICI cancellation and PAPR reduction in SC-FDMA systems using different methods can be investigated.
- PAPR reduction in SC-FDMA systems for MIMO applications using different coding techniques can be investigated.
- Impact of Carrier Frequency Offset on different PAPR reduction techniques can be investigated.
- Further, there are many aspects of SC-FDMA signals other than PAPR reduction not addressed in this thesis that would be worth investigating.

Bibliography

[1] Yiyan Wu and W. Y. Zou, "Orthogonal frequency division multiplexing: a multi-carrier modulation scheme," *IEEE Trans. Consum. Electron.*, vol. 41, no. 3, pp. 392–399, 1995.

[2] H. Myung, J. Lim, and D. Goodman, "Single carrier FDMA for uplink wireless transmission," *IEEE Veh. Technol. Mag.*, vol. 1, no. 3, pp. 30–38, Sep. 2006.

[3] H. Myung, J. Lim, and D. Goodman, "Peak-To-Average Power Ratio of Single Carrier FDMA Signals with Pulse Shaping," in *2006 IEEE 17th International Symposium on Personal, Indoor and Mobile Radio Communications*, 2006, pp. 1–5.

[4] D. Falconer, S. L. Ariyavisitakul, A. Benyamin-Seeyar, and B. Eidson, "Frequency domain equalization for single-carrier broadband wireless systems," *IEEE Commun. Mag.*, vol. 40, no. 4, pp. 58–66, Apr. 2002.

[5] H. Ochiai, "On instantaneous power distributions of single-carrier FDMA signals," *IEEE Wirel. Commun. Lett.*, vol. 1, no. 2, pp. 73–76, 2012.

[6] M. M. Rana, Jinsang Kim, and Won-Kyung Cho, "Performance analysis of sub-carrier mapping in LTE uplink systems," in *Digest of the 9th International Conference on Optical Internet (COIN 2010)*, 2010, pp. 1–3.

[7] Xiaodong Li and L. J. Cimini, "Effects of clipping and filtering on the performance of OFDM," *IEEE Commun. Lett.*, vol. 2, no. 5, pp. 131–133, May 1998.

[8] X. Wang, T. T. Tjhung, and C. S. Ng, "Reduction of peak-to-average power ratio of OFDM system using a companding technique," *IEEE Trans. Broadcast.*, vol. 45, no. 3, pp. 303–307, 1999.

[9] T. Jiang and G. Zhu, "Nonlinear Companding Transform for Reducing Peak-to-Average Power Ratio of OFDM Signals," *IEEE Trans. Broadcast.*, vol. 50, no. 3, pp. 342–346, Sep. 2004.

[10] R. W. Bäuml, R. F. H. Fischer, and J. B. Huber, “Reducing the peak-to-average power ratio of multicarrier modulation by selected mapping,” *Electron. Lett.*, vol. 32, no. 22, p. 2056, 1996.

[11] L. J. Cimini and N. R. Sollenberger, “Peak-to-average power ratio reduction of an OFDM signal using partial transmit sequences,” *IEEE Commun. Lett.*, vol. 4, no. 3, pp. 86–88, Mar. 2000.

[12] A. Mohammad, A. Zekry, and F. Newagy, “A time domain SLM for PAPR reduction in SC-FDMA systems,” *2012 IEEE Glob. High Tech Congr. Electron. GHTCE 2012*, no. 1, pp. 143–147, 2012.

[13] A. Sayed-Ahmed, M. Shokair, and E.-S. El-Rabaie, “C42. PAPR reduction for LFDMA using a reduced complexity PTS scheme,” in *2012 29th National Radio Science Conference (NRSC)*, 2012, pp. 515–522.

[14] F. E. Abd El-Samie, F. S. Al-Kamali, M. I. Dessouky, B. M. Sallam, and F. Shawki, “Performance enhancement of SC-FDMA systems using a companding technique,” *Ann. des Telecommun. Telecommun.*, vol. 65, no. 5–6, pp. 293–300, 2010.

[15] E. Sun, P. Si, R. Yang, Y. Sun, and Y. Zhang, “Power Function Companding Scheme for Peak-to-Average Power Ratio Reduction of SC-FDMA Signals,” in *2011 10th IEEE/ACIS International Conference on Computer and Information Science*, 2011, pp. 53–57.

[16] E. Sun, R. Yang, and Y. Zhang, “Raised Cosine-Like Companding Scheme for Peak-to-Average Power Ratio Reduction of SCFDMA Signals,” *Wirel. Pers. Commun.*, vol. 67, no. 4, pp. 913–921, Dec. 2012.

[17] F. S. Al-Kamali, M. I. Dessouky, B. M. Sallam, F. Shawki, and F. E. Abd El-Samie, “A new single carrier FDMA system based on the discrete cosine transform,” in *2009 International Conference on Computer Engineering & Systems*, 2009, pp. 555–560.

[18] A. Khan, A. Arif, T. Nawaz, and S. Baig, “Walsh Hadamard transform based transceiver design for SC-FDMA with discrete wavelet transform,” *China Commun.*, vol. 14, no. 5, pp. 193–206, May 2017.

[19] H. G. Myung and D. J. Goodman, *Single carrier FDMA: A new air interface for long term evolution*. Chichester, UK: John Wiley & Sons, Ltd, 2008.

[20] S. L. Miller and R. J. O'Dea, "Peak power and bandwidth efficient linear modulation," *IEEE Trans. Commun.*, vol. 46, no. 12, pp. 1639–1648, 1998.

[21] S. C. Cripps, *RF power amplifiers for wireless communications*. Artech House, 2006.

[22] Y. Rahmatallah and S. Mohan, "Peak-to-average power ratio reduction in ofdm systems: A survey and taxonomy," *IEEE Commun. Surv. Tutorials*, vol. 15, no. 4, pp. 1567–1592, 2013.

[23] T. Jiang and Y. Wu, "An overview: peak-to-average power ratio reduction techniques for OFDM signals," *Broadcast. IEEE Trans.*, vol. 54, no. 2, pp. 257–268, 2008.

[24] Seung Hee Han and Jae Hong Lee, "An overview of peak-to-average power ratio reduction techniques for multicarrier transmission," *IEEE Wirel. Commun.*, vol. 12, no. 2, pp. 56–65, Apr. 2005.

[25] H. Ochiai and H. Imai, "On clipping for peak power reduction of OFDM signals," in *Globecom '00 - IEEE. Global Telecommunications Conference. Conference Record (Cat. No.00CH37137)*, vol. 2, pp. 731–735.

[26] H. Ochiai and H. Imai, "Performance analysis of deliberately clipped OFDM signals," *IEEE Trans. Commun.*, vol. 50, no. 1, pp. 89–101, 2002.

[27] H. Saeedi, M. Sharif, and F. Marvasti, "Clipping noise cancellation in OFDM systems using oversampled signal reconstruction," *IEEE Commun. Lett.*, vol. 6, no. 2, pp. 73–75, Feb. 2002.

[28] R. O'Neill and L. B. Lopes, "Envelope variations and spectral splatter in clipped multicarrier signals," in *Proceedings of 6th International Symposium on Personal, Indoor and Mobile Radio Communications*, vol. 1, pp. 71–75.

[29] J. Armstrong, "Peak-to-average power reduction for OFDM by repeated clipping and frequency domain filtering," *Electron. Lett.*, vol. 38, no. 5, p. 246, 2002.

[30] Hangjun Chen and A. M. Haimovich, "Iterative estimation and cancellation of clipping

noise for OFDM signals," *IEEE Commun. Lett.*, vol. 7, no. 7, pp. 305–307, Jul. 2003.

[31] R. van Nee and A. de Wild, "Reducing the peak-to-average power ratio of OFDM," in *VTC '98. 48th IEEE Vehicular Technology Conference. Pathway to Global Wireless Revolution (Cat. No.98CH36151)*, vol. 3, pp. 2072–2076.

[32] G. Chen, R. Ansari, and Y. Yao, "Improved peak windowing for PAPR reduction in OFDM," *IEEE Veh. Technol. Conf.*, pp. 4–8, 2009.

[33] H.-B. Jeon, J.-S. No, and D.-J. Shin, "A New PAPR Reduction Scheme Using Efficient Peak Cancellation for OFDM Systems," *IEEE Trans. Broadcast.*, vol. 58, no. 4, pp. 619–628, Dec. 2012.

[34] J. Song and H. Ochiai, "Performance Analysis for OFDM Signals With Peak Cancellation," *IEEE Trans. Commun.*, vol. 64, no. 1, pp. 261–270, Jan. 2016.

[35] Xiao Huang, Jianhua Lu, Justin Chuang, and Junli Zheng, "Companding transform for the reduction of peak-to-average power ratio of OFDM signals," in *IEEE VTS 53rd Vehicular Technology Conference, Spring 2001. Proceedings (Cat. No.01CH37202)*, vol. 2, pp. 835–839.

[36] X. Huang, J. Lu, J. Zheng, J. Chuang, and J. Gu, "Reduction of peak-to-average power ratio of OFDM signals with companding transform," *Electron. Lett.*, vol. 37, no. 8, p. 506, 2001.

[37] Xianbin Wang, T. T. Tjhung, and C. S. Ng, "Reply to the comments on 'Reduction of peak-to-average power ratio of OFDM system using a companding technique,'" *IEEE Trans. Broadcast.*, vol. 45, no. 4, pp. 420–422, 1999.

[38] T. G. Pratt, N. Jones, L. Smee, and M. Torrey, "OFDM Link Performance With Companding for PAPR Reduction in the Presence of Non-Linear Amplification," *IEEE Trans. Broadcast.*, vol. 52, no. 2, pp. 261–267, Jun. 2006.

[39] T. A. Wilkinson, A. E. Jones, and S. K. Barton, "Block coding scheme for reduction of peak to mean envelope power ratio of multicarrier transmission schemes," *Electron. Lett.*, vol. 30, no. 25, pp. 2098–2099, Dec. 1994.

[40] Y. Zhang, A. Yongacoglu, J.-Y. Chouinard, and L. Zhang, "OFDM peak power reduction by sub-block-coding and its extended versions," in *1999 IEEE 49th Vehicular Technology Conference (Cat. No.99CH36363)*, vol. 1, pp. 695–699.

[41] J. A. Davis and J. Jedwab, "Peak-to-mean power control in OFDM, Golay complementary sequences, and Reed-Muller codes," *IEEE Trans. Inf. Theory*, vol. 45, no. 7, pp. 2397–2417, 1999.

[42] Y. Louet and A. Le Glaunec, "Peak-factor reduction in OFDM by Reed-Muller channel coding a new soft decision decoding algorithm," in *2000 10th Mediterranean Electrotechnical Conference. Information Technology and Electrotechnology for the Mediterranean Countries. Proceedings. MeleCon 2000 (Cat. No.00CH37099)*, vol. 2, pp. 872–875.

[43] Heekwan Lee and S. W. Golomb, "A new construction of 64-QAM golay complementary sequences," *IEEE Trans. Inf. Theory*, vol. 52, no. 4, pp. 1663–1670, Apr. 2006.

[44] B. S. Krongold and D. L. Jones, "PAR reduction in OFDM via active constellation extension," *IEEE Trans. Broadcast.*, vol. 49, no. 3, pp. 258–268, 2003.

[45] Z. Yang, H. Fang, and C. Pan, "ACE With Frame Interleaving Scheme to Reduce Peak-to-Average Power Ratio in OFDM Systems," *IEEE Trans. Broadcast.*, vol. 51, no. 4, pp. 571–575, Dec. 2005.

[46] Y. Zhou and T. Jiang, "A novel clipping integrated into ACE for PAPR reduction in OFDM systems," in *2009 International Conference on Wireless Communications & Signal Processing*, 2009, pp. 1–4.

[47] R. S. Prabhu and E. Grayver, "Active constellation modification techniques for OFDM PAR reduction," in *2009 IEEE Aerospace conference*, 2009, pp. 1–8.

[48] B. M. Kang, H.-G. Ryu, and S. B. Ryu, "A PAPR Reduction Method using New ACE (Active Constellation Extension) with Higher Level Constellation," in *2007 IEEE International Conference on Signal Processing and Communications*, 2007, pp. 724–727.

[49] J. He and Z. Yan, “Improving convergence rate of active constellation extension algorithm for PAPR reduction in OFDM,” in *2013 IEEE International Conference on Information and Automation (ICIA)*, 2013, pp. 280–284.

[50] M.-J. Hao and C.-H. Lai, “PAPR reduction with Adjustable Circle Constrain for OFDM systems,” in *2009 International Symposium on Intelligent Signal Processing and Communication Systems (ISPACS)*, 2009, pp. 323–326.

[51] B. S. Krongold and D. L. Jones, “An Active-Set Approach for OFDM PAR Reduction via Tone Reservation,” *IEEE Trans. Signal Process.*, vol. 52, no. 2, pp. 495–509, Feb. 2004.

[52] Luqing Wang and C. Tellambura, “Analysis of Clipping Noise and Tone-Reservation Algorithms for Peak Reduction in OFDM Systems,” *IEEE Trans. Veh. Technol.*, vol. 57, no. 3, pp. 1675–1694, May 2008.

[53] H. Li, T. Jiang, and Y. Zhou, “An Improved Tone Reservation Scheme With Fast Convergence for PAPR Reduction in OFDM Systems,” *IEEE Trans. Broadcast.*, vol. 57, no. 4, pp. 902–906, Dec. 2011.

[54] S. Zabre, J. Palicot, Y. Louet, and C. Lereau, “SOCP Approach for OFDM Peak-to-Average Power Ratio Reduction in the Signal Adding Context,” in *2006 IEEE International Symposium on Signal Processing and Information Technology*, 2006, pp. 834–839.

[55] J.-C. Chen, M.-H. Chiu, Y.-S. Yang, and C.-P. Li, “A Suboptimal Tone Reservation Algorithm Based on Cross-Entropy Method for PAPR Reduction in OFDM Systems,” *IEEE Trans. Broadcast.*, vol. 57, no. 3, pp. 752–756, Sep. 2011.

[56] Dae-Woon Lim, Hyung-Suk Noh, Hyun-Bae Jeon, Jong-Seon No, and Dong-Joon Shin, “Multi-Stage TR Scheme for PAPR Reduction in OFDM Signals,” *IEEE Trans. Broadcast.*, vol. 55, no. 2, pp. 300–304, Jun. 2009.

[57] J. Tellado, “Peak to Average Ratio Reduction for Multi-carrier Modulation,” PhD Thesis, Stanford University, Stanford, CA, USA, 1999.

[58] J. Tellado and J. M. Cioffi, “Peak power reduction for multicarrier transmission,” in

Proc. IEEE Global Communications Conference (CLOBECOM), 1998.

[59] S. H. Han, J. M. Cioffi, and J. H. Lee, "Tone injection with hexagonal constellation for peak-to-average power ratio reduction in OFDM," *IEEE Commun. Lett.*, vol. 10, no. 9, pp. 646–648, Sep. 2006.

[60] J.-C. Chen and C.-K. Wen, "PAPR Reduction of OFDM Signals Using Cross-Entropy-Based Tone Injection Schemes," *IEEE Signal Process. Lett.*, vol. 17, no. 8, pp. 727–730, Aug. 2010.

[61] H. Breiling, S. H. Muller-Weinfurtner, and J. B. Huber, "SLM peak-power reduction without explicit side information," *IEEE Commun. Lett.*, vol. 5, no. 6, pp. 239–241, Jun. 2001.

[62] Chin-Liang Wang and Yuan Ouyang, "Low-complexity selected mapping schemes for peak-to-average power ratio reduction in OFDM systems," *IEEE Trans. Signal Process.*, vol. 53, no. 12, pp. 4652–4660, Dec. 2005.

[63] S. H. Han and J. H. Lee, "Modified Selected Mapping Technique for PAPR Reduction of Coded OFDM Signal," *IEEE Trans. Broadcast.*, vol. 50, no. 3, pp. 335–341, Sep. 2004.

[64] Yung-Lyul Lee, Young-Hwan You, Won-Gi Jeon, Jong-Ho Paik, and Hyoung-Kyu Song, "Peak-to-average power ratio in MIMO-OFDM systems using selective mapping," *IEEE Commun. Lett.*, vol. 7, no. 12, pp. 575–577, Dec. 2003.

[65] C. P. Li, S. H. Wang, and C. L. Wang, "Novel low-complexity SLM schemes for PAPR reduction in OFDM systems," *IEEE Trans. Signal Process.*, vol. 58, no. 5, pp. 2916–2921, 2010.

[66] S. H. Müller and J. B. Huber, "OFDM with reduced peak-to-average power ratio by optimum combination of partial transmit sequences," *Electron. Lett.*, vol. 33, no. 5, p. 368, 1997.

[67] L. Yang, R. S. Chen, Y. M. Siu, and K. K. Soo, "PAPR Reduction of an OFDM Signal by Use of PTS With Low Computational Complexity," *IEEE Trans. Broadcast.*, vol. 52, no. 1, pp. 83–86, Mar. 2006.

[68] S. H. Han and J. H. Lee, “PAPR reduction of OFDM signals using a reduced complexity PTS technique,” *IEEE Signal Process. Lett.*, vol. 11, no. 11, pp. 887–890, 2004.

[69] A. Alavi, C. Tellambura, and I. Fair, “PAPR reduction of OFDM signals using partial transmit sequence: An optimal approach using sphere decoding,” *IEEE Commun. Lett.*, vol. 9, no. 11, pp. 982–984, 2005.

[70] G. D. Mandyam, “Sinusoidal transforms in OFDM systems,” *IEEE Trans. Broadcast.*, vol. 50, no. 2, pp. 172–184, 2004.

[71] F. S. Al-kamali, M. I. Dessouky, B. M. Sallam, F. Shawki, and F. E. A. El-Samie, “Transceiver scheme for single-carrier frequency division multiple access implementing the wavelet transform and peak-to-average-power ratio reduction methods,” *IET Commun.*, vol. 4, no. 1, p. 69, 2010.

[72] E. Sun, R. Yang, P. Si, Y. Sun, and Y. Zhang, “Raised Cosine-like companding scheme for peak-to-average power ratio reduction of SCFDMA signals,” in *2010 Global Mobile Congress*, 2010, pp. 1–5.

[73] L. Wang, G. Wu, L. Dan, and Y. Xiao, “A Time-Domain PTS without Side Information in SC-FDMA Systems,” in *2011 7th International Conference on Wireless Communications, Networking and Mobile Computing*, 2011, pp. 1–4.

[74] G. Chen, S. H. Song, and K. Ben Letaief, “A low-complexity precoding scheme for PAPR reduction in SC-FDMA systems,” in *2011 IEEE Wireless Communications and Networking Conference*, 2011, pp. 1358–1362.

[75] D. D. Falconer, “Linear precoding of OFDMA signals to minimize their instantaneous power variance,” *IEEE Trans. Commun.*, vol. 59, no. 4, pp. 1154–1162, 2011.

[76] S. Ben Slimane, “Reducing the Peak-to-Average Power Ratio of OFDM Signals Through Precoding,” *IEEE Trans. Veh. Technol.*, vol. 56, no. 2, pp. 686–695, Mar. 2007.

[77] C. H. G. Yuen and B. Farhang-Boroujeny, “Analysis of the Optimum Precoder in SC-FDMA,” *IEEE Trans. Wirel. Commun.*, vol. 11, no. 11, pp. 4096–4107, Nov. 2012.

[78] C. A. Azurdia-Meza, K. Lee, and K. Lee, “PAPR Reduction in SC-FDMA by Pulse Shaping Using Parametric Linear Combination Pulses,” *IEEE Commun. Lett.*, vol. 16, no. 12, pp. 2008–2011, Dec. 2012.

[79] C. A. Azurdia-Meza, K. Lee, and K. Lee, “PAPR Reduction in Single Carrier FDMA Uplink by Pulse Shaping Using a β-α Filter,” *Wirel. Pers. Commun.*, vol. 71, no. 1, pp. 23–44, Jul. 2013.

[80] J. Ji, G. Ren, and H. Zhang, “PAPR reduction in coded SC-FDMA systems via introducing few bit errors,” *IEEE Commun. Lett.*, vol. 18, no. 7, pp. 1258–1261, 2014.

[81] L. Zhuang, L. Liu, J. Li, K. Shao, and G. Wang, “Discrete sine and cosine transforms in single carrier modulation systems,” *Wirel. Pers. Commun.*, vol. 78, no. 2, pp. 1313–1329, 2014.

[82] Z. Feng, X. Tao, W. Liu, and Z. Hu, “PAPR Reduction in SC-IFDMA Using a Piece-Wise Linear Nyquist Filter,” *IEEE Commun. Lett.*, vol. 19, no. 3, pp. 487–490, Mar. 2015.

[83] F. S. Al-Kamal *et al.*, “An Efficient Transceiver Scheme for SC-FDMA Systems Based on Discrete Wavelet Transform and Discrete Cosine Transform,” *Wirel. Pers. Commun.*, vol. 83, no. 4, pp. 3133–3155, 2015.

[84] K. Wu, G. Ren, and M. Yu, “PAPR Reduction of SC-FDMA Signals Using Optimized Additive Pre-distortion,” *IEEE Commun. Lett.*, vol. 19, no. 8, pp. 1446–1449, Aug. 2015.

[85] J. Ji, G. Ren, and H. Zhang, “PAPR Reduction of SC-FDMA Signals Via Probabilistic Pulse Shaping,” *IEEE Trans. Veh. Technol.*, vol. 64, no. 9, pp. 3999–4008, Sep. 2015.

[86] Y. Xia and J. Ji, “Reducing PAPR of SC-FDMA signals through simple amplitude predistortion,” *ETRI J.*, vol. 37, no. 5, pp. 922–928, 2015.

[87] G. Ren, J. Ji, J. Wu, and K. Wu, “Side information embedding and detection scheme for selected mapping based single-carrier frequency-division multiple access systems,” *IET Commun.*, vol. 10, no. 11, pp. 1294–1302, 2016.

[88] H. Y. Liang, C. Y. Yang, K. H. Lin, and C. H. Cheng, "Using Improved Product-Coded Modulation Codes to Reduce the Peak-to-Average Power Ratio in Single-Carrier Frequency Division Multiple Access Systems," *Wirel. Pers. Commun.*, vol. 91, no. 3, pp. 1345–1357, 2016.

[89] A. Khelil, D. Slimani, L. Talbi, and J. LeBel, "SLM localised SC-FDMA performance evaluation based on 30 GHz channel measurement for 5G," *Electron. Lett.*, vol. 52, no. 18, pp. 1573–1574, Sep. 2016.

[90] S. Kamal, C. A. Azurdia Meza, N. H. Tran, and K. Lee, "Low-PAPR Hybrid Filter for SC-FDMA," *IEEE Commun. Lett.*, vol. 21, no. 4, pp. 905–908, Apr. 2017.

[91] T. Lee and H. Ochiai, "A New Trellis Shaping Design for Peak Power Reduction of SC-FDMA Signals with High-Order QAM," *IEEE Trans. Veh. Technol.*, vol. 66, no. 6, pp. 5030–5042, 2017.

[92] H.-Y. Liang and H.-C. Chu, "Improving the peak-to-average power ratio of single-carrier frequency division multiple access systems by using an improved constellation extension scheme with error correction," *Telecommun. Syst.*, vol. 65, no. 3, pp. 377–386, Jul. 2017.

[93] M. R. Hossain and K. T. Ahmmed, "Efficient PAPR Reduction in DCT-SCFDMA System Based on Absolute Exponential Companding Technique with Pulse Shaping," *Wirel. Pers. Commun.*, vol. 97, no. 3, pp. 3449–3463, Dec. 2017.

[94] H. Chen, H.-Y. Liang, H.-C. Chu, and C.-B. Lin, "Improving the peak-to-average power ratio of the single-carrier frequency-division multiple access system through the integration of tone injection and tone reservation techniques," *Int. J. Commun. Syst.*, vol. 31, no. 1, p. e3408, Jan. 2018.

[95] M. A. Abd El-Hamed, A. Zekry, S. S. Elagooz, and F. E. Abd El-Samie, "Blind selective mapping for single-carrier frequency division multiple access system," *Digit. Signal Process.*, vol. 75, pp. 25–37, Apr. 2018.

[96] M. R. Hossain and K. T. Ahmmed, "Non-linear companding based hybrid PAPR reduction approach for DCT-SCFDMA system," *IET Commun.*, vol. 12, no. 12, pp.

1468–1476, Jul. 2018.

[97] H. Sakran, “An efficient joint algorithm for reducing PAPR of SC-FDMA system in cognitive radio networks,” *Wirel. Networks*, vol. 25, no. 3, pp. 1117–1124, Apr. 2019.

[98] T. Jiang, W. Xiang, P. Richardson, D. Qu, and G. Zhu, “On the Nonlinear Companding Transform for Reduction in PAPR of MCM Signals,” *IEEE Trans. Wirel. Commun.*, vol. 6, no. 6, pp. 2017–2021, Jun. 2007.

[99] T. Jiang, Y. Yang, and Y.-H. Y. H. Song, “Exponential Companding Technique for PAPR Reduction in OFDM Systems,” *IEEE Trans. Broadcast.*, vol. 51, no. 2, pp. 244–248, Jun. 2005.

[100] H. Gong, W. Ye, S. Feng, and F. Ke, “A threshold companding scheme for reducing peak-to-average power ratio of OFDM signals,” *Proc. - 2005 Int. Conf. Wirel. Commun. Netw. Mob. Comput. WCNM 2005*, vol. 1, no. 2, pp. 553–556, 2005.

[101] Y. Jiang, “New companding transform for PAPR reduction in OFDM,” *IEEE Commun. Lett.*, vol. 14, no. 4, pp. 282–284, 2010.

[102] J. Hou *et al.*, “Peak-to-Average Power Ratio Reduction of OFDM Signals With Nonlinear Companding Scheme,” *IEEE Trans. Broadcast.*, vol. 56, no. 2, pp. 258–262, Jun. 2010.

[103] F. El-Samie, F. Al-kamali, A. Al-nahari, and M. Dessouky, *SC-FDMA for Mobile Communications*. CRC Press, 2013.

[104] D. Wulich and L. Goldfeld, “Bound of the distribution of instantaneous power in single carrier modulation,” *IEEE Trans. Wirel. Commun.*, vol. 4, no. 4, pp. 1773–1778, Jul. 2005.

[105] J. Kim and Y. Shin, “An effective clipped companding scheme for PAPR reduction of OFDM signals,” *IEEE Int. Conf. Commun.*, no. 1, pp. 668–672, 2008.

[106] H. Ochoa-Domínguez and K. R. Rao, *Discrete Cosine Transform*. II edition, Taylor & Francis Group: CRC Press, 2019.

[107] K. R. Rao and P. Yip, *Discrete Cosine Transform*. Academic Press, 1990.

[108] F. E. Abd El-Samie, F. S. Al-kamali, M. I. Dessouky, B. M. Sallam, and F. Shawki, "Performance enhancement of SC-FDMA systems using a companding technique," *Ann. Telecommun. - Ann. des télécommunications*, vol. 65, no. 5–6, pp. 293–300, Jun. 2010.

[109] N. Ahmed and K. R. Rao, "Walsh-Hadamard Transform," in *Orthogonal Transforms for Digital Signal Processing*, Berlin, Heidelberg: Springer Berlin Heidelberg, 1975, pp. 99–152.

[110] Y. A. Geadah and M. J. G. Corinthios, "Natural, Dyadic, and Sequency Order Algorithms and Processors for the Walsh-Hadamard Transform," *IEEE Trans. Comput.*, vol. C–26, no. 5, pp. 435–442, May 1977.

[111] K. R. Rao, D. N. Kim, and J. J. Hwang, *Fast Fourier Transform - Algorithms and Applications*. Springer, Netherlands, 2010.

[112] "WARPLab framework." [Online]. Available: http://warpproject.org/trac/wiki/WARPLab. [Accessed: 26-Mar-2019].

[113] "WARP repository." [Online]. Available: http://warpproject.org/trac. [Accessed: 26-Mar-2019].

[114] J. B. Doré, R. Gerzaguet, N. Cassiau, and D. Ktenas, "Waveform contenders for 5G: Description, analysis and comparison," *Phys. Commun.*, vol. 24, pp. 46–61, 2017.

List of Publications

International Journals

1. K.Shri Ramtej and S. Anuradha, "Non Linear Companding Transform to Mitigate PAPR in DCT Based SC-FDMA System," *Wireless Personal Communications*, vol. 112, no. 1, pp. 503–522, May 2020. doi:10.1007/s11277-020-07057-z. (**SCI**)
2. K.Shri Ramtej and S.Anuradha, "Experimental Validation of Improved Exponential Companding Technique for SC-FDMA Systems using WARP Hardware," *Journal of Circuits, Systems and Computers*, doi: 10.1142/S0218126620501546. (**SCI**)
3. K.Shri Ramtej and S.Anuradha, "Performance analysis of hybrid PAPR reduction technique for LTE uplink communications," *Physical Communication*, vol. 29, pp. 103–111, Aug. 2018. (**SCI**)
4. K.Shri Ramtej and S.Anuradha, "On Companding Techniques to Mitigate PAPR in SC-FDMA Systems," *International Journal of Wireless and Mobile Computing*, vol. 18, no. 3, pp.295–302, Mar, 2020. doi: 10.1504/IJWMC.2020.106778. (**Scopus**)
5. K.Shri Ramtej and S.Anuradha, "Logarithmic Companding Technique to Improve Performance of SC-FDMA Systems," *Indian Journal of Science and Technology*, vol 9(S1), doi: 10.17485/ijst/2016/v9iS1/107905, Dec, 2016. (**Scopus**)
6. K.Shri Ramtej and S.Anuradha, "Walsh Hadamard Transform based SC-FDMA System using WARP Hardware," *ETRI Journal*. (**SCI-Accepted**)

International Conferences

1. K.Shri Ramtej and S.Anuradha, "Modified μ-Law Companding Transform for PAPR Reduction in SC-FDMA Systems," *Optical and Wireless Technologies, Lecture Notes in Electrical Engineering,* vol 546, MNIT Jaipur, 2020, pp. 377–386. DOI: 10.1007/978-981-13-6159-3_40 (**Springer**)
2. K.Shri Ramtej and S. Anuradha, "Exponential Companding Transform to Mitigate PAPR in SC-FDMA Systems," *2019 PhotonIcs & Electromagnetics Research Symposium* - (PIERS-Spring), Rome, Italy, 2019, pp. 4174-4179. DOI: 10.1109/PIERS-Spring46901.2019.9017360 (**IEEE**)

3. K.Shri Ramtej and S.Anuradha, "PAPR Reduction in LTE Uplink Communications by Airy Companding Transform," *9th International Conference on Computing, Communication and Networking Technologies*, IISC Bangalore, pp. 1-5, 2018. (**IEEE**)
4. K.Shri Ramtej and S. Anuradha, "New Error Function Companding for PAPR Reduction in LTE Uplink Communications," *23rd National Conference on Communications (NCC)*, IIT Madras, pp. 287-291, Mar 2- 4, 2017. (**IEEE**)